Universidad Politécnica de Valencia
Departamento de Ingeniería Electrónica

Towards the Full Control of Sound with Sonic Crystals and Acoustic Metamaterials

Presentado por: D. Daniel Torrent Martí
Dirigida por: Profesor José Sánchez-Dehesa

Acknowledgments

Agradecimientos

Contents

List of Figures

List of Tables

Resum de la tesi doctoral

Cap al control total del so amb cristals sònics i metamaterials acústics

de

D. Daniel Torrent Martí
Doctor en Ciències pel Departament d'Enginyeria Electrònica
Universitat Politècnica de València, Juny 2008

L'objectiu d'aquest treball ha sigut obtenir expressions matemàtiques per als paràmetres acústics efectius de sistemes heterogenis al límit dhomogenetització, la qual cosa ha permès el disseny de nous dispositius refractius funcionals en un ampli rang de longituds d'ona.

Matemàticament aquest problema ha sigut tractat mitjanant la teoria de la dispersió múltiple, ja que les geometries del problema són principalment circulars i lesmentada teoria ha demostrat ser la més adequada en aquest cas. Per a obtenir els paràmetres efectius s'han desenvolupat dos mètodes d'homogeneïtzació que han demostrat ser complementaris. El primer es basa en la propagació d'ones elàstiques a través de mitjans periòdics, mentre que el segon es basa en les propietats de dispersió acústica de sistemes finits de cilindres.

Com a principals aplicacions de la teoria desenvolupada cal destacar, per l'interès i la novetat en el camp de l'acústica, les lents de gradient díndex i els dispositius d'invisibilitat acústica. Aquestes lents consisteixen en materials on la velocitat de propagació del so varia segons les coordenades, i permet així un control de la trajectòria del so. En aquest treball es proposa una d'aquestes lents, que té la peculiaritat de ser totalment transparent i, per tant, tota l'energia sonora incident és recollida pel focus.

Els dispositius d'invisibilitat permeten ocultar al seu interior un objecte de manera que siga indetectable per al so. La complexitat d'aquests resideix que han d'estar fets de materials amb una densitat de massa anisòtropa. Aquest treball ha demostrat com cal dissenyar aquests dispositius mitjanant estructures de cilindres fets amb dos tipus de materials isòtrops.

Resumen de la tesis doctoral

Hacia el Control Total del Sonido con Cristales Sónicos y Metamateriales Acústicos

de

D. Daniel Torrent Martí

Doctor en Ciencias por el Departamento de Ingeniería Electrónica
Universidad Politécnica de Valencia, Junio 2008

El objetivo de este trabajo ha sido obtener expresiones matemáticas para los parámetros acústicos efectivos de sistemas heterogéneos en el límite de homogeneización, lo que ha permitido el diseño de nuevos dispositivos refractivos funcionales en un amplio rango de longitudes de onda.

Matemáticamente este problema ha sido tratado mediante la teoría de dispersión múltiple, ya que las geometrías del problema son principalmente circulares y dicha teoría ha demostrado ser la más adecuada en ese caso.

Para obtener los parámetros efectivos se han desarrollado dos métodos de homogeneización que han demostrado ser complementarios. El primero se basa en la propagación de ondas elásticas a través de medios periódicos mientras que el segundo se basa en las propiedades de dispersión acústica de sistemas finitos de cilindros.

Como principales aplicaciones de la teoría desarrollada cabe destacar, por su interés y novedad en el campo de la acústica, las lentes de gradiente de índice y los dispositivos de invisibilidad acústica. Estas lentes consisten en materiales donde la velocidad de propagación del sonido varía en función de las coordenadas, permitiendo así un control de la trayectoria del sonido. En este trabajo se propone una de estas lentes con la peculiaridad de ser totalmente transparente, y por tanto, toda la energía sonora incidente es recogida por el foco.

Los dispositivos de invisibilidad permiten ocultar en su interior un objeto de modo que sea indetectable para el sonido. La complejidad de estos reside en que deben estar hechos de materiales con una densidad de masa anisótropa. Este trabajo ha demostrado como diseñar estos dispositivos mediante estructuras de cilindros hechos con dos tipos de materiales isótropos.

Abstract of the doctor thesis

Towards the Full Control of Sound with Sonic Crystals and Acoustic Metamaterials

by

D. Daniel Torrent Martí
Doctor of Philosophy in the Ingeniería Electrónicadepartment
Politecnic University of Valencia, Valencia, June 2008

The aim of this work has been to obtain mathematical expressions for the effective acoustic parameters of heterogeneous systems in the homogenization limit, what has allowed the design of new refractive devices working in a wide wavelength range.

Mathematically this problem has been treated by means of the multiple scattering theory, because the geometries of the problem are mainly circular and such theory is the best one in this case.

To obtain the effective parameters two homogenization methods have been developed, which has been shown to be complementary. The first is based in elastic wave propagation through periodic media while the second is based in the acoustic scattering properties of finite clusters of cylinders.

The main applications of the developed theory are, due to its interest and novelty in the field of acoustics, the gradient index lens and the acoustic cloaking devices. These lenses are materials where the propagation speed of sound change as a function of the spacial coordinates, allowing then the control of the sound trajectory. In this work has been proposed one of these lenses with the peculiarity of being fully transparent, and then, all the incident energy is located at the focus of the lens.

Acoustic cloaking devices can hide inside them an object such that it be undetectable for sound. The complexity of these consists in that they have to be made of materials with an anisotropic mass density. This work has shown how to design these devices by means of cylinder structures made of two types of isotropic materials.

Part I

Theory

Chapter 1

Introduction

In this chapter the basic equations of acoustics and elasticity are derived, but always focusing on wave propagation. Here, only linear wave phenomena are considered, so that the non linear elements will be neglected. Finally, a brief introduction to sonic crystals will be made.

1.1 Acoustics

In the present work a fluid is considered as a continuous medium defined by certain velocity field $\boldsymbol{V}(\boldsymbol{r},t)$,$\boldsymbol{r}$ being the position vector of a point in the fluid and t the time.

This fluid is assumed to be made of point particles of mass dm free to move around the space. If a particle is at position $\boldsymbol{r}$ at the time t, after a time Δt it will be at position $\boldsymbol{r}'$ given by

$$\boldsymbol{r}' = \boldsymbol{r} + \boldsymbol{V}(\boldsymbol{r},t)\Delta t \tag{1.1.1}$$

This change in the position of the particle implies a change in its velocity, which now will be

$$\boldsymbol{V}'(\boldsymbol{r}',t') = \boldsymbol{V}'(\boldsymbol{r}+\boldsymbol{V}\Delta t, t+\Delta t) \approx \boldsymbol{V}(\boldsymbol{r},t) + [\boldsymbol{V}(\boldsymbol{r},t)\cdot\boldsymbol{\nabla}]\,\boldsymbol{V}(\boldsymbol{r},t)\Delta t + \frac{\partial \boldsymbol{V}(\boldsymbol{r},t)}{\partial t}\Delta t \tag{1.1.2}$$

thus the acceleration of the particle is, by definition

$$\boldsymbol{a} \equiv \lim_{\Delta t\to 0}\left[\frac{\boldsymbol{V}\,' - \boldsymbol{V}}{\Delta t}\right] = \frac{\partial \boldsymbol{V}}{\partial t} + (\boldsymbol{V}\cdot\boldsymbol{\nabla})\boldsymbol{V} \tag{1.1.3}$$

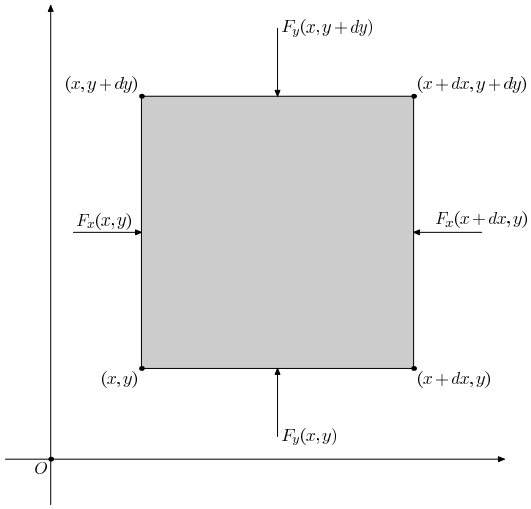

Figure 1.1: Force diagram acting on a fluid element with mass dm.

This acceleration is the reaction of the fluid to some force field. In the present work the acoustic pressure acts as the exciting field. Then, the force due to this field is the responsible of the acceleration of the particles in the fluid.

In figure 1.1 it is shown a diagram of the forces acting on certain volume element, where the z component has not been shown for clarity. The forces along x can be expressed as

$$F_x(x,y) - F_x(x+dx,y) = \frac{P(x,y) - P(x+dx,y)}{dx} dxdydz = -\frac{\partial P(x,y)}{\partial x} dV \tag{1.1.4}$$

and Newton's second law

$$\Sigma F_x = dma_x \tag{1.1.5}$$

The above equations leads to

$$-\frac{\partial P(x,y)}{\partial x} = \rho a_x \tag{1.1.6}$$

The generalization to the three spacial coordinates gives

$$-\boldsymbol{\nabla} P = \rho \boldsymbol{a} \tag{1.1.7}$$

Equation (1.1.3) establishes a relation between the acceleration and the spatial and temporal derivatives of the particle velocity field $\boldsymbol{V}$, thus with

the above equation it is possible to obtain the first relation between the basic variables of a fluid

$$-\boldsymbol{\nabla} P = \rho \left[\frac{\partial \boldsymbol{V}}{\partial t} + (\boldsymbol{V} \cdot \boldsymbol{\nabla}) \boldsymbol{V} \right] \tag{1.1.8}$$

The next relation between the basic variables is very simple to obtain: it is the well known continuity equation. This equation is obtained from the mass conservation law; that is, the decreasing mass in a given volume equals the mass flux through the boundary of such volume; i.e.

$$\frac{\partial}{\partial t} \iiint_V \rho dV = - \iint_S \rho \boldsymbol{V} \cdot d\boldsymbol{S} \tag{1.1.9}$$

The right hand side of the above equation can be converted into a volume integral with Gauss' theorem,

$$\iiint_V \frac{\partial \rho}{\partial t} dV = - \iiint_V \boldsymbol{\nabla} \cdot (\rho \boldsymbol{V}) dV \tag{1.1.10}$$

Therefore, the continuity equation is derived

$$\boldsymbol{\nabla} \cdot (\rho \boldsymbol{V}) + \frac{\partial \rho}{\partial t} = 0 \tag{1.1.11}$$

To complete the description of a fluid another equation should be needed relating the basic variables of the fluid: density ρ, particle velocity vector$\boldsymbol{V}$ and pressure P. This equation is called the "state equation" and can be derived with the definition of the compressibility or bulk modulus B

$$B \equiv \rho \frac{\Delta P}{\Delta \rho} \tag{1.1.12}$$

it is assumed that this definition also holds in differential form so that

$$B = \rho \frac{dP}{d\rho} \rightarrow dP = \frac{B}{\rho} d\rho \tag{1.1.13}$$

If the pressure is a function of the spacial and time coordinates and of the density ρ

$$P = P(\mathbf{r}, t; \rho), \tag{1.1.14}$$

the state equation is

$$\frac{\partial P}{\partial t} dt + d\boldsymbol{r} \cdot \boldsymbol{\nabla} P = \frac{B}{\rho} \frac{\partial \rho}{\partial t} dt + \frac{B}{\rho} d\boldsymbol{r} \cdot \boldsymbol{\nabla} \rho \tag{1.1.15}$$

and dividing by dt

$$\frac{\partial P}{\partial t} + \boldsymbol{V} \cdot \boldsymbol{\nabla} P = \frac{B}{\rho}\frac{\partial \rho}{\partial t} + \frac{B}{\rho}\boldsymbol{V} \cdot \boldsymbol{\nabla}\rho \tag{1.1.16}$$

Solving for the derivative of the density in the continuity equation (1.1.11) and inserting above, the following result is obtained

$$\frac{\partial P}{\partial t} + \mathbf{V} \cdot \nabla P = -B\nabla \cdot \mathbf{V} \tag{1.1.17}$$

Equation (1.1.17) and (1.1.8) forms the basic equations to derive the sound wave equation, as will be shown in the next section. These equations are non linear, so the next step is to derive the linear approximation for them.

1.2 Acoustic waves

In equation (1.1.8) the non linear term $\boldsymbol{V} \cdot \boldsymbol{\nabla}\boldsymbol{V}$ can be suppressed, and the density ρ will be assumed to be a function of space coordinates. This last approximation can be understood considering that the time variations of the density are second orders terms, which multiplied by the time derivative of the particle velocity $\boldsymbol{V}$ will be a negligible quantity. Then the linear approximation to equation (1.1.8) will be

$$\boldsymbol{\nabla} P + \rho\frac{\partial \boldsymbol{V}}{\partial t} = 0 \tag{1.2.1}$$

In equation (1.1.17) the non linear term is $\boldsymbol{V} \cdot \boldsymbol{\nabla} P$, neglecting this term the linear version of this equation is

$$\frac{\partial P}{\partial t} + B\boldsymbol{\nabla} \cdot \boldsymbol{V} = 0 \tag{1.2.2}$$

It is worth to express these two equations with the variables being explicitly indicated, that is

$$\boldsymbol{\nabla} P(\boldsymbol{r}, t) + \rho(\boldsymbol{r})\frac{\partial \boldsymbol{V}(\boldsymbol{r}, t)}{\partial t} = 0 \tag{1.2.3a}$$

$$\frac{\partial P(\boldsymbol{r}, t)}{\partial t} + B(\boldsymbol{r})\boldsymbol{\nabla} \cdot \boldsymbol{V}(\boldsymbol{r}, t) = 0 \tag{1.2.3b}$$

These equations are the basic equations for the acoustic field. If equation (1.2.3b) is derivated respect to the time, with the help of equation (1.2.3a)

$$\frac{\partial^2 P(\boldsymbol{r},t)}{\partial t^2} - B(\boldsymbol{r})\boldsymbol{\nabla}\cdot\left[\rho^{-1}(\boldsymbol{r})\boldsymbol{\nabla}P(\boldsymbol{r},t)\right] = 0 \tag{1.2.4}$$

For the case of an harmonic pressure field of angular frequency ω

$$P(\boldsymbol{r},t) = P(\boldsymbol{r})e^{i\omega t} \tag{1.2.5}$$

by expanding the second term of equation (1.2.4), the following inhomogeneous Helmholtz equation is obtained

$$\left[\boldsymbol{\nabla}^2 + k^2(\boldsymbol{r})\right]P(\boldsymbol{r}) = -\rho(\boldsymbol{r})\boldsymbol{\nabla}\rho^{-1}(\boldsymbol{r})\cdot\boldsymbol{\nabla}P(\boldsymbol{r}) \tag{1.2.6}$$

with

$$k^2(\boldsymbol{r}) = \frac{\rho(\boldsymbol{r})}{B(\boldsymbol{r})}\omega^2 \tag{1.2.7}$$

1.2.1 Isotropic medium

When both the bulk modulus B and the density ρ are constant, equation (1.2.6) reduces to the well known homogeneous Helmholtz equation

$$\boldsymbol{\nabla}^2 P + k^2 P = 0 \tag{1.2.8}$$

The solution of this equation are plane waves of the form

$$P(\boldsymbol{r},\boldsymbol{k}) = e^{i\boldsymbol{k}\cdot\boldsymbol{r}} \tag{1.2.9}$$

with $\boldsymbol{k} = k(\cos\theta_0, \sin\theta_0)$ defining the direction of propagation of the plane wave with wave number $k = \omega\rho/B$. This expression for the wave number shows that the speed of sound for these waves is

$$c = \frac{\omega}{k} = \sqrt{\frac{B}{\rho}} \tag{1.2.10}$$

1.2.2 Anisotropic medium

The wave equation for an anisotropic acoustic medium can be obtained by using a phenomenological argument. Such anisotropic medium will be made

by placing sound scatters in a periodic lattice and letting the wavelength be larger than the lattice parameter.

In this approach, both the bulk modulus B and the density ρ will be periodic functions of the spacial coordinates. The starting point will be the basic linear acoustic equations (1.2.3a) and (1.2.3b)(omitting the explicit dependence space and time)

$$\boldsymbol{\nabla} P(\boldsymbol{r},t) + \rho(\boldsymbol{r}) \frac{\partial \boldsymbol{V}(\boldsymbol{r},t)}{\partial t} = 0 \tag{1.2.11a}$$

$$\frac{\partial P(\boldsymbol{r},t)}{\partial t} + B(\boldsymbol{r}) \boldsymbol{\nabla} \cdot \boldsymbol{V}(\boldsymbol{r},t) = 0 \tag{1.2.11b}$$

Now, it is assumed that both the bulk modulus $B(\boldsymbol{r})$ and the density $\rho(\boldsymbol{r})$ are periodic functions of the position vector $\boldsymbol{r}$. The goal is to find the form of the above equations in the low frequency limit, that is, for the case in which the spacial periodicity defined by the wavelength is larger than the periodicity of the acoustic parameters B and ρ.

Plane wave-like solution can be proposed for both the pressure field and the particle velocity, being these functions of the form

$$\Psi(\boldsymbol{r},t) = \Psi(\omega,\boldsymbol{k}) e^{i\boldsymbol{k}\cdot\boldsymbol{r}} e^{-i\omega t} \tag{1.2.12}$$

where the wave number $\boldsymbol{k} = \boldsymbol{k}(\boldsymbol{r})$ is a function of the spacial coordinates. It is obvious that in the low frequency limit this dependence will disappear and the wave number will be constant along the crystal, and then the solutions are plane waves.

The spacial derivatives of functions given above are

$$\frac{\partial \Psi(\boldsymbol{r},t)}{\partial x_i} = i\Psi(\boldsymbol{r},t) \sum_j \chi_{ij}(\boldsymbol{r}) k_j(\boldsymbol{r}) \tag{1.2.13}$$

where the tensorial quantity χ_{ij} is defined by

$$\chi_{ij}(\boldsymbol{r}) = \delta_{ij} + \frac{x_j}{k_j(\boldsymbol{r})} \frac{\partial k_j(\boldsymbol{r})}{\partial x_i} \tag{1.2.14}$$

Note that this quantity is a function of the spacial coordinates and the wave number. The only assumption that is needed to do now is that in the low frequency limit this quantity becomes finite and different than zero. This quantity will be the responsible of the anisotropy, as will be shown later.

With this definition the equations of motion (1.2.11a) and (1.2.11b) are:

$$iP(\boldsymbol{r},t)\sum_l \chi_{kl}(\boldsymbol{r})k_l(\boldsymbol{r}) + \rho(\boldsymbol{r})\frac{\partial V_k(\boldsymbol{r},t)}{\partial t} = 0 \tag{1.2.15a}$$

$$\frac{\partial P(\boldsymbol{r},t)}{\partial t} + iB(\boldsymbol{r})\sum_k\sum_j \chi_{kj}(\boldsymbol{r})k_j(\boldsymbol{r})V_k(\boldsymbol{r},t) = 0 \tag{1.2.15b}$$

The second equation can be simplified by defining some kind of "effective particle velocity"

$$V_j^*(\boldsymbol{r},t) = \sum_k \chi_{kj}(\boldsymbol{r})V_k(\boldsymbol{r},t) \tag{1.2.16}$$

yielding

$$\frac{\partial P(\boldsymbol{r},t)}{\partial t} + iB(\boldsymbol{r})\sum_j k_j(\boldsymbol{r})V_j^*(\boldsymbol{r},t) = 0 \tag{1.2.17}$$

The above equation is suitable for being averaged in the unit cell of the lattice defined by the periodic system, but not in its present form. When the average is taken over a unit cell, it is expected that, in the long wavelength limit, the pressure field be constant in this unit cell, as well as the wave number. But the "effective particle velocity" has an unknown behavior due to the quantities χ_{ij}, whose dependence in the spacial coordinates is unknown. In order to average it is necessary to divide the equation by the bulk modulus B, and then average,

$$\left\langle \frac{1}{B(\boldsymbol{r})} \right\rangle \frac{\partial P(\boldsymbol{r},t)}{\partial t} + i\sum_j k_j \left\langle V_j^*(\boldsymbol{r},t)\right\rangle = 0, \tag{1.2.18}$$

where it has been assumed that we work in the low frequency limit and the wave number does not depend on the spacial coordinates. Since the bulk modulus does not interact with the periodicity of the lattice, the average can be taken easily. For the case of one scatterer per unit cell

$$\left\langle \frac{1}{B(\boldsymbol{r})} \right\rangle = \frac{1}{V_d}\int_{\text{cell}} \frac{1}{B(\boldsymbol{r})}dV = \frac{f}{B_a} + \frac{1-f}{B_b} \tag{1.2.19}$$

where B_a and B_b are the bulk modulus of the scatter and of the background, respectively. The quantity f is the filling fraction of the scatter, that is, the area of the scatter divided by the area of the unit cell. Note that this result

is independent of the number of dimensions of the problem; that is, it is also for three dimensions (3D) and it is independent of the shape of the scatterer.

Defining the effective bulk modulus as

$$\frac{1}{B^*} \equiv \left\langle \frac{1}{B(\boldsymbol{r})} \right\rangle = \frac{f}{B_a} + \frac{1-f}{B_b} \tag{1.2.20}$$

and the unit cell-averaged particle velocity as

$$v_j(\boldsymbol{r},t) \equiv \left\langle V_j^*(\boldsymbol{r},t) \right\rangle \tag{1.2.21}$$

the final form of the equation is

$$\frac{1}{B^*}\frac{\partial P(\boldsymbol{r},t)}{\partial t} + i\sum_j k_j v_j(\boldsymbol{r},t) = 0 \tag{1.2.22}$$

or

$$\frac{1}{B^*}\frac{\partial P(\boldsymbol{r},t)}{\partial t} + \boldsymbol{\nabla}\cdot\boldsymbol{v}(\boldsymbol{r},t) = 0 \tag{1.2.23}$$

which has the same form of equation (1.2.11b) but with a constant bulk modulus; now it is the equation of a homogeneous medium.

The same procedure can be done for equation (1.2.15a), but it has to be expressed as a function of the effective particle velocity vector V_j^*, to do that this equation has to be multiplied by χ_{kj} and summed for all k, yielding

$$iP(\boldsymbol{r},t)\sum_l\sum_k \chi_{kj}(\boldsymbol{r})\chi_{kl}(\boldsymbol{r})k_l(\boldsymbol{r}) + \rho(\boldsymbol{r})\frac{\partial V_j^*(\boldsymbol{r},t)}{\partial t} = 0 \tag{1.2.24}$$

Again this equation cannot be averaged because the product of $\rho(\boldsymbol{r})$ and $V_j^*(\boldsymbol{r},t)$. Let us divide by the density first and after averaging, we arrive to

$$iP(\boldsymbol{r},t)\sum_l \rho_{jl}^{-1}k_l + \frac{\partial v_j(\boldsymbol{r},t)}{\partial t} = 0 \tag{1.2.25}$$

where the reciprocal density tensor has been defined as

$$\rho_{jl}^{-1} = \left\langle \rho^{-1}(\boldsymbol{r})\sum_k \chi_{kj}(\boldsymbol{r})\chi_{kl}(\boldsymbol{r}) \right\rangle \tag{1.2.26}$$

Equation (1.2.25) can also be expressed as a function of the mass density tensor as

$$ik_l P(\boldsymbol{r},t) + \sum_j \rho_{lj}\frac{\partial v_j(\boldsymbol{r},t)}{\partial t} = 0 \tag{1.2.27}$$

or, in vectorial differential form

$$\boldsymbol{\nabla} P(\boldsymbol{r},t) + \rho : \frac{\partial v(\boldsymbol{r},t)}{\partial t} = 0 \tag{1.2.28}$$

solving for the pressure field we arrive to the following wave equation

$$\sum_{i,k} \rho_{ik}^{-1} \frac{\partial^2 P}{\partial x_k \partial x_i} - \frac{1}{B^*} \frac{\partial^2 P}{\partial t^2} = 0 \tag{1.2.29}$$

The wave equation is obviously anisotropic, due to the presence of the cross terms in the partial derivatives. When assuming plane wave solutions of the form

$$P(\boldsymbol{r},t) = P(\omega) e^{i\boldsymbol{k}\cdot\boldsymbol{r}} e^{-i\omega t} \tag{1.2.30}$$

Since the wave vector components are $k_i = k \cos\theta_i$, the following relationship between the frequency and the wave number is found

$$\omega^2 = k^2 B^* \sum_{i,k} \rho_{ki}^{-1} \cos\theta_i \cos\theta_k \tag{1.2.31}$$

Therefore the relation between the effective speed of sound tensor c_{ki} and the reciprocal density tensor ρ_{ki}^{-1} is similar to that of the isotropic case

$$c_{ki}^2 = B^* \rho_{ki}^{-1} \tag{1.2.32}$$

1.3 Elastic waves

A solid medium under deformation is better defined in terms of a displacement vector field $\boldsymbol{u} = \boldsymbol{u}(\boldsymbol{r},t)$. A displacement vector relates the initial position of a point in the medium before the deformation, $\boldsymbol{r}$, with its position after the deformation $\boldsymbol{r}' = \boldsymbol{r}'(\boldsymbol{r},t)$

$$\boldsymbol{u} = \boldsymbol{r}' - \boldsymbol{r} \tag{1.3.1}$$

The line element $|d\boldsymbol{r}|$ before the deformation and after it $|d\boldsymbol{r}'|$ can be related with the displacement vector through the quantity

$$|d\boldsymbol{r}'|^2 = |d\boldsymbol{r} + d\boldsymbol{u}|^2 = \sum_k dx_k dx_k + \sum_k du_k du_k + 2\sum_k du_k dx_k \tag{1.3.2}$$

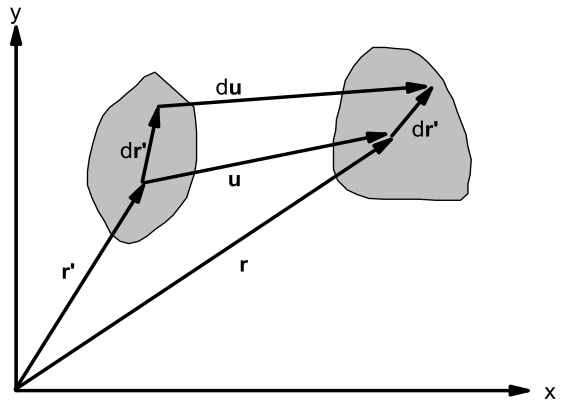

Figure 1.2: Coordinates definition in a solid medium under deformation.

Since

$$du_k = \sum_m \frac{\partial u_k}{\partial x_m} dx_m \tag{1.3.3}$$

the line element will be

$$|d\boldsymbol{r}'|^2 = |d\boldsymbol{r}|^2 + \sum_{k,l,m} \frac{\partial u_k}{\partial x_m} \frac{\partial u_k}{\partial x_l} dx_l dx_m + 2 \sum_{k,m} \frac{\partial u_k}{\partial x_m} dx_m dx_k \tag{1.3.4}$$

where the term containing the partial derivatives $\partial_l u_k \partial_m u_k$ can be neglected (in the linear approximation). The final form for the line element is

$$|d\boldsymbol{r}'|^2 = |d\boldsymbol{r}|^2 + 2 \sum_{m,k} E_{mk} dx_m dx_k \tag{1.3.5}$$

where the tensor E_{mk} is defined in a clearly symmetrical form as

$$E_{mk} = \frac{1}{2} \left(\frac{\partial u_k}{\partial x_m} + \frac{\partial u_m}{\partial x_k} \right) \tag{1.3.6}$$

The tensor E_{mk} is called the strain tensor, and it relates the deformation of line element of some elastic medium with the displacement vector $\boldsymbol{u}$.

This strain or deformation appears in a solid as the consequence of some external (or internal) force field $\boldsymbol{F}$ defined through a stress tensorial field σ_{ik} by means of

$$F_i = \int_S \sum_k \sigma_{ik} dS_k = \int_V \sum_k \frac{\partial \sigma_{ik}}{\partial x_k} dV \tag{1.3.7}$$

when this force is due to a hydrostatic pressure, the stress tensor is related with it by

$$\sigma_{ik} = -P\delta_{ik} \tag{1.3.8}$$

This stress tensor can be related with the movement of the solid through Newton's second law

$$\rho a_i = \sum_k \frac{\partial \sigma_{ik}}{\partial x_k}, \tag{1.3.9}$$

where a_i is the i component of the acceleration vector $\boldsymbol{a}$,

$$a_i = \frac{dv_i}{dt} = \frac{\partial v_i}{\partial t} + \sum_k \frac{\partial v_i}{\partial x_k} v_k \tag{1.3.10}$$

The convective term $v_k \partial_k v_i$ is a non linear term and is neglected here, while the time derivative can be related with the displacement vector

$$\frac{\partial v_i}{\partial t} = \frac{\partial}{\partial t}\frac{\partial x_i}{\partial t} = \frac{\partial^2 u_i}{\partial t^2} \tag{1.3.11}$$

Finally Newton second law is obtained

$$\rho \frac{\partial^2 u_i}{\partial t^2} = \sum_k \frac{\partial \sigma_{ik}}{\partial x_k} \tag{1.3.12}$$

The stress tensor will be assumed to be some function of the strain. This function should be expressed in a Taylor series, being the zero order term null (there is no stress if there is no strain) and neglecting the orders higher than one because of the linear assumption, then the more general form for this function is

$$\sigma_{ik} = \sum_{lm} C_{iklm} E_{lm} \tag{1.3.13}$$

It can be shown [LL] that for an isotropic medium this relation can be expressed as

$$\sigma_{ik} = \sum_l \lambda \delta_{ik} E_{ll} + 2\mu E_{ik} \tag{1.3.14}$$

and as a function of the displacement vector $\boldsymbol{u}$

$$\sigma_{ik} = \sum_l \lambda \delta_{ik} \frac{\partial u_l}{\partial x_l} + \mu \left(\frac{\partial u_k}{\partial x_i} + \frac{\partial u_i}{\partial x_k} \right) \tag{1.3.15}$$

By inserting the above expression into Newton's second law and reordering indexes this equation is

$$\rho\frac{\partial^2 u_i}{\partial t^2} = (\lambda+\mu)\frac{\partial}{\partial x_i}\sum_l \frac{\partial u_l}{\partial x_l} + \mu\sum_k \frac{\partial^2 u_k}{\partial x_k^2} \tag{1.3.16}$$

where it has been assumed that the Lamé constants λ and μ are not functions of the spacial coordinates. In the present work the elastic field will be considered only inside cylinders, where the elastic parameters are constant and there is no need to derive the inhomogeneous wave equation.

Finally, the wave equation in vectorial form is

$$\rho\frac{\partial^2 \boldsymbol{u}}{\partial t^2} = (\lambda+\mu)\boldsymbol{\nabla}(\boldsymbol{\nabla}\cdot\boldsymbol{u}) + \mu\nabla^2\boldsymbol{u} \tag{1.3.17}$$

The displacement vector $\boldsymbol{u}$ can be expressed, by using Helmholtz decomposition, as a function of a scalar potential ϕ and a vectorial potential $\boldsymbol{A}$

$$\boldsymbol{u} = -\boldsymbol{\nabla}\phi + \boldsymbol{\nabla}\times\boldsymbol{A} \tag{1.3.18}$$

and the wave equation is satisfied if the potentials function satisfy the equations

$$\frac{\partial^2\phi}{\partial t^2} = \frac{\lambda+2\mu}{\rho}\nabla^2\phi \tag{1.3.19}$$

$$\frac{\partial^2\boldsymbol{A}}{\partial t^2} = \frac{\mu}{\rho}\nabla^2\boldsymbol{A} \tag{1.3.20}$$

In the present work elasticity is only considered when working with two dimensional systems(2D), then the displacement vector $\boldsymbol{u}$ will lay always in the xy plane. With this limitation to the displacement vector the only non zero component of the potential vector $\boldsymbol{A}$ will be the z component, so that

$$\boldsymbol{A} = A_z\hat{\boldsymbol{z}} \tag{1.3.21}$$

and the displacement vector in Cartesian coordinates

$$u_x = -\frac{\partial\phi}{\partial x} + \frac{\partial A_z}{\partial y} \tag{1.3.22a}$$

$$u_y = -\frac{\partial\phi}{\partial y} - \frac{\partial A_z}{\partial x} \tag{1.3.22b}$$

although it is more useful to express this vector in polar coordinates

$$u_r = -\frac{\partial \phi}{\partial r} + \frac{1}{r}\frac{\partial A_z}{\partial \theta} \tag{1.3.23a}$$

$$u_\theta = -\frac{1}{r}\frac{\partial \phi}{\partial \theta} - \frac{\partial A_z}{\partial r} \tag{1.3.23b}$$

In this coordinate system it is obvious that both the scalar and vectorial potential functions can be expanded in series of Bessel functions

$$\phi = \sum_q A_q^l J_q(k_l r) e^{iq\theta} \tag{1.3.24a}$$

$$A_z = \sum_q A_q^t J_q(k_t r) e^{iq\theta} \tag{1.3.24b}$$

The displacement vector components are

$$u_r = \sum_q \left[-k_l A_q^l J_q'(k_l r) + \frac{iq}{r} A_q^t J_q(k_t r) \right] e^{iq\theta} \tag{1.3.25a}$$

$$u_\theta = \sum_q \left[-\frac{iq}{r} A_q^l J_q(k_l r) - k_t A_q^t J_q'(k_t r) \right] e^{iq\theta} \tag{1.3.25b}$$

For applying the boundary conditions it is necessary to express as well the stress tensor in polar coordinates. In [LL] the strain tensor in such system is given

$$E_{rr} = \frac{\partial u_r}{\partial r} \tag{1.3.26a}$$

$$E_{\theta\theta} = \frac{1}{r}\frac{\partial u_\theta}{\partial \theta} + \frac{u_r}{r} \tag{1.3.26b}$$

$$2E_{r\theta} = \frac{1}{r}\frac{\partial u_r}{\partial \theta} + \frac{\partial u_\theta}{\partial r} - \frac{u_\theta}{r} \tag{1.3.26c}$$

By writing equation (1.3.14) in polar coordinates

$$\sigma_{rr} = (\lambda + 2\mu) E_{rr} + \lambda E_{\theta\theta} \tag{1.3.27a}$$

$$\sigma_{\theta\theta} = (\lambda + 2\mu) E_{\theta\theta} + \lambda E_{rr} \tag{1.3.27b}$$

$$\sigma_{r\theta} = 2\mu E_{r\theta} \tag{1.3.27c}$$

we arrive to the final form of the stress tensor

$$\sigma_{rr} = (\lambda + 2\mu)\frac{\partial u_r}{\partial r} + \frac{\lambda}{r}\frac{\partial u_\theta}{\partial \theta} + \frac{\lambda}{r}u_r \tag{1.3.28a}$$

$$\sigma_{\theta\theta} = \frac{\lambda + 2\mu}{r}\frac{\partial u_\theta}{\partial \theta} + \frac{\lambda + 2\mu}{r}u_r + \lambda\frac{\partial u_r}{\partial r} \tag{1.3.28b}$$

$$\sigma_{r\theta} = \frac{\mu}{r}\frac{\partial u_r}{\partial \theta} + \mu\frac{\partial u_\theta}{\partial r} - \frac{\mu}{r}u_\theta \tag{1.3.28c}$$

1.4 Boundary conditions

Boundary conditions at an interface between two media are different depending on the media involved. For instance, the conditions at a fluid-fluid interface are not the same than that at a fluid-elastic interface. However they can be generalized for an elastic-elastic interface and then particularize for the fluid by considering this medium as an elastic medium with no shear waves.

The general boundary conditions for an elastic-elastic interface are continuity of the displacement vector and the continuity of the normal component of the stress tensor, respectively

$$\boldsymbol{u}^- = \boldsymbol{u}^+ \tag{1.4.1}$$

$$\sum_i \sigma^-_{ni} n_i = \sum_i \sigma^+_{ni} n_i, \tag{1.4.2}$$

where the signs $\pm$ indicates that the quantities have to be evaluated at both media. If one or both of the media is a fluid, the first condition is replaced by the continuity of the normal component of the particle velocity.

In the present work, where boundaries are mainly defined by cylinders, the possible situations are listed below

- Fluid Cylinder in a Fluid Background

$$\frac{1}{\rho_b}\frac{\partial P^-(r)}{\partial r}\bigg|_{r=R_a} = \frac{1}{\rho_a}\frac{\partial P^+(r)}{\partial r}\bigg|_{r=R_a} \tag{1.4.3a}$$

$$P^-(R_a) = P^+(R_a) \tag{1.4.3b}$$

- Solid Cylinder in a Fluid Background

$$0 = \sigma^{+}_{r\theta}(R_a) \tag{1.4.4a}$$

$$\frac{1}{k^2 c_b^2 \rho_b} \frac{\partial P^{-}(r)}{\partial r}\bigg|_{r=R_a} = u^{+}_{r}(R_a) \tag{1.4.4b}$$

$$-P^{-}(R_a) = \sigma^{+}_{rr}(R_a) \tag{1.4.4c}$$

- Fluid Cylinder in a Solid Background

$$\sigma^{-}_{r\theta}(R_a) = 0 \tag{1.4.5a}$$

$$u^{-}_{r}(R_a) = \frac{1}{k^2 c_b^2 \rho_b} \frac{\partial P^{+}(r)}{\partial r}\bigg|_{r=R_a} \tag{1.4.5b}$$

$$\sigma^{-}_{rr}(R_a) = -P^{+}(R_a) \tag{1.4.5c}$$

- Solid Cylinder in a Solid Background

$$u^{-}_{\theta}(R_a) = u^{+}_{\theta}(R_a) \tag{1.4.6a}$$

$$u^{-}_{r}(R_a) = u^{+}_{r}(R_a) \tag{1.4.6b}$$

$$\sigma^{-}_{rr}(R_a) = \sigma^{+}_{rr}(R_a) \tag{1.4.6c}$$

$$\sigma^{-}_{r\theta}(R_a) = \sigma^{+}_{r\theta}(R_a) \tag{1.4.6d}$$

For the special case of an anisotropic fluid cylinder the normal component of the particle velocity is

$$v_r = \frac{i}{\omega}\left[\rho^{-1}_{rr}\frac{\partial P}{\partial r} + \frac{\rho^{-1}_{r\theta}}{r}\frac{\partial P}{\partial \theta}\right], \tag{1.4.7}$$

where the reciprocal density tensor is expressed in polar coordinates.

When the boundary is a plane with normal vector $\boldsymbol{n} = \hat{\boldsymbol{x}}$ it is obvious that the above expressions are valid replacing $r \to x$ and $\theta \to y$.

1.5 Two Dimensional Phononic Crystals and Metamaterials

Phononic crystal is a name that, in general, refers to periodic arrangements of solid scatterers embedded in a solid matrix. This periodicity makes that

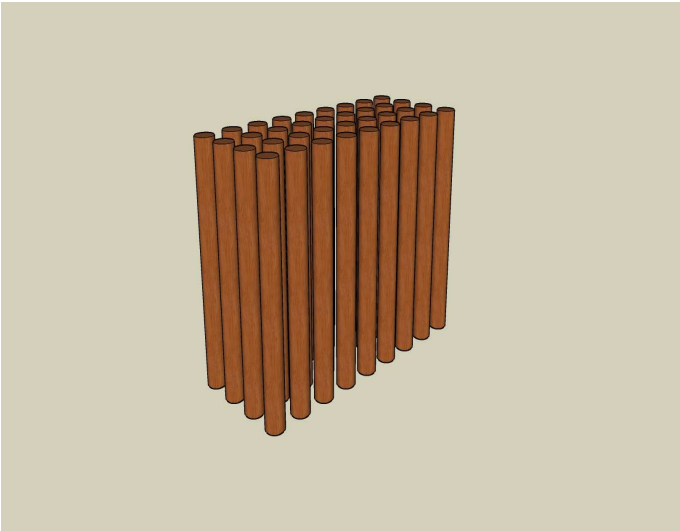

Figure 1.3: Two dimensional sonic crystal. The cylindrical symmetry of the problem makes possible the reduction to the 2D plane.

elastic wave propagation through the crystal presents a behavior analogous to that well known in solid state physics and in photonic crystals physics(for electromagnetic wave propagation).

When the background is not a solid matrix but a fluid medium it is common to refer to this crystal as "sonic crystal", because the only waves that propagates through the medium are acoustic waves, although, of course, elastic modes are excited inside the scatterer.

In the present work the wave propagation is reduced basically to a two dimensional(2D) problem; it is assumed that all the fields have no z dependence of interest. All the scatterers considered here, otherwise indicated, are cylinders and, therefore, the 2D geometry reduces to the circle.

The problem mainly solved here is sound propagation in periodic arrangements of both fluid and elastic cylinders in a (non viscous) fluid background, although effects of disorder will also be analyzed. The case of a solid background will be considered at the end of this manuscript as "future work".

Moreover, the propagation of sound is studied in the long wavelength limit, where the periodic arrangement of scatterers leads to an effective medium and the dispersion relation for waves becomes linear. This limit is called the "homogenization limit" and within this limit, the phononic or

sonic crystals define a new class of acoustic metamaterials with acoustic properties unknown in nature.

Chapter 2

Scattering of waves by a single cylinder: The T Matrix

In this chapter the basic equations of wave scattering are reported. First, two types of incidents fields are introduced. Later, the relation of the scattered field with these incidents fields, called the T matrix, is derived for the main types of cylinders. Finally, some properties of the scattered field are discussed and some comments on convergence for numerical simulations are done.

2.1 Scattering of waves

When an external field reaches a close region defined by some boundary $\partial\sigma$ and having acoustic parameters different to that of the surrounding medium, a phenomenon called "scattering" occurs. The phenomenon consists on the excitation of a certain scattered field as a result of this variation of medium parameters. The close region is called the scatterer and, in the present work, unless otherwise specified, the boundary $\partial\sigma$ will be a line in polar coordinates. In other words, the scattering problem will be solved mainly in 2D.

The external field can be always expressed in terms of regular Bessel functions $J_q(\cdot)$ of the two dimensional spacial coordinates $\boldsymbol{r} = (r, \theta)$ and the field wave number k,

$$P^0(\boldsymbol{r}) = \sum_{q=-\infty}^{\infty} A_q^0 J_q(kr) e^{iq\theta} \tag{2.1.1}$$

The excited field cannot be constructed only with regular Bessel functions, but a irregular part must be added. This irregular part is formed with the Bessel functions of the second kind $Y_q(\cdot)$, and the resulting functions are called Hankel functions $H_q(\cdot) = J_q(\cdot) + iY_q(\cdot)$. In terms of Hankel functions the scattered field is expressed as

$$P^{\text{sc}}(\boldsymbol{r}) = \sum_{q=-\infty}^{\infty} A_q H_q(kr) e^{iq\theta} \tag{2.1.2}$$

In a general problem, coefficients A_q^0 of the incident field are the inputs and the scattered field coefficients A_q are the output. The coefficients A_q depend on both the physical nature of the scatterer and the external field. The dependence of the physical nature of the scatterer is obtained mathematically by means of the boundary conditions, which are different for each type of cylinder, as will be shown later. However, for the case of the external field, P^0, a general expression can be obtained by physical arguments.

All the scattering processes analyzed in this work are linear in frequency. This means that if the external field is the field associated to some wavenumber k, the scattered field will be associated to the same wavenumber k, where k is related with the frequency as usually $\omega = c_b k$, being c_b the speed of sound in the medium. Then, to obtain the scattered field, a function of the type

$$A_q = f(A_0^0, A_{\pm 1}^0, A_{\pm 2}^0, \cdots, A_{\pm s}^0) \tag{2.1.3}$$

must be found for each A_q.

If the linear behavior is imposed to the response of the external field, it is obvious that the function f must be a matrix, that is, the general form of the above relation will be

$$A_q = \sum_s T_{qs}(k; x) A_s^0, \tag{2.1.4}$$

where the argument x indicates that the matrix elements T_{qs} are dependent of some set of physical constants x. Nevertheless, in the present work this notation is simplified and only the wavenumber dependence will be explicitly indicated in some special cases. The matrix elements T_{qs} form what is called as the "transition matrix" or simply the "T matrix". The expression of this T matrix depends not only on the physical nature of the cylinder but also on the external shape of the cylinder.

In this chapter, after showing the expressions for the most commonly used incident fields, will be computed the T matrix of a fluid cylinder (circular and with arbitrary cross section) and of an elastic cylinder (only circular). In chapter 4 another types of scatterers will be considered and their T matrix computed.

2.2 Incident fields

Here, only two types of 2D incident fields are used: the plane wave and the punctual source. Both are basic fields and can be used to understand the response of a given system to more complicated sources. Independently of the functional form of the incident fields, when working in multiple scattering these fields have to be expanded in regular Bessel functions in different reference frames. The goal of this section is not only introduce the fields, but also show how they can be expanded in Bessel functions.

2.2.1 The plane wave

The plane wave is a field distribution defined by some wavenumber $\boldsymbol{k_0} = k_{0x}\hat{\boldsymbol{x}} + k_{0y}\hat{\boldsymbol{y}} = k(\cos\theta_0, \sin\theta_0)$ and some complex amplitude C_0, and has a functional form

$$P^0(\boldsymbol{r}) = C_0 e^{i\boldsymbol{k_0}\cdot\boldsymbol{r}} \tag{2.2.1}$$

the integral definition of the Bessel functions shown in Appendix A allow us to express this field as

$$P^0(\boldsymbol{r}) = C_0 e^{i\boldsymbol{k_0}\cdot\boldsymbol{r}} = C_0 \sum_q i^q e^{-iq\theta_0} J_q(kr) e^{iq\theta} \tag{2.2.2}$$

The coefficients A_q^0 in (2.1.1) are quickly obtained,

$$A_q^0 = C_0 i^q e^{-iq\theta_0} \tag{2.2.3}$$

Now let us assume that the same field has to be given in another reference frame $\boldsymbol{r'}$ such that, as shown in figure 2.2.2

$$\boldsymbol{r'} = \boldsymbol{r} - \boldsymbol{R'} \tag{2.2.4}$$

where $\boldsymbol{R'}$ is a vector which goes from the origin in the frame $\boldsymbol{r}$ to that of the frame $\boldsymbol{r'}$. The expression needed could be obtained by Graf's addition theorem (see Appendix A). For the case of plane waves a more simple approach can be used,

$$P^0(\boldsymbol{r}) = C_0 e^{i\boldsymbol{k_0}\cdot\boldsymbol{r}} = C_0 e^{i\boldsymbol{k_0}\cdot\boldsymbol{R'}} e^{i\boldsymbol{k_0}\cdot\boldsymbol{r'}} = C_0 e^{i\boldsymbol{k_0}\cdot\boldsymbol{R'}} \sum_q i^q e^{-iq\theta_0} J_q(kr') e^{iq\theta'} \tag{2.2.5}$$

Therefore

$$A'^0_q = C_0 e^{i\boldsymbol{k_0}\cdot\boldsymbol{R'}} i^q e^{-iq\theta_0} = C_0 e^{i\boldsymbol{k_0}\cdot\boldsymbol{R'}} A^0_q \tag{2.2.6}$$

When working in multiple scattering theory this operationmoves the origin of coordinates to the center of some cylinder. In this situation the vector $\boldsymbol{R'}$ is the position vector of the cylinder.

Any incident field can be expanded in a sum (discrete or continuous) of plane waves, the resulting field being the sum of the response to all these plane waves. In general, the incident field will be

$$P^0(\boldsymbol{r}) = \sum_{\theta_0} C_{\theta_0} e^{i\boldsymbol{k_0}\cdot\boldsymbol{r}} \tag{2.2.7}$$

2.2.2 The punctual source

The punctual source of order s is defined by a Hankel function of the same order. For a source located in $\boldsymbol{R_s}$

$$P^0(\boldsymbol{r}) = C_s H_s(kr_s) e^{is\theta_s} \tag{2.2.8}$$

where $\boldsymbol{r_s} = \boldsymbol{r} - \boldsymbol{R_s}$ and C_s is a complex constant (see figure 2.1).

This field can be expressed in the frame $\boldsymbol{r'}$ of the previous section by means of the Graf's addition theorem (see Appendix A),

$$P^0(\boldsymbol{r}) = C_s \sum_q H_{s-q}(kR'_s) e^{i(s-q)\Phi'_s} J_q(kr') e^{iq\theta'} \tag{2.2.9}$$

where the vector $\boldsymbol{R'_s} = (R'_s, \Phi'_s)$ is the position vector of the source in the $'$ frame, and is given by

$$\boldsymbol{R'_s} = \boldsymbol{R_s} - \boldsymbol{R'} \tag{2.2.10}$$

When working with multiple scattering the $'$ is some cylinder, so that $\boldsymbol{R'}$ is the position vector of this cylinder.

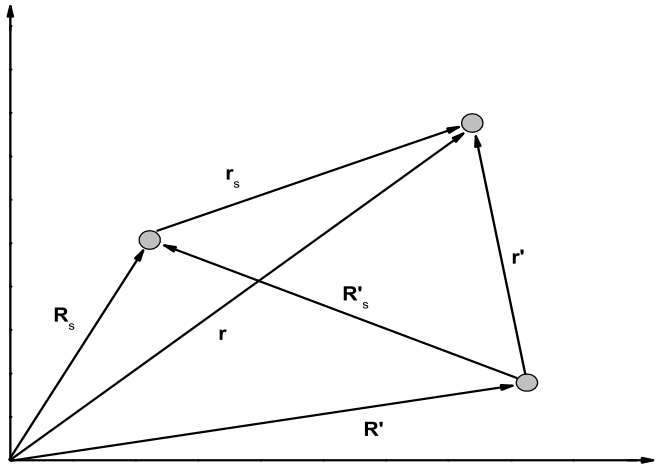

Figure 2.1: Coordinate definitions for the incident fields.

If a more general source is needed, it can be modeled with a linear combination of all the s-sources

$$P^0(\boldsymbol{r}) = \sum_s C_s H_s(kr_s) e^{is\theta_s}, \tag{2.2.11}$$

and the response of the system will be the addition of the responses to all the individual sources.

2.3 T Matrix of a fluid cylinder

The concept of fluid-like cylinder seems of non physical sense, due to the fact that is difficult to believe that a fluid could be confined in a circular shaped region and surrounded by another fluid. But it will be shown later that this fluid-like cylinder can be made possible in several ways.So it is important to begin by analyzing this type of cylinders. The T matrix of this system is very easy to obtain, and two important cases are derived from it: the rigid cylinder and the void.

Let us consider a fluid cylinder of radius R_a and acoustic parameters v_a and ρ_a. Let us also assume that some external field, defined by the coefficients A_q^0, impinges the cylinder. In the region outside the cylinder, as shown

previously, the total acoustic field is

$$P^+(\boldsymbol{r}) = \sum_q A_q^0 J_q(kr)e^{iq\theta} + \sum_q A_q H_q(kr)e^{iq\theta} \tag{2.3.1}$$

Inside the cylinder there are no sources, and the total field can be expressed in terms of regular Bessel functions with associated wavenumber k_a

$$P^-(\boldsymbol{r}) = \sum_q B_q^{\text{in}} J_q(k_a r)e^{iq\theta} \tag{2.3.2}$$

Now the boundary conditions should be applied at the circular surface. These boundary conditions are (see section 1.4):

$$P^+(\boldsymbol{R_a}) = P^+(\boldsymbol{R_b}) \tag{2.3.3}$$

$$\frac{1}{\rho_b}\frac{\partial P^+(\boldsymbol{r})}{\partial r}\bigg|_{r=R_a} = \frac{1}{\rho_a}\frac{\partial P^+(\boldsymbol{r})}{\partial r}\bigg|_{r=R_a} \tag{2.3.4}$$

These equations are equivalent to

$$\sum_q A_q^0 J_q(kR_a)e^{iq\theta} + \sum_q A_q H_q(kR_a)e^{iq\theta} = \sum_q B_q^{\text{in}} J_q(k_a R_a)e^{iq\theta}, \tag{2.3.5}$$

$$\frac{k}{\rho_b}\sum_q A_q^0 J_q'(kR_a)e^{iq\theta} + \frac{k}{\rho_b}\sum_q A_q H_q'(kR_a)e^{iq\theta} = \frac{k_a}{\rho_a}\sum_q B_q^{\text{in}} J_q'(k_a R_a)e^{iq\theta}, \tag{2.3.6}$$

where the ' implies derivatives respect to the argument.

The sums in q can be eliminated multiplying the equations by $e^{is\theta}$ and integrating from 0 to 2π.In this case only those terms such that $s = q$ are different than zero and the final form of the equations are

$$A_q^0 J_q(kR_a)e^{iq\theta} + A_q H_q(kR_a)e^{iq\theta} = B_q^{\text{in}} J_q(k_a R_a)e^{iq\theta} \tag{2.3.7a}$$

$$\frac{k}{\rho_b}A_q^0 J_q'(kR_a)e^{iq\theta} + \frac{k}{\rho_b}A_q H_q'(kR_a)e^{iq\theta} = \frac{k_a}{\rho_a}B_q^{\text{in}} J_q'(k_a R_a)e^{iq\theta} \tag{2.3.7b}$$

Now it is easy to obtain the relation between the coefficients A_q and A_q^0, which defines the T matrix. Note that in the obtained relation the coefficient

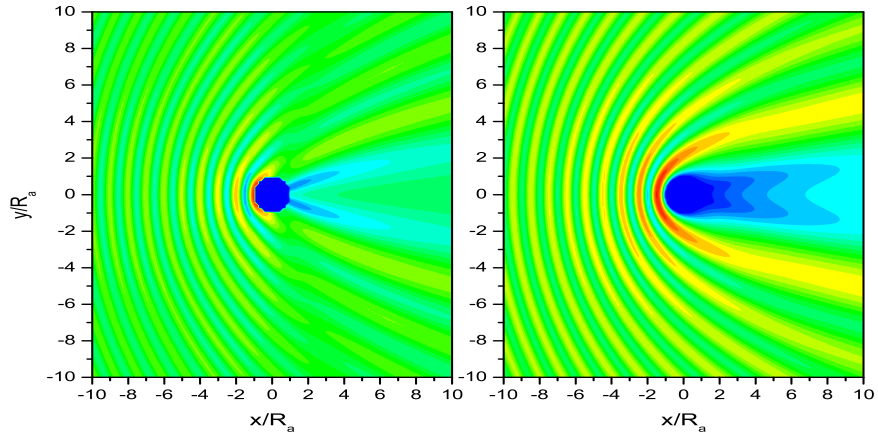

Figure 2.2: Comparison between the scattered field of a rigid cylinder (left panel) and of a void (right panel), for $kR_a = \pi(\lambda = 2R_a)$. Both the x axis and the y axis extends from $-10R_a$ to $10R_a$.

A_q only depends on the coefficient A_q^0; i.e., the T matrix is diagonal, $T_{sq} = T_q\delta_{sq}$, with T_q given by

$$T_q = -\frac{\rho_q J_q'(kR_a) - J_q(kR_a)}{\rho_q H_q'(kR_a) - H_q(kR_a)}, \tag{2.3.8}$$

where

$$\rho_q = \frac{\rho_a v_a}{\rho_b v_b}\frac{J_q(k_a R_a)}{J_q'(k_a R_a)} \tag{2.3.9}$$

The T matrix of two special cases can now be derived. The first one is the rigid cylinder, where the density of the cylinder ρ_a, in relation to the background ρ_b, approaches to infinity. In this situation also the quantity ρ_q approaches to infinity, so that the T matrix for the rigid cylinder is

$$T_q = -\frac{J_q'(kR_a)}{H_q'(kR_a)} \tag{2.3.10}$$

The second case is the void cylinder, which corresponds to the opposite situation: now the density of the cylinder, in relation to the background,

approaches to zero, then the T matrix for the void is

$$T_q = -\frac{J_q(kR_a)}{H_q(kR_a)} \tag{2.3.11}$$

Mathematically these two special cases seems very similar, but it can be seen in figure 2.2 how the scattering by a void is stronger than that of the rigid cylinder.

The T matrix allows to obtain the field outside the cylinder. When the field inside the cylinder is needed, it can be computed with the help of equation (2.3.7a), which solving for B_q^{in} gives

$$B_q^{\text{in}} = \frac{J_q(kR_a) + T_q H_q(kR_a)}{J_q(k_a R_a)} A_q^0 \tag{2.3.12}$$

for both the rigid and the void cylinders there is no field inside them.

2.4 T Matrix of an elastic cylinder

This section deals with a more realistic approach to the scattering by a solid cylinder. Now the solid cylinder is made of some elastic material, characterized by a given density ρ_a and lamé constans λ_a and μ_a, all of them defining the longitudinal and transversal speeds of sound

$$c_\ell = \sqrt{\frac{\lambda_a + 2\mu_a}{\rho_a}} \tag{2.4.1}$$

$$c_t = \sqrt{\frac{\mu_a}{\rho_a}} \tag{2.4.2}$$

In section 1.3 was shown that in a 2D elastic medium the displacement vector $\boldsymbol{u}$ can be expressed in polar coordinates as

$$u_r = -\frac{\partial \psi}{\partial r} + \frac{1}{r}\frac{\partial A_z}{\partial \theta} \tag{2.4.3}$$

$$u_\theta = -\frac{1}{r}\frac{\partial \psi}{\partial \theta} - \frac{\partial A_z}{\partial r} \tag{2.4.4}$$

Inside the elastic cylinder, with no sources, the potentials ψ and A_z are expressed as linear combinations of Bessel functions,

$$\psi = \sum_q B_q^{(\ell)} J_q(k_\ell r) e^{iq\theta} \tag{2.4.5}$$

$$A_z = \sum_q B_q^{(t)} J_q(k_t r) e^{iq\theta}, \tag{2.4.6}$$

with $k_\ell = k/c_\ell$ and $k_t = k/c_t$.

The field outside the cylinder will be the same that in the previous section, that is

$$P(\boldsymbol{r}) = \sum_q A_q^0 J_q(kr) e^{iq\theta} + \sum_q A_q H_q(kr) e^{iq\theta} \tag{2.4.7}$$

As explained in section 1.4 the coupling between the elastic field and the acoustic field occurs through the boundary conditions at the surface of the cylinder, which are

$$\sigma_{r\theta} = 0 \tag{2.4.8}$$

$$\sigma_{rr} = -P \tag{2.4.9}$$

$$u_r^- = u_r^+ \tag{2.4.10}$$

the first of the equations is

$$\frac{1}{r}\frac{\partial u_r}{\partial \theta} + \frac{\partial u_\theta}{\partial r} - \frac{1}{r} u_\theta = 0 \tag{2.4.11}$$

inserting in the above equation the expression for the vector displacement and the expansion of the potentials ψ and A_z the following relation between the coefficients $B_q^{(\ell,t)}$ is obtained

$$B_q^{(t)} = F_q B_q^{(\ell)} \tag{2.4.12}$$

with

$$F_q = \frac{2iq}{k_t^2 R_a^2}\left[\frac{J_q(k_\ell R_a) - k_\ell R_a J_q'(k_\ell R_a)}{J_q(k_t R_a) + 2J_q''(k_t R_a)}\right] \tag{2.4.13}$$

The second of the equations is

$$\frac{\lambda_a}{r} u_r + (\lambda_a + 2\mu_a)\frac{\partial u_r}{\partial_r} + \frac{\lambda_a}{r}\frac{\partial u_\theta}{\partial \theta} = -P \tag{2.4.14}$$

again, substituting the potentials and their expansions the following is obtained

$$\begin{aligned} -\frac{2iq\mu_a}{R_a^2}\left[J_q(k_t R_a) - k_t R_a J_q'(k_t R_a)\right] B_q^{(t)} + \\ k_\ell^2\left[\lambda_a J_q(k_\ell R_a) - 2\mu_a J_q''(k_\ell R_a)\right] B_q^{(\ell)} = \\ - A_q^0 J_q(kR_a) - A_q H_q(kR_a) \end{aligned} \tag{2.4.15}$$

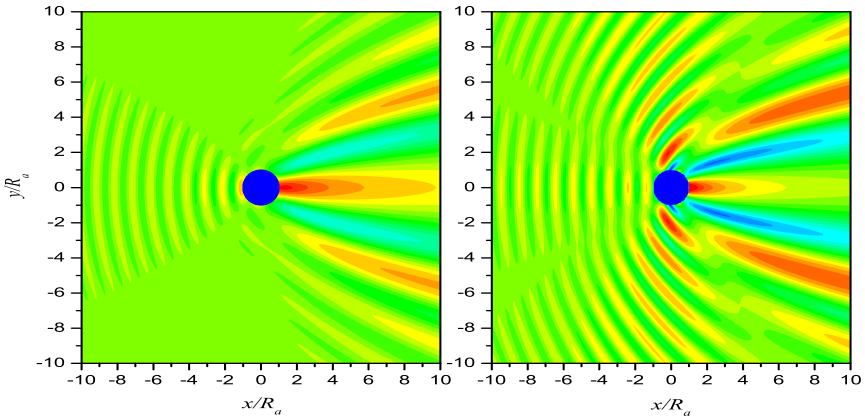

Figure 2.3: Comparison between the scattered fields for the case of a fluid cylinder (left panel) and an elastic cylinder (right panel). For $kR_a = \pi$ ($\lambda = 2R_a$). The density of the cylinders is $\rho_a = 2\rho_b$ and the longitudinal speed of sound is $c_\ell = 0.8c_b$. For the elastic cylinder the transversal speed of sound is $c_t = 0.5c_\ell$. The field inside the cylinders is not plotted for clarity.

which can be expressed as

$$G_q B_q^{(\ell)} = A_q^0 J_q(kR_a) + A_q H_q(kR_a) \tag{2.4.16}$$

where

$$G_q = \frac{2iq\mu_a F_q}{R_a^2}\left[J_q(k_t R_a) - k_t R_a J_q'(k_t R_a)\right] - k_\ell^2\left[\lambda_a J_q(k_\ell R_a) - 2\mu_a J_q''(k_\ell R_a)\right] \tag{2.4.17}$$

Finally, the last boundary condition is

$$-\frac{\partial\psi}{\partial r} + \frac{1}{r}\frac{\partial A_z}{\partial\theta} = \frac{1}{\rho_b\omega^2}\frac{\partial P}{\partial r} \tag{2.4.18}$$

then

$$-k_\ell B_q^{(\ell)} J_q'(k_\ell R_a) + \frac{iq}{R_a} B_q^{(t)} J_q(k_t R_a) = \frac{1}{\rho_b k c_b^2}\left[A_q^0 J_q'(kR_a) + A_q H_q'(kR_a)\right] \tag{2.4.19}$$

This expression can be cast in

$$I_q B_q^{(\ell)} = A_q^0 J_q'(kR_a) + A_q H_q'(kR_a) \tag{2.4.20}$$

with

$$I_q = \rho_b k c_b^2 \left[-k_\ell J_q'(k_\ell R_a) + \frac{iq}{R_a} F_q J_q(k_t R_a) \right] \tag{2.4.21}$$

Then, equations (2.4.16) and (2.4.20) can be solved to obtain the relation between the coefficients A_q^0 and A_q, relation which defines the T matrix, arriving to an expression identical to that of the fluid-like cylinder

$$T_q = -\frac{\rho_q J_q'(kR_a) - J_q(kR_a)}{\rho_q H_q'(kR_a) - H_q(kR_a)} \tag{2.4.22}$$

but now the factor ρ_q has a more complex form

$$\rho_q = \frac{G_q}{I_q} \tag{2.4.23}$$

If the field inside the cylinder is needed, from equation 2.4.16 the coefficient $B_q^{(l)}$ is

$$B_q^{(\ell)} = \frac{J_q(kR_a) + T_q H_q(kR_a)}{G_q} A_q^0 \tag{2.4.24}$$

The procedure to obtain the T matrix is so lug that it is worth to explain a brief recipe to obtain it. The following steps have to be followed

- Compute the quantity F_q with (2.4.13)
- Compute the quantity G_q with (2.4.17)
- Compute the quantity I_q with (2.4.21)
- Compute the quantity ρ_q with (2.4.23)
- Compute the quantity T_q with (2.4.22)
- The coefficients A_q are just $A_q = T_q A_q^0$

If the field inside the cylinder is needed

- The coefficients $B_q^{(\ell)}$ can be computed with (2.4.24)
- The coefficients $B_q^{(\ell)}$ are $B_q^{(t)} = F_q B_q^{(\ell)}$

In figure 2.3 it is shown the acoustic field scattered by a fluid cylinder and by an elastic cylinder of similar physical properties.

2.5 T Matrix of a fluid scatter with arbitrary cross section

When the cylinder has a geometry other than the circular cylinder a more complex approach must be used. In this work only circular cylinders has been considered, but the result for a fluid cylinder with arbitrary cross section will be showed for possible reference.

Defining the matrix elements H_{sq} and J_{sq}

$$\Upsilon_{sq} = \frac{1}{4}\oint d\sigma \boldsymbol{n} \cdot \left[\frac{\rho_a}{\rho_b} J_s(k_a r_\sigma) e^{is\theta_\sigma} \nabla \Upsilon_q(k_a r_\sigma) e^{-iq\theta_\sigma} - \right.$$
$$\left. \Upsilon_q(k r_\sigma) e^{iq\theta_\sigma} \nabla J_s(k_a r_\sigma) e^{is\theta_\sigma}\right] \quad (2.5.1)$$

where $\Upsilon = H(J)$. The T matrix is defined by the equation

$$\sum_r H_{rq} T_{rs} = -J_{qs} \quad (2.5.2)$$

and therefore

$$T = -H^{'-1} J \quad (2.5.3)$$

2.6 Far field and form factor

Two dimensional pressure maps are very visual and allows to understand some aspects of the sound scattering by obstacles. How ever, it is difficult to compare two different pressure maps. One dimensional plots are more suitable to make comparisons.

A very useful quantity to understand the scattering properties of obstacles is the form factor, derived from the far field distribution. This far field is an asymptotic expression of the scattered field when $r \to \infty$. Employing the asymptotic form of Hankel functions for large arguments (equation A.1.14)

$$P^{sc}(r,\theta) = \sum_q A_q H_q(kr) e^{iq\theta} \approx \sqrt{\frac{2}{\pi kr}} e^{-i\pi/4} e^{ikr} \sum_q (-i)^q A_q e^{iq\theta} \quad (2.6.1)$$

the scattered far field is defined as

$$\sigma_{sc}(k,\theta) \equiv \lim_{r\to\infty} \left|\sqrt{r} P^{sc}(r,\theta)\right| = \left|\sqrt{\frac{2}{\pi k}} \sum_q (-i)^q A_q e^{iq\theta}\right| \quad (2.6.2)$$

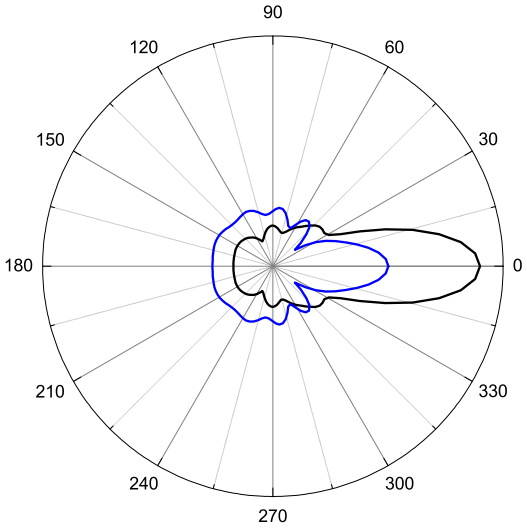

Figure 2.4: Scattered far field for a rigid and a fluid cylinder. The wavelength is equal to the radius of both cylinders, $\lambda = R_a$. For the fluid cylinder, the density is $\rho_a = 2\rho_b$ and the speed of sound is $c_a = 0.8c_b$.

if the quantity is computed for $\theta = 0$ is called the "forward scattered field" and is denoted by σ_{fwd}, and if the quantity is computed for $\theta = \pi$ is called the "back scattered field", denoted by σ_{back}.

In figure 2.4 the far field has been plotted for the case of the rigid and the fluid cylinder. Obviously the scattered fields are higher in the forward direction, which is the direction of the incident field.

In figure 2.5 the back scattered field has been plotted as a function of the frequency for the different cylinders explained in the last section. It is clear that the elastic one has the more complex spectrum. It happens due to the fact that the elastic cylinder has a more complex structure, with both longitudinal and transversal waves propagating, thus there are more resonances and more complex effects.

The angular integral of the scattered far field is called the form factor

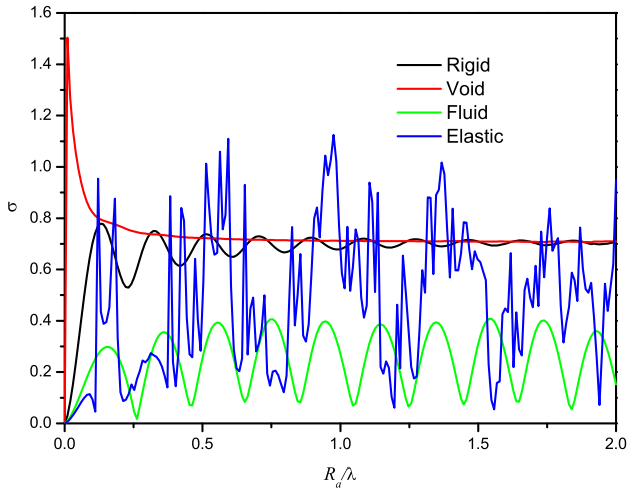

Figure 2.5: Back Scattering field for the case of the rigid, void, fluid and elastic cylinder. The fluid and elastic cylinder's properties are the same as in figure 2.3.

$F(k)$

$$F(k) \equiv \int_0^{2\pi} \sigma_{sc}^2(k,\theta)d\theta = \int_0^{2\pi} \left| \sqrt{\frac{2}{\pi k}} \sum_q (-i)^q A_q e^{iq\theta} \right|^2 d\theta = \frac{4}{k} \sum_q |A_q|^2 \tag{2.6.3}$$

2.7 Comments on convergence

The scattered pressure is obtained as an infinite sum of Hankel functions:

$$P^{sc}(r,\theta) = \sum_{q=-\infty}^{\infty} A_q H_q(kr) e^{iq\theta} \tag{2.7.1}$$

Obviously this sum has to be computed to a maximum value $q = Q_{max}$, large enough to ensure that the value computed has some desired error. However, convergence in these series is so good that the desired error can be the double precision of a desktop computer. It means that the procedure is

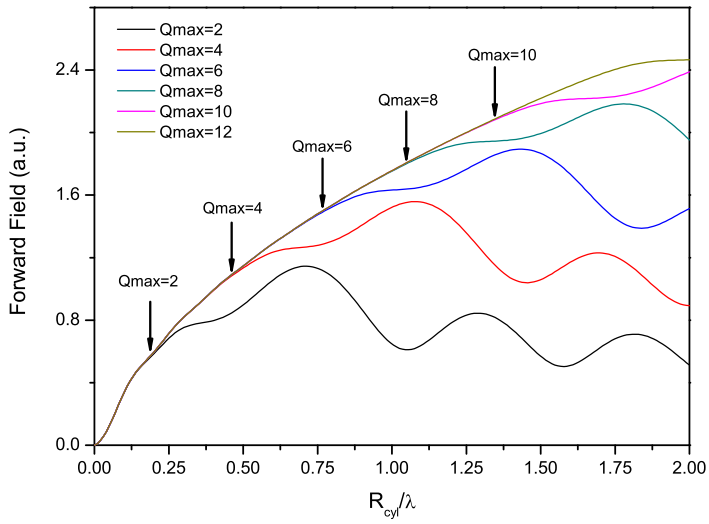

Figure 2.6: Convergence analysis. The improvement of the result is evident when increasing the number of Bessel functions Q_{max}. In the present work the wavelength is normally larger than the cylinder radius, $R_{cyl}/\lambda < 1$, therefore $Q_{max} = 4$ is a good choice.

to increase the number of Hankel functions till the computer cannot compute different values.

A good procedure should be to choose some Q_{max} and then check the result. Following this value has to be increased by one $Q_{max} = Q_{max} + 1$ and compare the result with the previous one. This procedure has to be done till there is no difference between the previous one (or the difference be equal to some defined errror).

In figure 2.6 has been plot the forward scattered field by one rigid cylinder as a function of the normalized frequency. The plot has been computed for several Q_{max}. It is evident that the number of Hankel functions depends on the frequency at which the field is computed, being larger as the frequency is increased.

In this work cylinders are placed in regular lattice of lattice constant a. It means that the maximum value of the radius of the cylinders will be $R_a \approx a/2$, which is the limit for the close packing condition. The maximum

frequency employed here use to be under the diffraction limit, that is, when the wavelength is similar to the lattice constant $\lambda \approx a$, though sometimes this limit has been exceeded. But it can be say that, in general, the maximum ratio R_a/λ is about 1/2.

In figure 2.6 it is shown that, for this limiting case, only 4 Hankel functions should be needed. But it is not necessary to use so much functions for low frequency calculations, as shown as well in the same figure. To choose the correct number of functions, in this work the following rule has been used

$$Q_{max} = Q_0 + kR_a \tag{2.7.2}$$

where Q_0 is equal to 1, 2 or 3.

As will be seen later, when more than one cylinder is implied in the problem there appear some multiple scattering terms. These terms makes that the number of functions needed be increased. So that, if for a single cylinder the problem converges for say $Q_{max} = 2$, if two or even more cylinders are implied it has not to be necessary true, it depends on how close each other are the cylinders. This is the reason why the value Q_0 has to be analyzed for different situations. Also, if more than one cylinder is implied, the rule used can be

$$Q_{max} = Q_0 + \frac{k}{N}\sum_{i=1}^{N} R_i \tag{2.7.3}$$

being N the number of cylinders. For the frequencies employed in this work it has been found that $Q_0 = 3$ ensures convergence in almost all the ranges.

A convergence analysis is always recommendable. This analysis is easy to do in these problems, due to the fact that the convergence is managed by only one parameter. For few cylinders few Hankel functions does not affect the time of CPU to compute the field, but when there are many cylinders the size of the matrices involved is highly increased by only few functions, so it is important to ensure that only the necessary functions are used.

Chapter 3

Multiple Scattering of waves

The multiple scattering of waves is here fully analyzed. Firstly, scatterers arbitrarily located are considered. Afterwords, scatterers will be ordered in infinite rows and, finally, the case of scatterers ordered in a periodic infinite system is studied. These three forms of ordering sets of scatters allows to understand different aspects of wave propagation in heterogeneous media. It is shown that the three methods are complementary each other.

3.1 Arbitrarily located scatterers

Consider a cluster of N parallel cylinders with arbitrary transversely section located at $\boldsymbol{R}_\alpha$, with $\alpha = 1, 2, ..., N$. If an external field $P^0(r, \theta)$ impinges the cluster, the total scattered field will be given by the sum of the scattered field by each individual cylinder, that is

$$P^{SC}(r, \theta) = \sum_{\alpha} \sum_{q=-\infty}^{\infty} (A_\alpha)_q H_q(kr_\alpha) e^{iq\theta_\alpha} \tag{3.1.1}$$

where $H_q(\cdot)$ is the q-Th order Hanker function of first kind and $(r_\alpha, \theta_\alpha)$ are the polar coordinates with the origin translated to the center of the α-cylinder, i.e, $\boldsymbol{r}_\alpha = \boldsymbol{r} - \boldsymbol{R}_\alpha$, as shown in figure 3.1. Here, $k = \omega/c_b$ and $(A_\alpha)_q$ are the coefficients to be determined.

The total field incident on the α-cylinder can be expressed as a linear combination of Bessel functions

$$P^0_\alpha(r_\alpha, \theta_\alpha) = \sum_{s} (B_\alpha)_s J_s(kr_\alpha) e^{is\theta_\alpha} \tag{3.1.2}$$

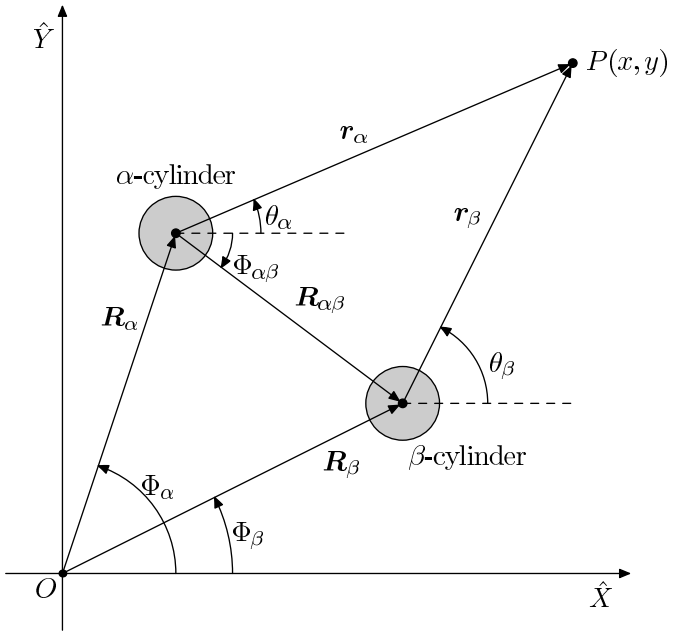

Figure 3.1: Definition of variables employed in the multiple scattering theory

these coefficients are related with the $(A_\alpha)_q$ by means of the T matrix

$$(A_\alpha)_q = \sum_s (T_\alpha)_{qs}(B_\alpha)_s \tag{3.1.3}$$

being (T_α) the T matrix of the α-cylinder.

The total field (3.1.2) incident the α-cylinder is the sum of the external field $P^0(r,\theta)$ and the field scattered by all the cylinders except α. The external field can be expressed in the α frame by using the method explained in the previous chapter. The scattered field can also be expressed in the α reference frame by means of the Graft's addition theorem explained in Appendix A. It is obtained that

$$P^0_\alpha(r_\alpha,\theta_\alpha) = \sum_q (A^0_\alpha)_q J_q(kr_\alpha)e^{iq\theta_\alpha} + \sum_{\beta\neq\alpha}(A_\beta)_s H_{q-s}(kr_{\alpha\beta})e^{i(s-q)\theta_{\alpha\beta}} J_q(kr_\alpha)e^{iq\theta_\alpha}, \tag{3.1.4}$$

where the coefficients $(A^0_\alpha)_q$ are those of the external field in the α frame of reference. Details of the variables employed are given in figure 3.1. From the

equation above and (3.1.2), the relation between $(B_\alpha)_q$ and $(A_\beta)_s$ coefficients is

$$(B_\alpha)_q = (A^0_\alpha)_q + \sum_{\beta\neq\alpha}(A_\beta)_s H_{q-s}(kr_{\alpha\beta})e^{i(s-q)\theta_{\alpha\beta}} \tag{3.1.5}$$

finally, multiplying this equation by $(T_\alpha)_{qr}$ and summing for all q we get

$$(A_\alpha)_r - \sum_s\sum_\beta(G_{\alpha\beta})_{rs}(A_\beta)_s = \sum_q(T_\alpha)_{qr}(A^0_\alpha)_q \tag{3.1.6}$$

where

$$(G_{\alpha\beta})_{rs} = \sum_q(1-\delta_{\alpha\beta})(T_\alpha)_{qr}H_{q-s}(kr_{\alpha\beta})e^{i(s-q)\theta_{\alpha\beta}} \tag{3.1.7}$$

The equation above has been derived for a cylinder of arbitrary section with some non-diagonal T matrix. However, in the present work, the multiple scattering theory has been mainly applied to circular cylinders, where the T matrix is diagonal, $(T_\alpha)_{qr} = (T_\alpha)_q\delta_{qr}$. In this situation the above equations are

$$(A_\alpha)_q - \sum_s\sum_\beta(G_{\alpha\beta})_{qs}(A_\beta)_s = (T_\alpha)_q(A^0_\alpha)_q \tag{3.1.8}$$

$$(G_{\alpha\beta})_{qs} = (1-\delta_{\alpha\beta})(T_\alpha)_q H_{q-s}(kr_{\alpha\beta})e^{i(s-q)\theta_{\alpha\beta}} \tag{3.1.9}$$

Returning to the general expression 3.1.6, in principle the multi-polar expansions are infinite, but the angular momentum index is truncated to some maximum value $s_{\max}$ such that $|s| <= s_{\max}$. In this case, the set of equations (3.1.6) defines a system of $N(2s_{\max}+1)$ linear equations. The inversion of the M matrix defined by

$$(M_{\alpha\beta})_{rs} = \delta_{rs}\delta_{\alpha\beta} - (G_{\alpha\beta})_{rs} \tag{3.1.10}$$

gives the solution of the problem

$$(A_\alpha)_q = \sum_\beta\sum_r\sum_s(M^{-1}_{\alpha\beta})_{qr}(T_\alpha)_{rs}(A^0_\alpha)_s \tag{3.1.11}$$

The solution is obtained in terms of the position and properties of each cylinder and of the external field.

Also note that, for the case of a plane wave of amplitude C_0 and propagation angle θ_0, the coefficients $(A^0_\alpha)_q$ are

$$(A^0_\alpha)_q = C_0 e^{i\boldsymbol{k}_0\cdot\boldsymbol{R_\alpha}} i^q e^{-iq\theta_0} \tag{3.1.12}$$

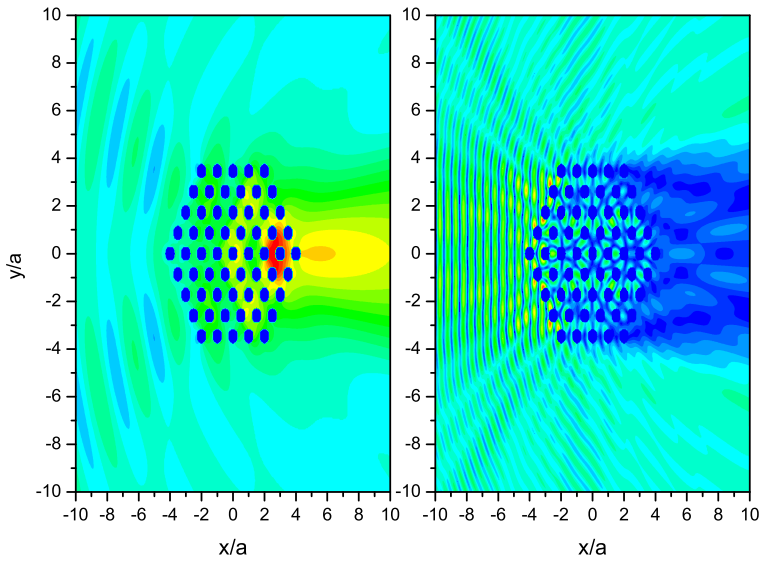

Figure 3.2: Scattering of an hexagonal cluster of rigid cylinders embedded in an hexagonal lattice of constant a. Two wavelengths are used in this simulation: $\lambda = 4a$ in the left panel and $\lambda = a$ in the right one. It is clear how the behavior is different in both situations. When $\lambda = 4a$ the cluster of cylinders behaves like a fluid cylinder, as can be seen by the focusing effect. For the case $\lambda = a$ some diffracted waves are excited, as will be explained in the next section.

and for the punctual source of order s and amplitude C_s

$$(A_\alpha^0)_q = C_s H_{s-q}(kr'_s)e^{i(s-q)\Phi'_s} \tag{3.1.13}$$

Finally, the total pressure at any point of the plane is the addition of the incident field and the total scattered field, that is

$$P(r,\theta) = P^0(r,\theta) + \sum_\alpha \sum_{q=-\infty}^{\infty} (A_\alpha)_q H_q(kr_\alpha)e^{iq\theta_\alpha} \tag{3.1.14}$$

In figure 3.2 the pressure field is plotted for the case of a plane wave incident in an hexagonal cluster of cylinders, arranged also in an hexagonal lattice of constant a. For the plot of the left panel the wavelength is four times the lattice constant($\lambda = 4a$). In this case the cluster behaves like a single homogeneous medium. Is in this range of wavelengths where this work focus.

In the right panel of figure 3.2 the wavelength equals the lattice constant ($\lambda = a$) and Bragg diffraction occurs. This phenomenon will be discussed in the next section.

Like for the simple cylinder, the scattered far field is a very useful quantity to characterize a cluster of cylinders. This scattered far field is computed for long r, then

$$P^{sc}(r,\theta) = \sum_\alpha \sum_{q=-\infty}^{\infty} (A_\alpha)_q H_q(kr_\alpha)e^{iq\theta_\alpha} \approx \sqrt{\frac{2}{\pi kr}}e^{-i\pi/4}e^{ikr}\sum_\alpha \sum_{q=-\infty}^{\infty}(-i)^q(A_\alpha)_q e^{-ikr_\alpha}e^{iq\theta_\alpha} \tag{3.1.15}$$

therefore the scattered far field is

$$\sigma_{sc}(k,\theta) = \left|\sqrt{\frac{2}{\pi k}}\sum_\alpha \sum_{q=-\infty}^{\infty}(-i)^q(A_\alpha)_q e^{-ikr_\alpha}e^{iq\theta_\alpha}\right| \tag{3.1.16}$$

and the scattering form factor

$$F(k) \equiv \int_0^{2\pi} \sigma_{sc}^2(k,\theta)d\theta = \frac{4}{k}\sum_\alpha \sum_{q=-\infty}^{\infty}|(A_\alpha)_q|^2 \tag{3.1.17}$$

3.2 Periodic arrays of scatterers: Reflectance and Transmittance

In some special situations it is interesting to analyze the reflectance and transmittance through slabs of cylinders infinite in one of the spacial dimensions. An infinite slab has the geometry shown in figure 3.3. Each row of cylinders extends from $-\infty$ to ∞, and all the cylinders in the row are identical. The distance between cylinders in a row is equal to a, and this distance is the same for all the rows. As shown in figure 3.3 the position vector of a cylinder α will be

$$\boldsymbol{R}_\alpha = \boldsymbol{R}_\ell + \boldsymbol{R}^\ell_\alpha = x_\ell \hat{\boldsymbol{x}} + (y_\ell + \alpha a)\hat{\boldsymbol{y}} \tag{3.2.1}$$

where α runs from $-\infty$ to ∞. The vector $\boldsymbol{R_\ell} = (x_\ell, y_\ell)$ defines the position of the central cylinder in a line. This central cylinder defines the x position of the line and the y relative displacement of lines. The vector $\boldsymbol{R}^\ell_\alpha$ defines the position of the α cylinder relative to the central one. This vector is obviously equal to $\alpha a\hat{\boldsymbol{y}}$

The incident field is a plane wave

$$P^0(\boldsymbol{r}) = e^{i\boldsymbol{k}_0\cdot\boldsymbol{r}} \tag{3.2.2}$$

with wavevector $\boldsymbol{k}_0 = k(\cos\theta_0, \sin\theta_0)$. This field makes the problem highly symmetrical, due to the fact that now the scattering coefficients of the α cylinder in the ℓ line differs from the scattering coefficients of the central cylinder only by a phase factor. It can be seen clearly writting the equation for the scattering coefficients when the incident field is a plane wave

$$(A^\ell_\alpha)_r - \sum_s \sum_m \sum_\beta (G^{\ell m}_{\alpha\beta})_{rs}(A^m_\beta)_s = \sum_s (T_\ell)_{rs} e^{i\boldsymbol{k}_0\cdot\boldsymbol{R_\ell}} e^{i\boldsymbol{k}_0\cdot\boldsymbol{R^\ell_\alpha}} A^0_s \tag{3.2.3}$$

note that the super index ℓ has been added in order to indicate that cylinders are located along lines.

The subindex α only appears in the right hand side of the above equation through the phase factor

$$e^{i\boldsymbol{k}_0\cdot\boldsymbol{R}^\ell_\alpha} = e^{i\alpha ka\sin\theta_0} \tag{3.2.4}$$

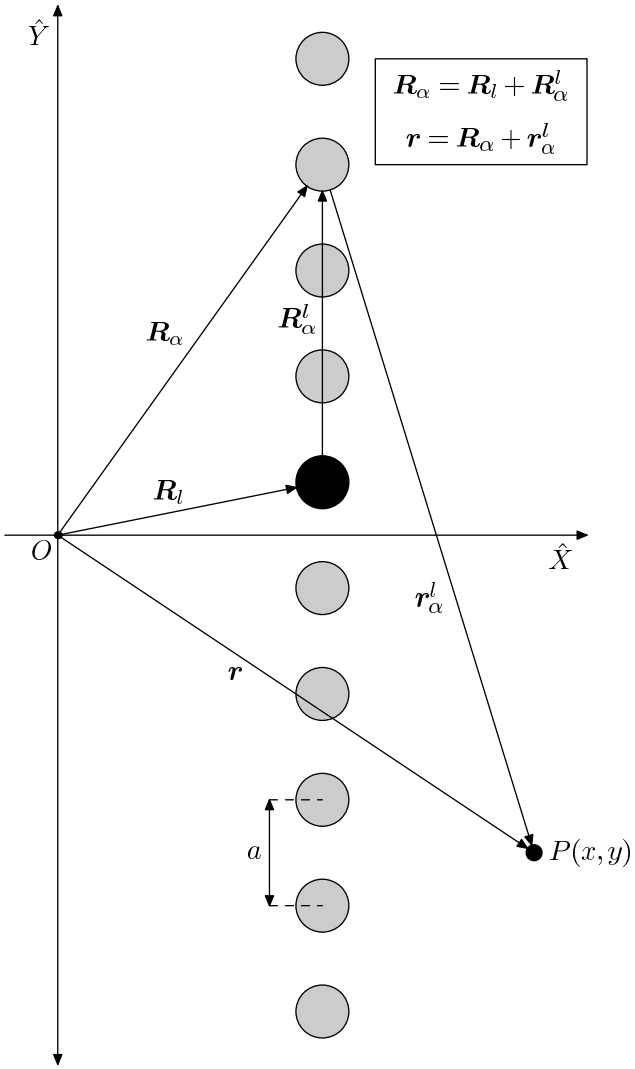

Figure 3.3: Geometry and coordinate definitions for the infinite line of cylinders. The distance between two successive cylinders is always a. Only one line is drawn for simplicity.

multiplying the equation 3.2.3 by the phase factor $e^{-i\alpha ka\sin\theta_0}$ and expressing the multiple scattering terms as

$$e^{-i\alpha ka\sin\theta_0}(G^{\ell m}_{\alpha\beta})_{rs}(A^m_\beta)_s = (G^{\ell m}_{\alpha\beta})_{rs}e^{i(\beta-\alpha)ka\sin\theta_0}e^{-i\beta ka\sin\theta_0}(A^m_\beta)_s \tag{3.2.5}$$

It is convenient define the quantities $(A_\ell)_r \equiv e^{-i\alpha ka\sin\theta_0}(A^\ell_\alpha)_r$, which are independent of α, because only terms involving relative coordinates of the cylinders appear in the equations, and the symmetry of the problem makes that this relative coordinates are the same for all the cylinders in one row. The final form for the equation (3.2.3) is

$$(A_\ell)_r - \sum_s\sum_m(\mathcal{G}_{\ell m})_{rs}(A_m)_s = \sum_s(T_\ell)_{rs}e^{i\boldsymbol{k}_0\cdot\boldsymbol{R}_\ell}i^s e^{-is\theta_0} \tag{3.2.6}$$

where the identity $A^0_s = i^s e^{-is\theta_0}$ has been used.

The lattice sums

$$(\mathcal{G}_{\ell m})_{rs} \equiv \sum_{\beta=-\infty}^{\infty}(G^{\ell m}_{0\beta})_{rs}e^{i\beta ka\sin\theta_0} \tag{3.2.7}$$

are calculated at the central cylinder. These lattice sums converges very slowly, but faster convergent expressions are given in Appendix A.

Once the coefficients $(A_\ell)_r$ are determined, the total field can be easily computed,

$$P(r,\theta) = e^{i\boldsymbol{k}_0\cdot\boldsymbol{r}} + \sum_q\sum_\alpha\sum_\ell(A^\ell_\alpha)_q H_q(kr^\ell_\alpha)e^{iq\theta^\ell_\alpha} \tag{3.2.8}$$

where the vector $\boldsymbol{r}^\ell_\alpha$ is

$$\boldsymbol{r}^\ell_\alpha = \boldsymbol{r} - \boldsymbol{R}_\alpha = \boldsymbol{r} - \boldsymbol{R}_\ell - \boldsymbol{R}^\ell_\alpha \tag{3.2.9}$$

using

$$(A^\ell_\alpha)_q H_q(kr^\ell_\alpha)e^{iq\theta^\ell_\alpha} = (A_\ell)_q H_q(kr^\ell_\alpha)e^{i\alpha ka\sin\theta_0}e^{iq\theta^\ell_\alpha} \tag{3.2.10}$$

and the result of Appendix A

$$\sum_{\alpha=-\infty}^{\infty}e^{i\alpha ka\sin\theta_0}H_q(kr^\ell_\alpha)e^{iq\theta^\ell_\alpha} = \sum_{\nu=-\infty}^{\infty}C^\pm_{\nu q}e^{i\boldsymbol{k}^\pm_\nu\cdot(\boldsymbol{r}-\boldsymbol{R}_\ell)} \tag{3.2.11}$$

the total field will be

$$P(r,\theta) = e^{i\boldsymbol{k}_0\cdot\boldsymbol{r}} + \sum_q\sum_\ell\sum_{\nu=-\infty}^{\infty}(A_\ell)_q C^\pm_{\nu q}e^{i\boldsymbol{k}^\pm_\nu\cdot(\boldsymbol{r}-\boldsymbol{R}_\ell)}, \tag{3.2.12}$$

which can be cast in a more compact form as

$$P(r,\theta) = e^{i\boldsymbol{k}_0\cdot\boldsymbol{r}} + \sum_{\nu=-\infty}^{\infty} C_\nu^{\pm} e^{i\boldsymbol{k}_\nu^{\pm}\cdot\boldsymbol{r}} \tag{3.2.13}$$

where

$$C_\nu^{\pm} = \sum_q \sum_\ell (A_\ell)_q C_{\nu q}^{\pm} e^{-i\boldsymbol{k}_\nu^{\pm}\cdot\boldsymbol{R}_\ell} \tag{3.2.14}$$

To better understand the physical meaning of the result above, it is worth to calculate the energy flux through the vertical segment $(y, y+a)$. This energy flux is the flux of the intensity vector

$$\vec{I} = \frac{1}{2\omega\rho_b}\Re[iP\nabla P^*] \tag{3.2.15}$$

where $\Re$ denotes the real part.

It is easy to show that

$$\begin{aligned} iP\nabla P^* = \\ \boldsymbol{k}_0 + \sum_\nu C_\nu^{*\pm} e^{i\boldsymbol{k}_0\cdot\boldsymbol{r}} e^{-i\boldsymbol{k}_\nu^{\pm}\cdot\boldsymbol{r}} \boldsymbol{k}_\nu^{\pm} + \sum_\nu C_\nu^{\pm} e^{-i\boldsymbol{k}_0\cdot\boldsymbol{r}} e^{i\boldsymbol{k}_\nu^{\pm}\cdot\boldsymbol{r}} \boldsymbol{k}_0 + \end{aligned} \tag{3.2.16}$$

the energy flux is then

$$\Phi = \int_y^{y+a} I_x dy \tag{3.2.17}$$

After integration it is easy to show that

$$\begin{aligned} \Phi = \frac{1}{2\omega\rho_b} \times \\ \left[ka\cos\theta_0 + ka\Re[C_0^{\pm} \pm C_0^{*\pm}]\cos\theta_0 \pm ka|\cos\theta_\nu| \sum_{\cos\theta_\nu\in\Re} |C_\nu^{\pm}|^2 \right] \end{aligned} \tag{3.2.18}$$

Then only modes with $\cos\theta_\nu$ real contributes to the energy flow, so that evanescent modes does not carries energy. The quantity $\Phi_0 = ka\cos\theta_0/2\omega\rho_b$ defines the incident flow to the slab. By dividing the total flow by this quantity, it can be obtained that the flow at the left hand side of the slab is

$$\frac{\Phi^-}{\Phi_0} = 1 - \frac{|\cos\theta_\nu|}{\cos\theta_0} \sum_{\cos\theta_\nu\in\Re} |C_\nu^-|^2 \tag{3.2.19}$$

For the flow at the right hand side,

$$\frac{\Phi^+}{\Phi_0} = 1 + 2\Re[C_0^+] + \frac{|\cos\theta_\nu|}{\cos\theta_0} \sum_{\cos\theta_\nu \in \Re} |C_\nu^+|^2 \tag{3.2.20}$$

In the expression above is possible to identify

$$\mathcal{R} = \frac{|\cos\theta_\nu|}{\cos\theta_0} \sum_{\cos\theta_\nu \in \Re} |C_\nu^-|^2 \tag{3.2.21a}$$

$$\mathcal{T} = 1 + 2\Re[C_0^+] + \frac{|\cos\theta_\nu|}{\cos\theta_0} \sum_{\cos\theta_\nu \in \Re} |C_\nu^+|^2 \tag{3.2.21b}$$

where the quantities $\mathcal{R}$ and $\mathcal{T}$ are defined, respectively, as the reflectance and transmittance. These quantities indicate how much energy flows through the slab and how much is reflected by it.

The total field is composed by the sum of the incident plane wave and a set of both propagating plane waves($\cos\theta_\nu$ real) and evanescent modes ($\cos\theta_\nu$ complex). Only the propagating modes transport energy, then the evanescent ones are relevant only for surface effects, which is not the purpose of the present work, so that the discussion about them will be omitted.

When there are more than one propagating mode the energy is distributed between the different diffracted waves. In the last case has no sense to talk about the reflection and transmission coefficients in the usual way. When there is only one mode (there is no diffraction) it is possible to talk about the relation between the incident and the reflected or transmitted plane wave.

When only the mode corresponding to $\nu = 0$ is the only propagating mode, the reflectance is

$$\mathcal{R} = |C_0^-|^2 \tag{3.2.22}$$

and the transmittance

$$\mathcal{T} = 1 + 2\Re[C_0^+] + |C_0^+|^2 = |1 + C_0^+|^2 \tag{3.2.23}$$

Therefore, for the left hand side of the slab, the reflectance coefficient is

$$r = C_0^- \tag{3.2.24}$$

and for the right hand side of the slab the transmittance coefficient is

$$t = 1 + C_0^+ \tag{3.2.25}$$

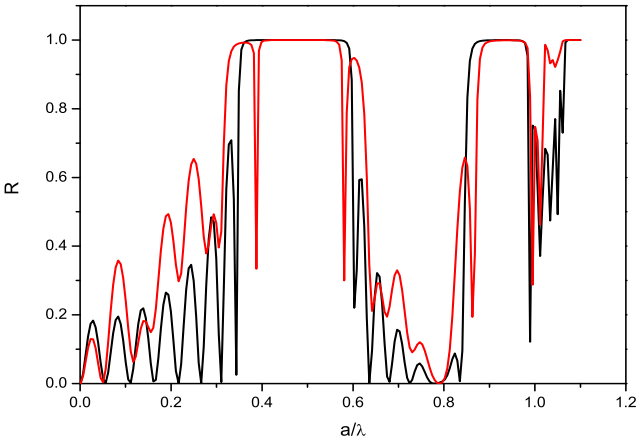

Figure 3.4: (Black line) Reflectance of an eight layers slab of rigid cylinders embedded in a square lattice of constant a. Cylinders have a radius of $R_a = 0.3a$ and the incidence is perpendicular to the ΓX direction.(Red line) The same structure but without the forth line of cylinders.

3.3 Periodic lattice: Band structure

If the cylinders are ordered in a 2D lattice, their α-positions are defined by the Bravos lattice $\boldsymbol{R} = n_1\boldsymbol{a}_1 + n_2\boldsymbol{a}_2$, where n_1 and n_2 are integers and $\boldsymbol{a}_1$ and $\boldsymbol{a}_2$ are the primitive vectors:

$$\boldsymbol{a}_1 = a_1\hat{\boldsymbol{x}} \tag{3.3.1a}$$

$$\boldsymbol{a}_2 = a_2\cos\phi\hat{\boldsymbol{x}} + a_2\sin\phi\hat{\boldsymbol{y}} \tag{3.3.1b}$$

Bloch's theorem allows to cast the total field as the product of a Bloch plane wave and a function with the periodicity of the lattice, that is

$$P(\boldsymbol{r}) = e^{i\boldsymbol{K}\cdot\boldsymbol{r}}u(\boldsymbol{r}) \tag{3.3.2}$$

This function verifies

$$P(\boldsymbol{r} + \boldsymbol{R}_\alpha) = e^{i\boldsymbol{K}\cdot\boldsymbol{R}_\alpha}P(\boldsymbol{r}), \tag{3.3.3}$$

where the vector $\boldsymbol{R}_\alpha$ is a vector of the Bravos lattice.

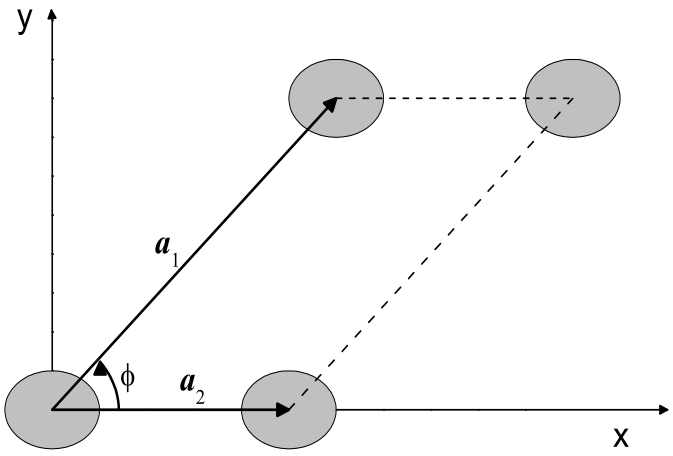

Figure 3.5: Arbitrary 2D lattice with one cylinder per unit cell. The 2D sonic crystal is built by a translation of the unit vectors $\boldsymbol{a}_1$ and $\boldsymbol{a}_2$.

The solutions of interest are the modes of the system, i.e., the solutions with no incident field. In this case the total field will be

$$P(\boldsymbol{r}) = \sum_{\alpha} P_{\alpha}^{\mathrm{SC}}(\boldsymbol{r}_{\alpha}) = \sum_{\alpha} P_{\alpha}^{\mathrm{SC}}(\boldsymbol{r} - \boldsymbol{R}_{\alpha}) \tag{3.3.4}$$

The total field in a point translated $\boldsymbol{r}+\boldsymbol{R}_{\beta}$ can be computed using Bloch's theorem

$$P(\boldsymbol{r} + \boldsymbol{R}_{\beta}) = e^{i\boldsymbol{K}\cdot\boldsymbol{R}_{\beta}} P(\boldsymbol{r}) \tag{3.3.5}$$

but it implies

$$P(\boldsymbol{r} + \boldsymbol{R}_{\beta}) = \sum_{\alpha} P_{\alpha}^{\mathrm{SC}}(\boldsymbol{r} - \boldsymbol{R}_{\alpha} + \boldsymbol{R}_{\beta}) \tag{3.3.6}$$

then it is obvious that the scattered field by the cylinder located at the origin and that of the cylinder located at the lattice point $\mathbf{R}_{\beta}$ are related by

$$P_{\beta}^{\mathrm{SC}}(\boldsymbol{r}_{\beta}) = e^{i\boldsymbol{K}\cdot\boldsymbol{R}_{\beta}} P_{0}^{\mathrm{SC}}(\boldsymbol{r}) \tag{3.3.7}$$

and this expression leads to a relation between the scattering coefficients

$$(A_q)_{\beta} = e^{i\boldsymbol{K}\cdot\boldsymbol{R}_{\beta}} A_q \tag{3.3.8}$$

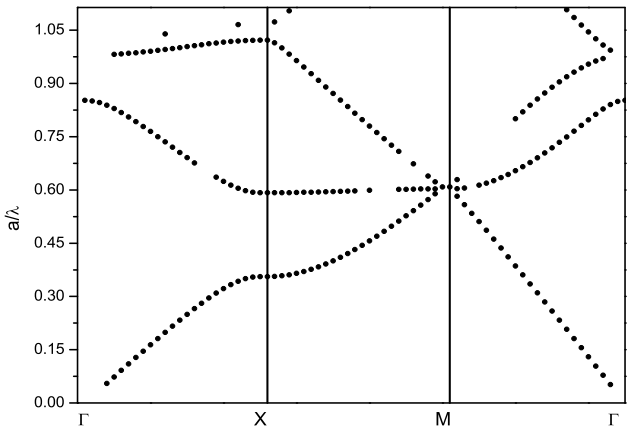

Figure 3.6: Band structure for a square lattice of rigid cylinders of radius $R_a = 0.3a$. There is a band gap in the ΓX direction, but it is not a complete band gap, therefore sound can propagate through the structure in the direction, for example, ΓM. The existence of full band gaps is a topic of intense research in acoustics.

where A_q are the scattering coefficients of the cylinder located at the origin. With the above relation and reminding that the incident field is null, equation 3.1.6 will be

$$A_r - \sum_S A_s \sum_\beta e^{i\boldsymbol{K}\cdot\boldsymbol{R}_\beta}(G_{0\beta})_{rs} = 0 \tag{3.3.9}$$

the lattice sums

$$S_{rs} = \sum_\beta e^{i\boldsymbol{K}\cdot\boldsymbol{R}_\beta}(G_{0\beta})_{rs} \tag{3.3.10}$$

are given in the appendix. These sums converges very slowly in real space but very quickly in the reciprocal space. Then the system to solve becomes

$$\boldsymbol{M}\cdot\boldsymbol{A} = 0 \tag{3.3.11}$$

where the matrix M is

$$M_{rs} = \delta_{rs} - S_{rs} \tag{3.3.12}$$

In order to obtain non trivial solutions of the above equations, the determinant of the matrix M must be equal to zero. It means that for a given

Bloch wave number $\boldsymbol{K}$, there will be some ω_n values which satisfies the condition $\det \boldsymbol{M} = 0$, that is, this condition defines a set of dispersion relations of the form $\omega_n = \omega_n(\boldsymbol{K})$. Each n defines a band, and the complete set of solutions is called the band structure. Note that the dispersion relation is periodic in the Bloch wavenumber $\boldsymbol{K}$, where the periodicity defines the first Brailling zone (BZ).

The first Brailling zone is defined by the reciprocal lattice vectors $\boldsymbol{b}_1$ and $\boldsymbol{b}_2$. These vectors have the property that, when adding some linear combination $h_1\boldsymbol{b}_1 + h_2\boldsymbol{b}_2$ of them to the wave vector $\boldsymbol{K}$, the band structure is the same. It is evident that it will happen provided that

$$(h_1\boldsymbol{b}_1 + h_2\boldsymbol{b}_2) \cdot \boldsymbol{R}_\beta = 2n\pi \tag{3.3.13}$$

The above equation is satisfied defining the vectors $\boldsymbol{b}_i$ such that

$$\boldsymbol{b}_i \cdot \boldsymbol{a}_j = 2\pi\delta_{ij} \tag{3.3.14}$$

or, expressing $\boldsymbol{b}_i$ and $\boldsymbol{a}_j$ in Cartesian coordinates

$$\sum_{l,m} b_{IL}\hat{\boldsymbol{x}}_l \cdot a_{Jim}\hat{\boldsymbol{x}}_m = \sum_{l} b_{IL}a_{Jul} = 2\pi\delta_{ij} \tag{3.3.15}$$

This last equation can be, in 2D, expressed in matrix form, being

$$\begin{pmatrix} b_{1x} & b_{1y} \\ b_{2x} & b_{2y} \end{pmatrix} \cdot \begin{pmatrix} a_{1x} & a_{2x} \\ a_{1y} & a_{2y} \end{pmatrix} = 2\pi \begin{pmatrix} 1 & 0 \\ 0 & 1 \end{pmatrix} \tag{3.3.16}$$

which allows to obtain the vectors $\boldsymbol{b}_i$ from matrix inversion

$$\begin{pmatrix} b_{1x} & b_{1y} \\ b_{2x} & b_{2y} \end{pmatrix} = \frac{2\pi}{a_{1x}a_{2y} - a_{2x}a_{2y}} \begin{pmatrix} a_{2y} & -a_{2x} \\ -a_{1y} & a_{1x} \end{pmatrix} \tag{3.3.17}$$

If the lattice vectors are defined as in equations (3.3.1) the reciprocal lattice vectors are

$$\boldsymbol{b}_1 = \frac{2\pi}{a_1}\hat{\boldsymbol{x}} - \frac{2\pi}{a_1 \tan\phi}\hat{\boldsymbol{y}} \tag{3.3.18a}$$

$$\boldsymbol{b}_2 = \frac{2\pi}{a_2 \sin\phi}\hat{\boldsymbol{y}} \tag{3.3.18b}$$

Equations (3.3.18) and (3.3.1) are the conventions used in the present work. The two isotropic lattices in 2D, the hexagonal and the square lattices, are defined by $a_1 = a_2 = a$ and $\phi = \pi/2$ or $\phi = \pi/3$, respectively.

In figure 3.6 a band structure is computed for the case of rigid cylinders embedded in a square lattice. The frequency range has been choosen to be the working frequency range in the present work:mainly under the diffraction limit ($\lambda = a$).

The main feature of this band structure is the existence of a band gap in the ΓX direction. There are no solutions for the dispersion relation $\omega = \omega(\boldsymbol{K})$ in this direction, then sound cannot propagate through it. However it can through other directions. The existence of gaps in all the directions of propagation is a topic of intense research in acoustics, but not in the present work.

In this work, we are interested in the low frequency limit. It is clear from figure 3.6 that, in this limit, the dispersion relation becomes linear. Here we say that the medium homogenizes to an effective medium. To obtain the acoustic parameters of this effective medium and its possible applications is the objective of the present work.

Chapter 4

T matrix of special scatterers

It is shown here how to compute the T matrix for non conventional scattering structures, that is, those that are not just fluid or elastic cylinders. The first case is a cluster of cylinders. The scattering properties of such system can be described by some effective T matrix, as if it were a single scatter. The second example that will be considered is the anisotropic fluid cylinder. It will be shown that, although it is a circular cylinder, its T matrix will be non-diagonal. Another interesting type of scatters are those where the acoustic properties change with the position, that is, non-homogeneous scatters. A special case of this type of cylinders will be shown. Finally, the third case corresponds to a linear chain of spheres that, under certain conditions, behaves as a 2D scatterer, whose effective T matrix is computed.

4.1 Effective T Matrix of a cluster of cylindrical scatterers

Section 3.1 showed that the total scattered field by a cluster of N scatterers is

$$P^{sc}(r,\theta) = \sum_{\alpha=1}^{N} \sum_{q=-\infty}^{\infty} (A_\alpha)_q H_q(kr_\alpha) e^{iq\theta_\alpha} \tag{4.1.1}$$

By using Graf's addition theorem the Hankel functions of this equation can be translated to the origin of coordinates, the total scattered field can be

expressed as

$$P^{sc}(r,\theta) = \sum_{p} A_p^{sc} H_p(kr) e^{ip\theta} \quad ; \quad r > R_\alpha^+ \tag{4.1.2}$$

where

$$A_p^{sc} = \sum_{\alpha=1}^{N} \sum_{q} J_{p-q}(kR_\alpha) e^{i(q-p)\Phi_\alpha} (A_\alpha)_q \tag{4.1.3}$$

and R_α^+ stands for the greater of R_α.

These equations show that the total scattered field can be expressed as the scattered field by only one cylinder (of some arbitrary shape) located at the origin. The relation between the coefficients A_s^{sc} and A_q^0 will define the effective T matrix of this hypothetical cylinder. To obtain the effective T matrix, the coefficients $(A_\alpha)_q$ given by equation (3.1.11) are inserted in (4.1.3),

$$A_p^{sc} = \sum_{\alpha,\beta=1}^{N} \sum_{q,r,s} J_{p-q}(kR_\alpha) e^{(q-p)\Phi_\alpha} (M_{\alpha\beta}^{-1})_{qr} (T_\beta)_{rs} (A_\beta^0)_s \tag{4.1.4}$$

This equation establishes a linear relation between the coefficients A_p^{sc} and $(A_\alpha^0)_s$. The relationship between $(A_\alpha^0)_q$ with that of the generic incident field A_q^0 are still needed.

In section 2.2 was derived this expression for a specific type of fields. If the incident field is a generic field of the form

$$P^0(r,\theta) = \sum_{q} A_q^0 J_q(kr) e^{iq\theta} \tag{4.1.5}$$

when translating the origin to the cylinder α the field is

$$P^0(r_\alpha,\theta_\alpha) = \sum_{q} A_q^0 \sum_{s} J_{q-s}(kR_\alpha) e^{i(q-s)\Phi_\alpha} J_s(kr_\alpha) e^{is\theta_alpha} \tag{4.1.6}$$

equation that defines the coefficients $(A_\alpha^0)_s$ as

$$(A_\alpha^0)_s = \sum_{q} J_{q-s}(kR_\alpha) e^{i(q-s)\Phi_\alpha} A_q^0 \tag{4.1.7}$$

inserting the above expression in (4.1.4), replacing the index q by t

$$A_p^{sc} = \sum_{\alpha,\beta} \sum_{q,r,s,t} J_{p-q}(kR_\alpha) e^{(q-p)\Phi_\alpha} (M_{\alpha\beta}^{-1})_{qr} (T_\beta)_{rs} J_{t-s}(kR_\beta) e^{i(t-s)\Phi_\beta} A_t^0 \tag{4.1.8}$$

Now the effective T matrix is finally obtained:

$$T_{pt}^{\text{eff}} = \sum_{\alpha,\beta} \sum_{q,r,s} J_{p-q}(kR_\alpha) e^{(q-p)\Phi_\alpha} (M_{\alpha\beta}^{-1})_{qr} (T_\beta)_{rs} J_{t-s}(kR_\beta) e^{i(t-s)\Phi_\beta} \quad (4.1.9)$$

Note taht this expression does not allow to compute the field inside the cluster. However this expression is very important since in the low frequency limit allows to calculate the effective medium properties of the cluster, as it will be shown later.

4.2 T Matrix of an anisotropic fluid like cylinder

Chapter 1 showed that in an anisotropic fluid-like material sound waves travel with an angle dependent speed of sound given by

$$c(\tau) = \sum_{i,j} c_{ij} \cos\tau_i \cos\tau_j \quad (4.2.1)$$

The tensor c_{ij} is related with the reciprocal density tensor by means of the bulk modulus of the medium as $c_{ij} = B_0 \rho_{ij}^{-1}$.

Now the T matrix of a cylinder of radius R_0 made of such anisotropic medium, embedded in an isotropic fluid with acoustic parameters equal to one, will be derived. If the absolute values of the variables are needed, the substitution $B_0 \to B_0/B_b$, $c_{ij} \to c_{ij}/c_b$ and $\rho_{ij} \to \rho_{ij}/\rho_b$ has to be done.

For $r > R_0$ the pressure field is given by the addition of incident and scattered fields, that is

$$P(r,\theta;k) = \sum_s A_s^0 J_s(kr) e^{is\theta} + \sum_s A_s H_s(kr) e^{is\theta} \quad (4.2.2)$$

For $r \leq R_0$ the proposed solution for wave propagation inside the cylinder is a linear combination of plane waves of the form

$$P(r,\theta;k) = \sum_s B_s J_s^a(kr/c,\theta) e^{is\theta} \quad (4.2.3)$$

where

$$J_s^a(kr/c,\theta) = \frac{i^{-s}}{2\pi} \int_0^{2\pi} e^{i\frac{kr}{c(\tau)}\cos(\tau-\theta)} e^{is(\tau-\theta)} d\tau \quad (4.2.4)$$

Applying the boundary conditions defined in (1.4)

$$\sum_s A_s^0 J_s(kR_0)e^{is\theta} + \sum_s A_s H_s(kR_0)e^{is\theta} = \sum_s B_s J_s^a(kR_0/v,\theta)e^{is\theta} \tag{4.2.5}$$

$$\frac{\partial}{\partial r}\left[\sum_s A_s^0 J_s(kr)e^{is\theta} + \sum_s A_s H_s(kr)e^{is\theta}\right]_{r=R_0} = \sum_s B_s v_r^s \tag{4.2.6}$$

where

$$v_r^s = \left[\rho_{rr}^{-1}\frac{\partial}{\partial r} + \frac{1}{r}\rho_{r\theta}\frac{\partial}{\partial\theta}\right]_{r=R_0} J_s^a(kr/c,\theta)e^{is\theta} \tag{4.2.7}$$

The radial functions in the right hand side of both equations are coupled with the angular variable θ, so that now is not possible just cancel the factors $e^{iq\theta}$ but is needed to multiply both equations by $\frac{1}{2\pi}e^{-iq\theta}$ and integrate from 0 to 2π, then

$$A_q^0 J_q(kR_0) + A_q H_q(kR_0) = \sum_s N_{qs} B_s \tag{4.2.8}$$

$$A_q^0 J_q'(kR_0) + A_q H_q'(kR_0) = \sum_s M_{qs} B_s \tag{4.2.9}$$

where the $'$ implies derivation respect to the argument and

$$N_{qs} = \frac{1}{2\pi}\int_0^{2\pi} J_s^a(kR_0/c,\theta)e^{i(s-q)\theta}d\theta \tag{4.2.10}$$

$$M_{qs} = \frac{1}{2k\pi}\int_0^{2\pi}\left[\rho_{rr}^{-1}\frac{\partial}{\partial r} + \frac{1}{r}\rho_{r\theta}\frac{\partial}{\partial\theta}\right]_{r=R_0}\left[J_s^a(kr/c,\theta)e^{is\theta}\right]e^{-iq\theta}d\theta \tag{4.2.11}$$

to calculate M_{qs} elements derivation has to be performed before integration. Using the relation

$$J_q(kr)H_q'(kr) - J_q'(kr)H_q(kr) = \frac{2i}{\pi kr} \tag{4.2.12}$$

toguether with (4.2.8) and (4.2.9) the following relationships are derived

$$A_q^0 = -\frac{i\pi kR_0}{2}\sum_s\left[H_q'(kR_0)N_{qs} - H_q(kR_0)M_{qs}\right]B_s \tag{4.2.13}$$

$$A_q = \frac{i\pi kR_0}{2}\sum_s\left[J_q'(kR_0)N_{qs} - J_q(kR_0)M_{qs}\right]B_s \tag{4.2.14}$$

defining the matrices

$$H_{sq} = \frac{i\pi kR_0}{2}\left[H'_q(kR_0)N_{qs} - H_q(kR_0)M_{qs}\right] \tag{4.2.15}$$

$$J_{sq} = \frac{i\pi kR_0}{2}\left[J'_q(kR_0)N_{qs} - J_q(kR_0)M_{qs}\right] \tag{4.2.16}$$

the above equations are, in matrix form,

$$A^0 = -HB \tag{4.2.17}$$

$$A = JB \tag{4.2.18}$$

$$A = -JH^{-1}A^0 \tag{4.2.19}$$

so that the T matrix of the cylinder is given by

$$T = -JH^{-1} \tag{4.2.20}$$

4.2.1 Calculus Of N_{qs} And M_{qs}

The matrix elements N_{qs} and M_{qs} have to be computed numerically. However their form in (4.2.10) and (4.2.11) is not the more suitable for a numerical computation, because it implies double integration which is not always very efficient. In this subsection it will be shown that these matrix elements can be expressed as integrations of the Bessel functions.

N_{qs}

Matrix elements N_{qs} can be expressed, using the integral form of J_s^a, as

$$N_{qs} = \frac{1}{2\pi}\int_0^{2\pi} d\theta \frac{i^{-s}}{2\pi}\int_0^{2\pi} e^{i\frac{kr}{c}\cos(\tau-\theta)}e^{is(\tau-\theta)}d\tau e^{i(s-q)\theta} \tag{4.2.21}$$

if the integration is made first with respect to θ, reordering terms it is found

$$N_{qs} = \frac{i^{q-s}}{2\pi}\int_0^{2\pi} e^{i(s-q)\tau}d\tau \frac{i^{-q}}{2\pi}\int_0^{2\pi} e^{i\frac{kr}{c}\cos(\theta-\tau)}d\theta e^{-iq(\theta-\tau)} \tag{4.2.22}$$

note that, as c is function of τ and not of θ the above equation is equivalent to

$$N_{qs} = \frac{i^{q-s}}{2\pi}\int_0^{2\pi} J_q(kr/c)e^{i(s-q)\tau}d\tau \tag{4.2.23}$$

M_{qs}

These elements are more complex to simplify because of the derivatives that have to be performed. It is convenient to split them into

$$M_{qs} = I_{qs}^{(r)} + I_{qs}^{(\theta)} \tag{4.2.24}$$

where

$$I_{qs}^{(r)} = \frac{1}{2\pi}\int_0^{2\pi}\left[\rho_{rr}^{-1}\frac{\partial}{\partial r}\right]_{r=R_0}\left[J_s^a(kr/c,\theta)e^{is\theta}\right]e^{-iq\theta}d\theta \tag{4.2.25}$$

$$I_{qs}^{(\theta)} = \frac{1}{2\pi}\int_0^{2\pi}\left[\frac{1}{r}\rho_{r\theta}\frac{\partial}{\partial \theta}\right]_{r=R_0}\left[J_s^a(kr/c,\theta)e^{is\theta}\right]e^{-iq\theta}d\theta \tag{4.2.26}$$

Applying the differential operators and using the integral definition of $J_s^a(kr/c,\theta)e^{is\theta}$, it is found that

$$I_{qs}^{(r)} = \frac{i^{-s}}{(2\pi)^2}\int_0^{2\pi}\int_0^{2\pi}\frac{ik}{c(\tau)}\rho_{rr}^{-1}\cos(\tau-\theta)e^{i\frac{kR_0}{c}\cos(\tau-\theta)}e^{is\tau}e^{-iq\theta}d\theta d\tau \tag{4.2.27}$$

$$I_{qs}^{(\theta)} = \frac{i^{-s}}{(2\pi)^2}\int_0^{2\pi}\int_0^{2\pi}\frac{ik}{c(\tau)}\rho_{r\theta}^{-1}\sin(\tau-\theta)e^{i\frac{kR_0}{c}\cos(\tau-\theta)}e^{is\tau}e^{-iq\theta}d\theta d\tau \tag{4.2.28}$$

But, it is known that

$$\begin{aligned}&\rho_{rr}^{-1}\cos(\tau-\theta)+\rho_{r\theta}^{-1}\sin(\tau-\theta) = \\ &\rho_{s+}^{-1}\cos(\tau-\theta)+\rho_{s-}^{-1}\cos(\tau+\theta)+\rho_{a-}^{-1}\sin(\tau-\theta)+\rho_{a+}^{-1}\sin(\tau+\theta)\end{aligned} \tag{4.2.29}$$

Therefore, the sum of $I_{qs}^{(r)}$ and $I_{qs}^{(\theta)}$ and then M_{qs}, can be expressed as a sum the following four integrals

$$I_{qs}^{(1)} = \frac{i^{-s}}{(2\pi)^2}\rho_{s+}^{-1}\int_0^{2\pi}\int_0^{2\pi}\frac{ik}{c}\cos(\tau-\theta)e^{i\frac{kR_0}{c}\cos(\tau-\theta)}e^{is\tau}e^{-iq\theta}d\theta d\tau \tag{4.2.30}$$

$$I_{qs}^{(2)} = \frac{i^{-s}}{(2\pi)^2}\rho_{s-}^{-1}\int_0^{2\pi}\int_0^{2\pi}\frac{ik}{c}\cos(\tau+\theta)e^{i\frac{kR_0}{c}\cos(\tau-\theta)}e^{is\tau}e^{-iq\theta}d\theta d\tau \tag{4.2.31}$$

$$I_{qs}^{(3)} = \frac{i^{-s}}{(2\pi)^2}\rho_{a-}^{-1}\int_0^{2\pi}\int_0^{2\pi}\frac{ik}{c}\sin(\tau-\theta)e^{i\frac{kR_0}{c}\cos(\tau-\theta)}e^{is\tau}e^{-iq\theta}d\theta d\tau \tag{4.2.32}$$

$$I_{qs}^{(4)} = \frac{i^{-s}}{(2\pi)^2}\rho_{a+}^{-1}\int_0^{2\pi}\int_0^{2\pi}\frac{ik}{c}\sin(\tau+\theta)e^{i\frac{kR_0}{c}\cos(\tau-\theta)}e^{is\tau}e^{-iq\theta}d\theta d\tau \tag{4.2.33}$$

defining

$$SC_p(x) = \frac{1}{2i^p}\left[e^{ix} + (-1)^p e^{-ix}\right] \quad ; p = 0, 1 \tag{4.2.34}$$

the integral

$$\int_0^{2\pi} SC_p(\tau \pm \theta) e^{\frac{ikR}{c}\cos(\tau-\theta)} e^{iq(\tau-\theta)} d\theta \tag{4.2.35}$$

can be expressed as a function of Bessel functions

$$\frac{2\pi i^{q\pm1}}{2i^p}\left[e^{i(\alpha\pm\alpha)} J_{q\pm1}(kR/c) - (-1)^p e^{-i(\alpha\pm\alpha)} J_{q\mp1}(kR/c)\right] \tag{4.2.36}$$

then the four integrals becomes

$$I_{qs}^{(1)} = \frac{i^{-(s-q)}}{2\pi}\rho_{s+}^{-1}\int_0^{2\pi}\frac{k}{c}\frac{1}{2}\left[J_{q-1}(kR_0/c) - J_{q+1}(kR_0/c)\right] e^{i(s-q)\tau} d\tau \tag{4.2.37a}$$

$$I_{qs}^{(2)} = \frac{i^{-(s-q)}}{2\pi}\rho_{s-}^{-1}\int_0^{2\pi}\frac{k}{c}\frac{1}{2}\left[e^{-2i\tau} J_{q-1}(kR/c) - e^{2i\tau} J_{q+1}(kR/c)\right] e^{i(s-q)\tau} d\tau \tag{4.2.37b}$$

$$I_{qs}^{(3)} = -\frac{i^{-(s-q)}}{2\pi}\rho_{a-}^{-1}\int_0^{2\pi}\frac{k}{c}\frac{i}{2}\left[J_{q-1}(kR_0/c) + J_{q+1}(kR_0/c)\right] e^{i(s-q)\tau} d\tau \tag{4.2.37c}$$

$$I_{qs}^{(4)} = \frac{i^{-(s-q)}}{2\pi}\rho_{a+}^{-1}\int_0^{2\pi}\frac{k}{c}\frac{i}{2}\left[e^{2i\tau} J_{q+1}(kR/c) + e^{-2i\tau} J_{q-1}(kR/c)\right] e^{i(s-q)\tau} d\tau \tag{4.2.37d}$$

By adding the four terms, we arrive to

$$M_{qs} = \frac{i^{-(s-q)}}{2\pi}\times \int_0^{2\pi}\frac{1}{c}\left[\rho_{rr}^{-1}(\tau)\frac{\partial J_q(kR_0/c)}{\partial(kR_0/c)} + i\rho_{r\tau}^{-1}(\tau+\pi/2)\frac{qc}{kR_0}J_q(kR_0/c)\right] e^{i(s-q)\tau} d\tau \tag{4.2.38}$$

which is a expression more suitable for numerical computations.

4.3 T Matrix of an radially stratified fluid cylinder

It is possible to solve numerically the case of a cylinder whose properties are a function of the coordinates; that is, the case of an inhomogeneous cylinder.

This section is devoted to solve the particular case of a cylinder whose density is equal to that of the background and whose refractive index, $n(r)$, has the form

$$n^2(r) = n_0^2 + (n_f^2 - n_0^2)\frac{r^2}{R_a} \tag{4.3.1}$$

where n_0 is the value of the refractive index at the center of the cylinder and n_f is the refractive index at the surface of the cylinder.

It will be shown later that fluid cylinders with these properties are possible to obtain.

The field satisfies the Helmholtz equation

$$\left[\nabla^2 + n^2(r)\omega^2\right]\psi(\mathbf{r}) = 0 \tag{4.3.2}$$

Due to the radial dependence of the refractive index the function ψ can be expanded in a Fourier series, as the usual solution of the wave equation,

$$\psi(\mathbf{r}) = \sum_q \psi_q(r)e^{iq\theta} \tag{4.3.3}$$

where the function ψ_q satisfies the radial equation

$$\frac{d^2\psi_q}{dr^2} + \frac{1}{r}\frac{d\psi_q}{dr} + \left(n^2(r)\omega^2 - \frac{q^2}{r^2}\right)\psi_q = 0 \tag{4.3.4}$$

for the form (4.3.1) the final equation to solve is

$$\frac{d^2\psi_q}{dr^2} + \frac{1}{r}\frac{d\psi_q}{dr} + \left(n_0^2\omega^2 + \frac{(n_f^2 - n_0^2)\omega^2 r^2}{R_a^2} - \frac{q^2}{r^2}\right)\psi_q = 0 \tag{4.3.5}$$

it is obvious that when $n_0 = n_f$ the equation reduces to Bessel equation.

The best way to solve the above equation is to expand the function ψ_q in power series of r. Due to the similarity of the equation with Bessel equation, the series proposed will be similar to that corresponding to Bessel functions

$$\psi_q(n_0\omega r) = \frac{(n_0\omega r)^q}{2^q}\sum_{n=0}^{\infty} c_n \frac{(-1)^n}{n!(n+q)!}(n_0\omega r/2)^{2n} \tag{4.3.6}$$

the sum in n starts in $n = 0$ because the solutions of interest here are only

regular solutions. Inserting this series in the differential equation leads to

$$\sum_{n=0}^{\infty}\Bigg[n(n+q)n_0^2\omega^2 c_n\frac{(-1)^n}{n!(n+q)!}(n_0\omega r/2)^{2n-2} + n_0^2\omega^2 c_n\frac{(-1)^n}{n!(n+q)!}(n_0\omega r/2)^{2n} + \frac{4(n_f^2-n_0^2)}{n_0^2R_a^2}\frac{(-1)^n}{n!(n+q)!}(n_0\omega r/2)^{2n+2}\Bigg]=0 \quad (4.3.7)$$

Note that the term c_0 is arbitrary, because the coefficient of r^{-2} equals to zero. The constant term shows that $c_1 = c_0$, and the other coefficients are related through

$$(n+2)(n+2+q)n_0^2\omega^2 c_{n+2}\frac{(-1)^{n+2}}{(n+2)!(n+2+q)!} + n_0^2\omega^2 c_{n+1}\frac{(-1)^{n+1}}{(n+1)!(n+1+q)!} + c_n\frac{(-1)^n}{n!(n+q)!}=0 \quad (4.3.8)$$

This equation can be cast into the following recursive relation

$$c_n = c_{n-1} - \frac{4(n_f^2-n_0^2)}{n_0^4\omega^2R_a^2}n(n+q)c_{n-2} \quad (4.3.9)$$

Once the field inside the cylinder is solved, the T matrix can be obtained as for the case of the fluid or elastic cylinder

$$T_q = -\frac{\rho_q J_q'(kR_a) - J_q(kR_a)}{\rho_q H_q'(kR_a) - H_q(kR_a)} \quad (4.3.10)$$

but now the quantity ρ_q is

$$\rho_q = \frac{k}{v_b}\frac{\psi_q(n_0\omega R_a)}{\psi_q'(n_0\omega R_a)}, \quad (4.3.11)$$

where

$$\psi_q'(n_0\omega R_a) = \frac{\partial\psi}{\partial r} = \frac{(n_0\omega)^q r^{q-1}}{2^q}\sum_{n=0}^{\infty}c_n\frac{(-1)^n(2n+q)}{n!(n+q)!}(n_0\omega r/2)^{2n} \quad (4.3.12)$$

4.4 T Matrix of infinite linear chain of spheres

4.4.1 Three Dimensional Multiple Scattering

Assume that a plane wave with wavenumber $\boldsymbol{k}$ impinges a cluster of spheres places at positions $\boldsymbol{R}_\alpha$. The plane wave can be expressed in spherical coordinates as

$$P_0(\mathbf{r}) = \sum_{l,m} a^0_{lm} j_l(kr) Y_{lm}(\hat{r}) \tag{4.4.1}$$

where

$$a^0_{lm} = 4\pi i^l Y^*_{lm}(\hat{k}) \tag{4.4.2}$$

here $\hat{x}$ stands for the spherical angular variables of a some vector $\mathbf{x}$, that is $\hat{x} = (\theta, \phi)$, and $Y_{lm}(\hat{x})$ is the spherical harmonics as a function of the angular variables (θ, ϕ)

$$Y_{lm}(\hat{x}) = \sqrt{\frac{2l+1}{4\pi}\frac{(l-|m|)!}{(l+|m|)!}} P_l^{|m|}(\cos\theta) e^{im\phi} \tag{4.4.3}$$

The total scattered field by the cluster will be the sum of the individual scattered fields of spheres,

$$P_{sc}(\mathbf{r}) = \sum_\alpha P^\alpha_{sc}(\mathbf{r}_\alpha) \tag{4.4.4}$$

where

$$P^\alpha_{sc}(\mathbf{r}_\alpha) = \sum_{l,m} a^\alpha_{lm} h_l(kr_\alpha) Y_{lm}(\hat{r}_\alpha) \tag{4.4.5}$$

For a single scatterer, the T matrix relates the incident and scattered field; which relates the coefficients a^α_{lm} of the scattered field expanion with the coefficients b_{lm} of the incident field expansion

$$a^\alpha_{lm} = t^\alpha_l b_{lm}, \tag{4.4.6}$$

where

$$t^\alpha_l = -\frac{\rho_q j_l'(kR_a) - j_l(kR_a)}{\rho_q h_l'(kR_a) - h_l(kR_a)} \tag{4.4.7}$$

and

$$\rho_q = \frac{k\rho_b}{k_a\rho_a}\frac{j_l(k_aR_a)}{j_l'(k_aR_a)} \tag{4.4.8}$$

In this work all the spheres will be considered equal($t_l^\alpha = t_l$). For a given sphere α, the incident field is formed by the sum of the external field P^0 plus the scattered field by all the others spheres, that is

$$P_0^\alpha(\mathbf{r}_\alpha) = P^0(\mathbf{r}) + \sum_{\beta\neq\alpha} P_{sc}^\beta(\mathbf{r}_\beta) \tag{4.4.9}$$

To relate this expression with the scattering coefficients a_{lm}^α it is necessary to express the fields on the right hand side of the above equations in the reference frame of the α scatter.

The incident field is a plane wave, which has a very simple expression for the change of coordinates

$$P^0(\mathbf{r}) = e^{i\mathbf{k}\cdot\mathbf{r}} = e^{i\mathbf{k}\cdot\mathbf{R}_\alpha} e^{i\mathbf{k}\cdot(\mathbf{r}-\mathbf{R}_\alpha)} = e^{i\mathbf{k}\cdot\mathbf{R}_\alpha} \sum_{l,m} a_{lm}^0 j_l(kr_\alpha) Y_{lm}(\hat{r}_\alpha) \tag{4.4.10}$$

being the coefficients a_{lm}^0 defined before.

The translation of the scattered field by the β sphere to the α frame is obtained by using the addition theorem,

$$P_{sc}^\beta(\mathbf{r}_\beta) = \sum_{l,m} a_{lm}^\beta h_l(kr_\beta) Y_{lm}(\hat{r}_\beta) \tag{4.4.11}$$

but

$$h_l(kr_\beta) Y_{lm}(\hat{r}_\beta) = \sum_{l'm'} j_{l'}(kr_\alpha) Y_{l'm'}(\hat{r}_\alpha) g_{l'm'lm}^{(h)}(\mathbf{R}_\beta - \mathbf{R}_\alpha) \tag{4.4.12}$$

then

$$P_{sc}^\beta(\mathbf{r}_\beta) = \sum_{l,m} a_{lm}^\beta \sum_{l'm'} j_{l'}(kr_\alpha) Y_{l'm'}(\hat{r}_\alpha) g_{l'm'lm}^{(h)}(\mathbf{R}_\beta - \mathbf{R}_\alpha) \tag{4.4.13}$$

Finally, the total field incident on the α cylinder is

$$P_0^\alpha(\mathbf{r}_\alpha) = \sum_{l'm'} b_{l'm'} j_{l'}(kr_\alpha) Y_{l'm'}(\hat{r}_\alpha) \tag{4.4.14}$$

and the relation betwen coefficients is

$$a_{lm}^\alpha = t_l e^{i\mathbf{k}\cdot\mathbf{R}_\alpha} a_{lm}^0 + t_l \sum_{\beta\neq\alpha} \sum_{l',m'} a_{l'm'}^\beta g_{lml'm'}^{(h)}(\mathbf{R}_\beta - \mathbf{R}_\alpha) \tag{4.4.15}$$

The external incident field is assumed to be perpendicular to the linear chain axis (the $\hat{z}$), then $e^{i\mathbf{k}\cdot\mathbf{R}_\alpha} = 1$ for all α, moreover, all the coefficients a^α_{lm} will be equal to that of the sphere located at the origin $a^0_{lm} \equiv a_{lm}$,then

$$a_{lm} = t_l a^0_{lm} + t_l \sum_{l',m'} a_{l'm'} \sum_{\beta\neq 0} g^{(h)}_{lml'm'}(\mathbf{R}_\beta) \tag{4.4.16}$$

in the appendix is shown that for the linear chain $g^{(h)}_{lml'm'} = \delta_{mm'} g^{(h)}_{lml'm}$, then

$$a_{lm} = t_l a^0_{lm} + t_l \sum_{l'} a_{l'm} \sum_{\beta\neq 0} g^{(h)}_{lml'm}(\mathbf{R}_\beta) \tag{4.4.17}$$

Then, given the matrix m defined by

$$(M_m)_{ll'} = \delta_{ll'} - t_l \sum_{\beta\neq 0} g^{(h)}_{lml'm}(\mathbf{R}_\beta) = \delta_{ll'} - t_l \tilde{g}^{(h)}_{lml'm}(ka) \tag{4.4.18}$$

where the coefficients $\tilde{g}^{(h)}_{lml'm}(ka)$ are given in appendix A, the coefficients a_{lm} can be computed by direct inversion of the matrix M, and then

$$a_{lm} = \sum_{l'} (M^{-1}_m)_{ll'} t_{l'} a^0_{l'm} \tag{4.4.19}$$

4.4.2 Infinite Linear Chain

The addition

$$\sum_\alpha h_l(kr_\alpha) Y_{lm}(\hat{r}_\alpha) \tag{4.4.20}$$

can be made analytically for the case of an infinite linear chain of spheres. If all the spheres are located along the z-axis, the set of vectors $\mathbf{r}_\alpha$ are

$$\mathbf{r}_\alpha = \mathbf{r} - \alpha a \hat{\mathbf{z}} \tag{4.4.21}$$

and we know that

$$\sum_{\alpha=-\infty}^{\infty} h_l(kr_\alpha) P_l^{|m|}(\cos\theta_\alpha) = \frac{i^{m-l}\pi}{ka} \sum_\nu e^{ikz\sin\theta_\nu} H_m(k\rho\cos\theta_\nu) P_l^{|m|}(\cos\theta_\nu) \tag{4.4.22}$$

but considering only a propagating mode and in the $x-y$ plane

$$\sum_{\alpha=-\infty}^{\infty} h_l(kr_\alpha) Y_{lm}(\hat{r}_\alpha) = \frac{i^{m-l}\pi}{ka} \sqrt{\frac{2l+1}{4\pi}\frac{(l-|m|)!}{(l+|m|)!}} P_l^{|m|}(0) H_m(k\rho) e^{im\phi} \tag{4.4.23}$$

Finally the total scattered field will be

$$P_{sc}(r,\phi) = \sum_{l,m}\sum_{l'}(M_m^{-1})_{ll'}t_{l'}a^0_{l'm}\frac{i^{m-l}\pi}{ka}\sqrt{\frac{2l+1}{4\pi}\frac{(l-|m|)!}{(l+|m|)!}}P_l^{|m|}(0)H_m(k\rho)e^{im\phi} \tag{4.4.24}$$

4.4.3 T Matrix

The coefficients $a^0_{l'm}$ of the expansion of a plane wave in spherical coordinates can be related with that of the plane wave but in polar coordinates easily,

$$a^0_{l'm} = 4\pi i^{l'}Y^*_{l'm}(\hat{k}) = 4\pi i^{l'}\sqrt{\frac{2l'+1}{4\pi}\frac{(l'-|m|)!}{(l'+|m|)!}}P_{l'}^{|m|}(0)e^{-im\phi_0} \tag{4.4.25}$$

then, as $A^0_m = i^m e^{-im\phi_0}$ the following relation is obtained

$$a^0_{l'm} = 4\pi i^{l'-m}\sqrt{\frac{2l'+1}{4\pi}\frac{(l'-|m|)!}{(l'+|m|)!}}P_{l'}^{|m|}(0)A^0_m \tag{4.4.26}$$

Inserting this expression in the corresponding to the total scattered field

$$\begin{aligned}P_{sc}(r,\phi) = {} & \frac{\pi}{ka}\sum_{l,l',m} i^{l'-l}(M_m^{-1})_{ll'}t_{l'}\times \\ & \sqrt{2l'+1}\sqrt{2l+1}\sqrt{\frac{(l'-|m|)!}{(l'+|m|)!}}\sqrt{\frac{(l-|m|)!}{(l+|m|)!}}P_{l'}^{|m|}(0)P_l^{|m|}(0)A^0_m H_m(k\rho)e^{im\phi}\end{aligned} \tag{4.4.27}$$

the sums for the angular variables $\sum_{l,m}$ can be reordered, that is

$$\sum_{l,m} = \sum_{l=0}^{\infty}\sum_{m=-l}^{l} = \sum_{m=-\infty}^{\infty}\sum_{l=|m|}^{\infty} \tag{4.4.28}$$

Then the total scattered field will be

$$P_{sc}(r,\phi) = \sum_{m=-\infty}^{\infty} T_m A^0_m H_m(k\rho)e^{im\phi} \tag{4.4.29}$$

with

$$T_m = \frac{\pi}{ka} \sum_{l=|m|}^{\infty} \sum_{l'=0}^{\infty} i^{l'-l} (M_m^{-1})_{ll'} t_{l'} \times$$
$$\sqrt{2l'+1}\sqrt{2l+1}\sqrt{\frac{(l'-|m|)!}{(l'+|m|)!}}\sqrt{\frac{(l-|m|)!}{(l+|m|)!}} P_{l'}^{|m|}(0) P_l^{|m|}(0) \quad (4.4.30)$$

where

$$P_l^{|m|}(0) = \frac{2^m \sqrt{\pi}}{\Gamma(\frac{1-l-m}{2})\Gamma(1+\frac{l-m}{2})} \quad (4.4.31)$$

Therefore the periodic array of spheres can be, provided that $a > \lambda$, considered a two dimensional scatterer. Another condition for it is that the field be computed at a distance such that the evanescent waves be negligible.

Chapter 5

Homogenization

5.1 Homogenization of an infinite medium

It has been shown in section 3.3 that when cylinders are extended in the plane laying in a regular lattice, the modes of the system satisfy a secular equation

$$\det M = 0, \tag{5.1.1}$$

where M is the multiple scattering matrix defined in (3.3.12). The solution of this equation is a function of the form

$$\omega = \omega(\boldsymbol{K}) \tag{5.1.2}$$

which is called the band structure or the dispersion relation.

Appendix B shows that, in the low frequency limit, the ratio between ω and $\boldsymbol{K}$ appearing in the matrix M is a new variable called the effective speed of sound c_{eff}, given by

$$c_{eff} \equiv \lim_{|\boldsymbol{k}|\to 0} \frac{\omega(\boldsymbol{K})}{|\boldsymbol{K}|} \tag{5.1.3}$$

The interpretation of this fusion is that in this limit the dispersion relation becomes linear, and the slope of this line is the effective speed of sound of the homogeneous effective medium. This is the so called homogenization limit.

The objective now is to determine the effective parameters of this new homogeneous medium.

5.1.1 Effective speed of sound

In appendix B it is found that the asymptotic form of the secular equation $\det M = 0$ becomes

$$\det \widehat{M} = 0, \tag{5.1.4}$$

where the matrix $\widehat{M}$ is the low frequency form of the M matrix and is given obtained in subsection B.2.4

$$\widehat{M} = \begin{pmatrix} A_{3\times 3} & B_{3\times Q} \\ C_{Q\times 3} & D_{Q\times Q} \end{pmatrix} \tag{5.1.5}$$

In principle the method to find the effective speed of sound could be the same than that used to obtain the band structure. In this case, some propagation direction θ should be chosen and the effective speed of sound in this direction would be obtained. However, the above matrix has a form that invites to solve analytically for the effective speed of sound as a function of the propagation angle θ.

The reason why the form of the $\widehat{M}$ matrix is special is that only the matrix A contains information about the two more relevant variables, which are the effective speed of sound c_{eff} and the propagation angle θ. Then it suggest that a factorization of the determinant could be possible.

This factorization can be done defining the matrix X as

$$X \equiv \begin{pmatrix} I_{3\times 3} & O_{3\times Q} \\ -D^{-1}C|_{Q\times 3} & D^{-1}_{Q\times Q} \end{pmatrix} \tag{5.1.6}$$

where I and O are the identity matrix and a null matrix of the sizes indicated.

The product MX is the key for the factorization, this product is

$$MX = \begin{pmatrix} A - BD^{-1}C|_{3\times 3} & BD^{-1}|_{3\times Q} \\ O_{Q\times 3} & I_{Q\times Q} \end{pmatrix} \tag{5.1.7}$$

the following relations are now evident

$$\det(MX) = \det M \det X = \det M \det D^{-1} \tag{5.1.8}$$

$$\det(MX) = = \det(A - BD^{-1}C) \tag{5.1.9}$$

Then, if $\det D \neq 0$ is assumed, the condition $\det M = 0$ is equivalent to $\det(A - BD^{-1}C) = 0$, but now the matrix $A - BD^{-1}C$ is a 3×3 so that the determinant can be manipulated easily.

Appendix B found that the matrix $BD^{-1}C$ has the form

$$BD^{-1}C = \begin{pmatrix} \Delta' & 0 & \Gamma' \\ 0 & 0 & 0 \\ \Gamma'^{*} & 0 & \Delta'^{*} \end{pmatrix} \tag{5.1.10}$$

and then

$$A - BD^{-1}C = \begin{pmatrix} 1-\Delta'-f\eta\frac{c^2}{1-c^2} & if\eta\frac{c}{1-c^2}e^{-i\theta} & f\eta\frac{e^{2i\theta}}{1-c^2}+\Gamma^{(0)}-\Gamma' \\ -if\zeta\frac{c}{1-c^2}e^{i\theta} & 1-f\zeta\frac{c^2}{1-c^2} & if\zeta\frac{c}{1-c^2}e^{-i\theta} \\ f\eta\frac{e^{-2i\theta}}{1-c^2}+\Gamma^{(0)*}-\Gamma'^{*} & -if\eta\frac{c}{1-c^2}e^{i\theta} & 1-\Delta'^{*}-f\eta\frac{c^2}{1-c^2} \end{pmatrix} \tag{5.1.11}$$

Defining the new variables

$$1-\Delta' \equiv \Delta \tag{5.1.12}$$

$$\Gamma^{(0)}-\Gamma' \equiv \Gamma \tag{5.1.13}$$

and, after straightforward manipulations,

$$\det(A - BD^{-1}C) = \det\begin{pmatrix} (1-c^2)\Delta - f\eta c^2 & if\eta c & f\eta + (1-c^2)\Gamma e^{2i\theta} \\ -if\epsilon c & 1-c^2-f\epsilon c^2 & if\epsilon c \\ f\eta + (1-c^2)\Gamma^{*}e^{-2i\theta} & -if\eta c & (1-c^2)\Delta^{*} - f\eta c^2 \end{pmatrix} \tag{5.1.14}$$

equating the above determinant to zero and solving for the effective speed of sound, the following relation is obtained (now $c = c_{eff}$)

$$c_{eff}^2 = \frac{|\Delta|^2 - |\Gamma|^2 - f^2\eta^2 - 2f\eta|\Gamma|\cos\Phi_\Gamma\cos 2\theta + 2f\eta|\Gamma|\sin\Phi_\Gamma\sin 2\theta}{(1+f\zeta)\left[(\Delta+f\eta)(\Delta^{*}+f\eta) - |\Gamma|^2\right]} \tag{5.1.15}$$

Note that the expression for c_{eff}^2 takes the form of an angle-dependent speed of sound in an anisotropic medium,

$$c_{eff}^2(\theta) = c_{s+}^2 + c_{s-}^2\cos 2\theta + c_{a+}^2\sin 2\theta \tag{5.1.16}$$

where the components of the velocity tensor are

$$c_{s+}^2 = \frac{|\Delta|^2 - |\Gamma|^2 - f^2\eta^2}{(1+f\zeta)\left[(\Delta+f\eta)(\Delta^*+f\eta) - |\Gamma|^2\right]} \tag{5.1.17a}$$

$$c_{s-}^2 = -\frac{2f\eta|\Gamma|\cos\Phi_\Gamma}{(1+f\zeta)\left[(\Delta+f\eta)(\Delta^*+f\eta) - |\Gamma|^2\right]} \tag{5.1.17b}$$

$$c_{a+}^2 = \frac{2f\eta|\Gamma|\sin\Phi_\Gamma}{(1+f\zeta)\left[(\Delta+f\eta)(\Delta^*+f\eta) - |\Gamma|^2\right]} \tag{5.1.17c}$$

these quantities are always given relative to the background. In order to know their absolute value, they might be multiplied by the speed of sound in the background c_b.

An alternate expression for the effective speed of sound in an anisotropic medium is

$$c_{eff}^2(\theta) = c_{xx}^2\cos^2\theta + c_{yy}^2\sin^2\theta + (c_{xy}^2 + c_{yx}^2)\sin\theta\cos\theta \tag{5.1.18}$$

being

$$c_{xx}^2 = c_{s+}^2 + c_{s-}^2 \tag{5.1.19a}$$

$$c_{yy}^2 = c_{s+}^2 - c_{s-}^2 \tag{5.1.19b}$$

$$c_{yx}^2 = c_{xy}^2 = c_{a+}^2 \tag{5.1.19c}$$

5.1.2 Effective bulk modulus

I has been shown in the introduction that the bulk modulus is a quantity that does not interact with the lattice structure. This explains why the effective homogeneous medium has a scalar bulk modulus and an anisotropic density.

For an infinite periodic system the effective bulk modulus was given by the lattice average

$$\frac{1}{B_{eff}} = \int_{cell}\frac{1}{B(\boldsymbol{r})}dV \tag{5.1.20}$$

so that, independently of the dimensions of the periodicity, the effective bulk modulus of a mixture can be find to be

$$\frac{1}{B_{eff}} = \sum_i \frac{f_i}{B_i} \tag{5.1.21}$$

where f_i is the area of the material type i divided by the area of the unit cell, that is, it is the filling fraction of the material i.

It is common to do not consider the background as one of the materials, then when the subindex i stands for the background, the filling fraction is set to $1-f$, where f is the total filling fraction of the inclusions. Then, the common expression is

$$\frac{1}{B_{eff}} = \frac{1-f}{B_b} + \sum_i \frac{f_i}{B_i}, \tag{5.1.22}$$

where the addition is performed over all the inclusions.

5.1.3 Effective density

Once the effective tensor c_{ij} and the effective bulk modulus B_{eff}have been obtained, the reciprocal density tensor is determined with the help of (1.2.32)

$$\rho_{ij}^{-1} = c_{ij}^2 B_{eff}^{-1} \tag{5.1.23}$$

where c_{ij}^2 and ρ_{ij}^{-1} are the components of the speed of sound and the reciprocal density tensors. With the reciprocal density tensor the effective medium is fully characterized.

5.2 Homogenization of a cluster of cylinders

In the previous section only perfectly infinite ordered systems of scatters were considered. However, in actual finite structures some disordering effects can appear. Here, it will be shown how to analyze these effects.

The homogenization method is based in the assumption that, given a finite cluster of cylinders, the scattered field by this cluster in the low frequency limit will be equal to that of a homogeneous cylinder (not necessarily a circular cylinder). Mathematically this homogenization condition is expressed as

$$\lim_{\lambda\to\infty} \frac{P^{sc}_{cluster}(\boldsymbol{r}) - P^{sc}_{cyl}(\boldsymbol{r})}{P^{sc}_{cyl}(\boldsymbol{r})} = 0 \tag{5.2.1}$$

as explained in Chapter 4, the scattered pressure by a cluster of cylinders can be expressed in terms of the effective T matrix of the cluster, then

$$P^{sc}_{cluster}(\boldsymbol{r}) = \sum_q \sum_s T^{eff}_{qs} A^0_s H_q(kr) e^{iq\theta} \tag{5.2.2}$$

and for the cylinder

$$P_{cyl}^{sc}(\boldsymbol{r}) = \sum_q \sum_s T_{qs}^{cyl} A_s^0 H_q(kr) e^{iq\theta} \tag{5.2.3}$$

With these definitions it is easy to show that the homogenization condition in the scattered field becomes

$$\lim_{\lambda \to \infty} \frac{T_{qs}^{eff}}{T_{qs}^{cyl}} = 1 \tag{5.2.4}$$

If the cluster is given a circular shape, it is expected that the homogeneous scatter be a circular cylinder. Only isotropic lattices will be considered here, because the anisotropic case is more complex to analyze with this approach, it means that the T matrices implied in the theory will be always diagonal matrices.

Finally, the homogenization conditions will be

$$\widehat{T}_q^{eff} = \widehat{T}_q^{cyl} \quad , \quad q = 0, \pm 1, \pm 2, \cdots \tag{5.2.5}$$

where $\widehat{X}$ means that the lower order term in the Taylor expansion of X has to be taken.

The effective T matrix for the cluster of cylinders is the input of the problem. It is the known function of the knwown variables, while the effective T matrix of the cylinder is a function of the parameters to determine.

With this approach, it is possible to determine not only the acoustic parameters but, as will be shown, the shape of the effective scatter (the radius of the effective cylinder). Then, the parameters to determine are the effective bulk modulus, the effective density (then the effective speed of sound is trivially determined) and the effective radius of the cluster. Three unknowns and infinite equations (q runs from 0 to $\pm\infty$), so that with only three equations could be enough to fully solve the problem. But in practice, the following procedure is employed:

- Define the effective radius
- Use the $q = 0$ equation to determine the effective bulk modulus
- Use the $q = 1$ equation to determine the effective density
- Use $v_{eff} = \sqrt{B_{eff}/\rho_{eff}}$ to determine the effective speed of sound
- Use the $q > 1$ equations to check the result

5.2.1 Effective shape

The effective shape of the cluster can be defined from a filling fraction consideration. Consider a cluster of scatters occupying some region of the plane. If this cluster of cylinder is going to be considered a homogeneous scatter, it is expected that the filling fraction of the system be independent of the size of the effective scatter. This filling fraction is defined as the ration between the total area occupied by the scatters in the cluster and the area of the effective scatter

$$f = \frac{\sum_i A_i}{A_{eff}} \tag{5.2.6}$$

The most common situation is that these cylinders be circular and equal each other and, as was explained before, be in an isotropic lattice. If the filling fraction is expected to be independent of the size of the scatter, it can be assumed to be equal to that of the infinite system. Then for a cluster of N cylinders of radius R_a in a lattice whose unit cell has an area A_d the above equation becomes

$$\frac{\pi R_a^2}{A_d} = \frac{N\pi R_a^2}{A_{eff}} \tag{5.2.7}$$

if the cluster is a circular cluster, the effective area will that of a cylinder of radius R_{eff}, then solving from the above equation

$$R_{eff} = \sqrt{\frac{NA_d}{\pi}} \tag{5.2.8}$$

for the square lattice of lattice constant a the area of the unit cell is $A_d = a^2$ and for the hexagonal one $A_d = \sqrt{3}a^2/2$.

5.2.2 Effective bulk modulus

The previous result for the effective bulk modulus is valid for both the isotropic or the anisotropic lattice, but only when the different materials are fluid materials and when the system is a periodic infinite system, so that the expression needs to be extended for some special situations of practical interest.

Firstly, the effective bulk modulus will be computed for a finite cluster of scatters embedded in regular lattices, following these lattice will be allowed to be disordered and finally the scatters will be considered to have elastic

properties. The background will be always considered a fluid background, leaving the elastic background for the last chapter.

The homogenization condition for $q = 0$ is

$$\widehat{T}_0^{eff} = \widehat{T}_0^{cyl} \tag{5.2.9}$$

it is assumed that the effective cylinder be a fluid cylinder, so that, using equation B.1.6

$$\widehat{T}_0^{cyl} = \frac{i\pi R_{eff}^2}{4}\left[\frac{B_b}{B_{eff}} - 1\right] \tag{5.2.10}$$

while for the cluster of cylinders the 0 element is

$$\widehat{T}_0^{eff} = \sum_\alpha (T_\alpha)_0 = \sum_\alpha \frac{i\pi R_\alpha^2}{4}\left[\frac{B_b}{B_\alpha} - 1\right] \tag{5.2.11}$$

where B_α is the bulk modulus if the cylinder is a fluid cylinder and the fluid-like bulk modulus defined in (B.1.20) if the cylinder is an elastic cylinder

$$B_\alpha = \lambda_\alpha + \mu_\alpha \tag{5.2.12}$$

then the homogenization equation is

$$R_{eff}^2\left[\frac{B_b}{B_{eff}} - 1\right] = \sum_\alpha R_\alpha^2\left[\frac{B_b}{B_\alpha} - 1\right] \tag{5.2.13}$$

the absence of the lattice structure in the above equation allows to write it as

$$\frac{1}{B_{eff}} = \frac{1-f}{B_b} + \sum_i \frac{f_i}{B_i} \tag{5.2.14}$$

which is the same result of the previous section.

This result shows that, effectively, the bulk modulus does not interacts with the lattice and with the order or disorder of the cluster. Provided that the system could be considered homogeneous, the effective bulk will be computed with the above equation.

5.2.3 Effective density

The effective density can be computed in a similar way from the equation for $q = 1$. As shown in equations (B.1.10) and (B.1.27) for both the elastic

cylinder the fluid cylinder the $q = 1$ element is

$$\widehat{T}_1^{cyl} = \frac{i\pi R_{eff}^2}{4}\frac{\rho_{eff} - \rho_b}{\rho_{eff} + \rho_b} \tag{5.2.15}$$

while for the cluster of cylinders it is shown that

$$\widehat{T}_1^{eff} = \sum_{\alpha,\beta}(\widehat{M}_{\alpha\beta}^{-1})_{11}(T_\beta)_1 = \frac{i\pi R_a^2}{4}\frac{\rho_a - \rho_b}{\rho_a + \rho_b}\sum_{\alpha,\beta}(\widehat{M}_{\alpha\beta}^{-1})_{11} \tag{5.2.16}$$

it has been assumed here that all the cylinders in the cluster are equal each other, leaving the discussion of mixture for later sections.

Defining the Δ factor as

$$\frac{1}{\Delta} = \frac{1}{N}\sum_{\alpha,\beta}(\widehat{M}_{\alpha\beta}^{-1})_{11} \tag{5.2.17}$$

the homogenization equation is

$$\frac{\rho_{eff} - \rho_b}{\rho_{eff} + \rho_b} = \frac{\rho_a - \rho_b}{\rho_a + \rho_b}\frac{f}{\Delta} \tag{5.2.18}$$

and solving for the effective density

$$\rho_{eff} = \frac{\rho_a(\Delta + f) + \rho_b(\Delta - f)}{\rho_a(\Delta - f) + \rho_b(\Delta + f)} \tag{5.2.19}$$

which is the previous result for the isotropic case, but with different expressions for the Δ factor.

Now the Δ factor is a real space convergent factor, while in the previous section was a reciprocal space convergent. This new expression allows to analyze finite size effects in the effective parameters, like disorder or small number of cylinders, as will be shown later.

5.2.4 Effective speed of sound

Once the effective bulk modulus and the effective density have been determined, the effective speed of sound is simply

$$c_{eff} = \sqrt{\frac{B_{eff}}{\rho_{eff}}} \tag{5.2.20}$$

and then the problem is solved.

5.2.5 Testing Condition

Once the effective parameters have been obtained it is worth to check how consistent is the method. So far, it has been imposed that the $q = 0$ and the $q = 1$ elements of both the effective T matrix and the cylinder T matrix be equal. Now the others elements will be used to check if they are equal.

As shown in section B, for $q > 1$ the T matrix elements of a fluid cylinder of density ρ_{eff} and radius R_{eff} are

$$T_q^{cyl} = \frac{i\pi R_{eff}^{2q}}{4^q} \frac{1}{q!(q-1)!} \frac{\rho_{eff} - \rho_b}{\rho_{eff} + \rho_b} \tag{5.2.21}$$

the ratio of the elements $q+1$ and q is a function only of the effective radius of the cylinder, then

$$\frac{\widehat{T}_{q+1}^{cyl}}{\widehat{T}_q^{cyl}} = \frac{1}{4q(q+1)} R_{eff}^2 = \frac{\widehat{T}_{q+1}^{eff}}{\widehat{T}_q^{eff}} \tag{5.2.22}$$

the right hand side of the above equation is a function of the cluster parameters and the integer q, while the effective radius is a constant for a given cluster. Defining the q-dependent radius as

$$R_{eff}^2(q) = 4q(q+1) \frac{\widehat{T}_{q+1}^{eff}}{\widehat{T}_q^{eff}} \tag{5.2.23}$$

it is expected that $R_{eff}(q) = R_{eff}$ for all q, but as will be shown later this is not always the case, being this analysis one way to check if the homogenization theory has been applied correctly.

Part II

Applications

Chapter 6

Clusters of rigid cylinders

The homogenization method is applied here to finite clusters of rigid cylinders. First, a large number of cylinders (151) are placed in a circular region, and the homogenization method is applied to study the effective acoustic parameters of this configuration. Later, the homogenization parameters are studied as a function of the number of cylinders in the cluster, showing that with only 7 scatterers a fluid-like cylinder can be built. In both cases experiments are performed to support the predictions simulated.

6.1 Characterization of a cluster of cylinders

The case of solid cylinders in air can be studied under the rigid cylinder approximation. For almost all solid materials their density is very high in comparison with that of air, therefore no sound waves will propagate through the cylinder. The rigid cylinder is also a good starting point to understand acoustic wave phenomena, because it is a basic scattering problem with no other parameters than the radius. Therefore all the phenomena involved here can be understood by means of the ratio between the wavelength and the cylinder radius ratio (filling fraction).

6.1.1 Theoretical analysis

The geometry considered here is a circular-shaped cluster of 151 cylinders, shown in figure 6.1. Cylinders are distributed in an hexagonal lattice, which

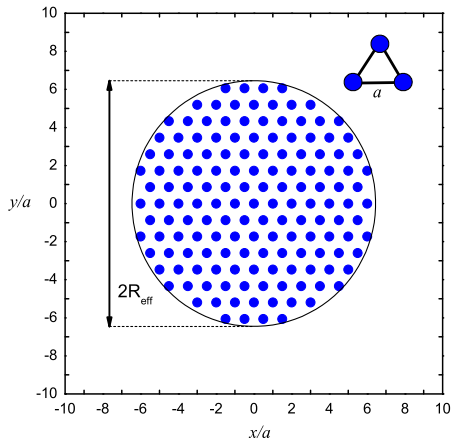

Figure 6.1: Cluster of 151 rigid cylinders to be characterized. The underlaying lattice is hexagonal with lattice constant a.

is an isotropic structure and it is better for making a circular region than the square lattice.

The first parameter to determine is the effective radius of the cluster. This parameter is computed with the help of (5.2.8) applied to the hexagonal lattice,

$$R_{eff} = \sqrt{\frac{N\sqrt{3}}{2\pi}}a \approx 6.451a \tag{6.1.1}$$

being a the lattice constant.

The circle associated to this value is drawn in figure 6.1 together with the cluster. It can be seen that the physical dimension of the cluster is consistent with the circle determined by R_{eff}.

The accuracy of R_{eff} can be studied with the properties of the effective T matrix. As shown in chapter 5, for a given q (5.2.23) is

$$R^2_{eff}(q) = 4q(q+1)\frac{\widehat{T}^{eff}_{q+1}}{\widehat{T}^{eff}_{q}} \tag{6.1.2}$$

Since it is impossible to get an exact circular cluster, different values for the effective radius will be obtained for different values of q. Then, the variations observed in R_{eff} will provide an account of how the cluster is different from

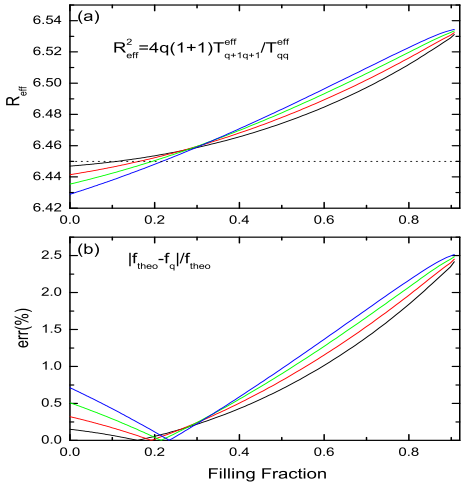

Figure 6.2: (a) Effective radius plotted as a function of the filling fraction calculated from equation (6.1.2) for four different q values. The horizontal line defines the value given by equation (6.1.1).(b) Relative error of the theoretically assumed filling fraction, compared with the ones obtained from the T matrix (see equation (6.1.2)) for four different q values.

a circular shape. Figure 6.2 (a) plots the values of R_{eff} obtained for four different values of q. It is shown that deviations from approximated in (6.1.1) (horizontal line) occur, but figure 6.2 shows that these variations are not very important. The relevance of these variations can be better understood if we represent a comparison of the associated filling fractions. On the one hand, for a given q, the value R_{eff} given by equation (B.3.16) is employed in calculating the filling fraction f_q of the lattice, then

$$f_q = N\left(\frac{R_a}{R_{eff}(q)}\right)^2 \tag{6.1.3}$$

On the other hand, the theoretical assumed filling fraction is defined as usual, $f_{theo} = f_{hex}$. The relative error $err(\%) = 100 \times |f_{theo} - f_q|/f_{theo}$, is shown in figure 6.2 (lower panel). Notice that the error is always smaller than 2.5%, which supports the validity of (6.1.1) to determine the effective radius of a homogenized cluster with external circular shape.

The other acoustic parameters for this cluster can be obtained with (5.2.14), (5.2.19) and (5.2.20) under the simplified assumption of $\rho_a \approx \infty$

(rigid cylinders)

$$\frac{1}{B_{eff}} = \frac{B_b}{1-f}, \tag{6.1.4}$$

$$\rho_{eff} = \frac{\Delta+f}{\Delta-f}\rho_b, \tag{6.1.5}$$

$$c_{eff} = \sqrt{\frac{\Delta-f}{\Delta+f}}\frac{c_b}{\sqrt{1-f}}. \tag{6.1.6}$$

For low f, the contribution to $\widehat{M}$ of matrix $\widehat{G}$ can be neglected. Then, matrix $\widehat{M}$ is simply the identity, so that $(\widehat{M}^{-1}_{\alpha\beta})_{11} \approx \delta_{\alpha\beta}$, and, moreover, $\Delta = 1$. Finally, B_{eff} remains the same but not ρ_{eff} and c_{eff} that now are

$$\rho_{eff} = \frac{1+f}{1-f}\rho_b, \tag{6.1.7}$$

$$c_{eff} = \frac{c_b}{\sqrt{1+f}}. \tag{6.1.8}$$

At this point it is interesting to stress that equation (6.1.7) recovers the Berryman' s effective density [Ber80, Ber92] and equation (6.1.8) recovers the heuristic model reported in reference [CSSP$^+$01] for c_{eff}. Moreover, these expressions have also been found in studying the refraction of water waves by the CPA method [HC05].

Continuous lines in both panels of figure 6.3 represent the effective parameters calculated by using equations (6.1.5) and (6.1.6). The result for c_{eff} fairly agrees with that calculated in reference [KAG03] for an infinite medium by a plane wave expansion method. The red dotted lines define the approximated values for ρ_{eff} and c_{eff} given by (6.1.7) and (6.1.8), respectively. As it is shown, the approximated model is valid over a wide range of filling fractions. The symbols wiht errors bars represent the parameters experimentally determined by using the method be explained in the next subsection.

To summarize, in a cluster of infinite-density cylinders in a fluid, ρ_{eff} increases and c_{eff} decreases for increasing filling fraction. The speed of sound goes to zero because the sound cannot propagate inside the cylinder (they have infinite density and, then, infinite acoustic impedance). Later will be shown the analysis of cylinders with more realistic acoustic parameters, but

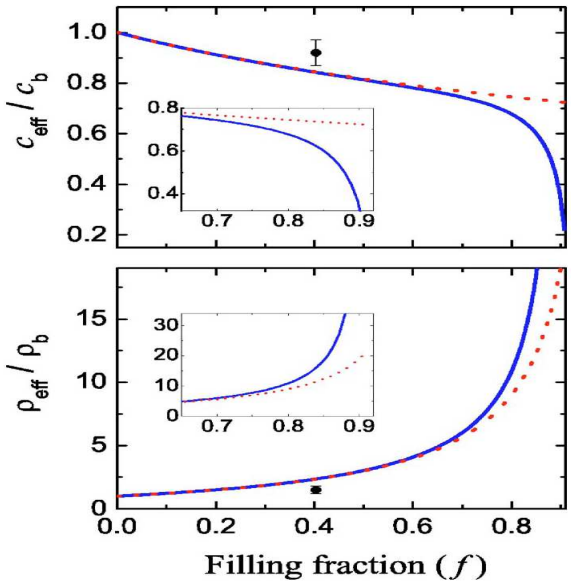

Figure 6.3: Effective acoustic parameters relative to the embedded medium calculated (blue continuous lines) for a homogenized cluster of 151 rigid cylinders. The red-dotted lines represent the values obtained by using the approach in (6.1.7) and (6.1.8). The black dots with error bars define the data obtained in the experimental characterization of 151 wooden cylinders.

now some other phenomena related with this particular case will be studied.

When disorder is introduced in a lattice of sonic or elastic scatterers many interesting phenomena might appear. Perhaps the more fundamental is related with the problem of localization. Acoustic localization has been predicted in sound propagation through liquid media containing air-filled bubbles [YA98]. More recently, widening of phononic band gaps has been found in certain disordered phononic systems due to strong Anderson localization [SSM05].

The homogenization method developed can be also employed to study how c_{eff} and ρ_{eff} change when the condition of ideal cluster is released (disordering effects). Two types of disordering effects are studied here. First, the possibility of having cylinders put at positions different to that of the hexagonal lattice (positional disorder) is analyzed. Second, cylinders with different radii are considered (structural disorder) in order to show their implications over the effective parameters.

Equations (6.1.5)and (6.1.6) give ρ_{eff} and c_{eff} as a function of f and Δ. The last parameter can be calculated for any arbitrary structure, ordered or not. Then, it is possible to study, for example, the homogenization of clusters of cylinders with positional disorder inside a certain region and to determine their effective parameters by calculating the corresponding value Δ.

In figure 6.4 the effective parameters for the homogenization of 151 cylinders with equal radii put inside an imaginary circle have been calculated for two cases of positional disorder. We first studied the "weakly disordered" case, which corresponds to assume the cylinders at random inside each one of the 151 hexagonal unit cells defined in the circle. In other words, every cylinder in the ordered lattice is randomly moved inside the unit cell. The resulting effective parameters are represented by blue continuous lines in figure and compared with the perfectly ordered case (black dotted lines). Notice that no appreciable difference appears between them because, in fact, both distributions of cylinders are equivalent in the long wavelength limit.

The second case corresponds to the "fully disordered" case; that is, inside the imaginary circle (the one defined by the ideal cluster) all the cylinders have been put at random. The red dashed lines in figure 6.4 define the results obtained after averaging over ten different configurations. The amount of

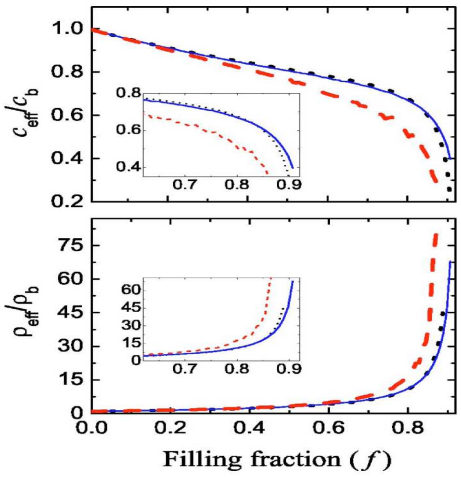

Figure 6.4: Effective acoustic parameters (relative to the embedded medium) defining a homogenized cluster of 151 rigid cylinders with positional disorder. The blue continuous lines define results corresponding to the "weakly disordered" case. The red dashed lines corresspond to the case randomly disordered. The parameters of the perfectly ordered case (black dotted lines) also appear for comparison purposes.

configurations employed is enough to guarantee that the standard deviation is lower than 10% even in the case of large filling fractions. Now, it is shown that deviations from the ideal case appear even at small filling fractions. The simulations predict effective parameters such that c_{eff} (ρ_{eff}) is always smaller (greater) than that of the corresponding ideal cluster. Note that for large filling fraction, the parameters of the disordered case do not converge to those of the ideal one though the touching of cylinders is achieved. The explanation for that disagreement is simple: the structure of voids between touching cylinders is different in the two configurations.

The case of a cluster made of cylinders that are different can be easily treated by taking into account that the diagonal terms are now

$$\widehat{T}_{00}^{eff} = \sum_{\alpha} (\widehat{T}_{\alpha})_{00}, \tag{6.1.9}$$

$$\widehat{T}_{00}^{eff} = \sum_{\alpha,\beta} (\widehat{M}_{\alpha\beta}^{-1})_{11} (\widehat{T}_{\alpha})_{11} \tag{6.1.10}$$

When the cluster is made of several i-types of cylinders equally distributed, the partial filling fraction f_i can be defined as

$$f_i \equiv N_i \left(\frac{R_i}{R_{eff}} \right)^2 \tag{6.1.11}$$

where N_i is the total number of cylinders of material i and radius R_i. The following expressions are easily obtained for the effective parameters

$$\frac{1}{B_{eff}} = \frac{1-f}{B_b} + \sum_i \frac{f_i}{B_i}, \tag{6.1.12}$$

$$\rho_{eff} = \frac{1 + \sum_i f_i \frac{\rho_i - \rho_b}{\rho_i + \rho_b}}{1 - \sum_i f_i \frac{\rho_i - \rho_b}{\rho_i + \rho_b}} \tag{6.1.13}$$

where B_i and ρ_i are, respectively, the bulk modulus and density of cylinders made of material i. The effective speed of sound could be obtained from the previous expressions as usual. The results above for B_{eff} were also obtained in reference [Ber80, Ber92] for a 3D case, where cylinders are replaced by spheres.

In the most general case, when all the cylinders are different, if the homogenized cluster is still considered as homogeneous and isotropic, its corresponding effective parameters are given by

$$\frac{1}{B_{eff}} = \frac{1+\zeta}{B_b}, \tag{6.1.14}$$

$$\rho_{eff} = \frac{1+\eta}{1-\eta}\rho_b, \tag{6.1.15}$$

where

$$\eta = -\frac{i4}{\pi R_{eff}^2} \widehat{T}_{11}^{eff}, \tag{6.1.16}$$

$$\zeta = -\frac{i4}{\pi R_{eff}^2} \widehat{T}_{00}^{eff}. \tag{6.1.17}$$

These expressions have been used to study the case of a cluster made of 151 rigid cylinders having different radii. The radii of the cylinders are considered to follow a normal distribution centered in a certain radius R_0, which defines the filling fraction in the x-axis. The function that defines the distribution of cylinders' radii for a given R_0 is

$$P(R) = \frac{1}{\sigma\sqrt{2\pi}} e^{-(R-R_0)^2/2\sigma^2} \tag{6.1.18}$$

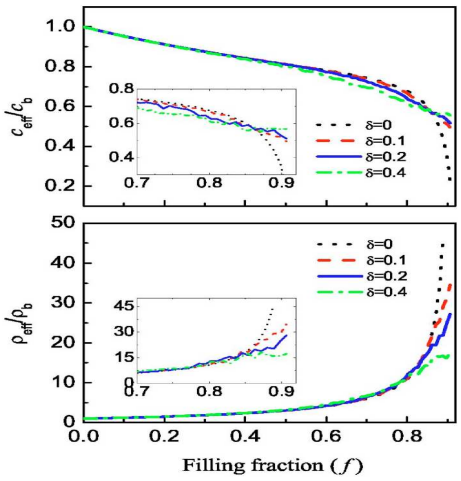

Figure 6.5: Effective parameters of a homogenized cluster of 151 rigid cylinders enclosed in a circle of radius $R_{eff} = 6.452a$. The values are calculated under the assumption that the lattice of cylinders has structural disorder. Three different degrees of disorder have been considered. The ideal case is represented by the lines $\delta = 0$.

Results have been obtained for three different values of the variance σ. This value has been defined assuming that there is a relative error δ in the radius of the cylinder and that $R_0\delta \approx 3\sigma^2$.

Results for $\delta = 0.1, 0.2$, and 0.4 are shown in figure 6.5 and compared with the case of an ideal cluster of identical cylinders($\delta = 0$). All the curves are obtained after averaging parameters of ten different configurations of cylinders. It can be concluded that structural disorder produces effective parameters that deviate from those obtained in clusters of identical cylinders only for large filling fractions.

Finally in figure 6.6 it is possible to see the comparison of the acoustic field generated when a plane wave with $\lambda = 4a$ reaches a circular cluster and a circular cylinder with the effective parameters of the cluster. The agreement between the pressure patterns is fairly good not only in the far field but also inside the cylinder and cluster, which is afurther support of the homogenization theory.

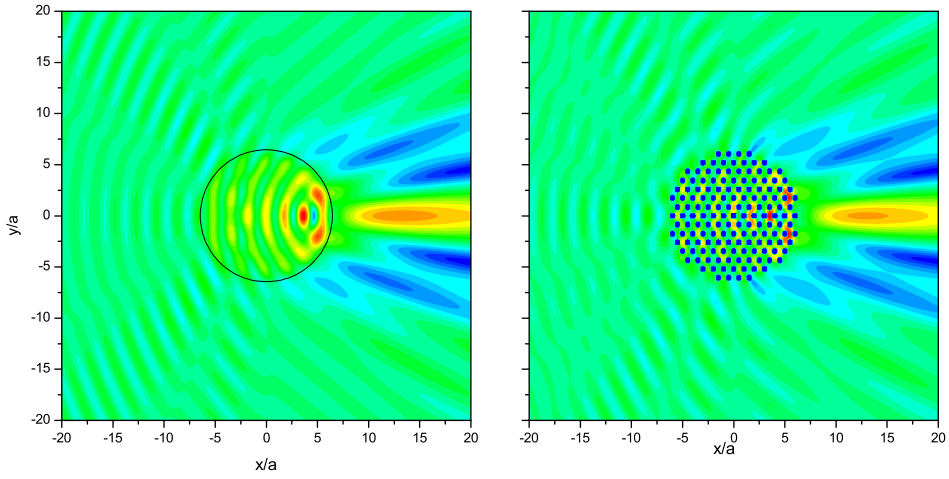

Figure 6.6: Comparison of the field scattered by a fluid cylinder and by a cluster of cylinders. The cluster is made of 151 rigid cylinders of radius $R_a = 0.3a$. The fluid cylinder has the acoustic parameters defined by the cluster in the low frequency limit, that is, the radius is $R_{cyl} = 6.451a$ and the effective speed of sound and density are, respectively, $v_{cyl} = 0.87v_b$ and $\rho_{cyl} = 1.9\rho_b$. The wavelength of the incident field is $\lambda = 4a$, which corresponds to the homogenization limit. It is clear that the acoustic field is very similar in both situations even inside the cylinder.

6.1.2 Experimental Characterization

Experimentally, the model of homogenization has been verified by analyzing a circular-shaped cluster made of 151 wooden cylinders 1 m long and radius 1 cm arranged in an hexagonal distribution with $a = 3$ cm ($f = 0.40$). Measurements have been performed in an echo-free chamber as follows. A white sound generated by an acoustic column speaker within a wide range of frequencies was employed as incident sound. Pressure maps were obtained by a set of two microphones. The first microphone was located at a distance $r_0 = 170$ cm from the center of the cluster, hanging from a robotic arm that allows its movement on the polar angle θ, and it is computer controlled using a stepper motor within a maximum resolution of 1° per step. The second microphone was fixed at approximately 220 cm from the loudspeaker, and it was used as a reference to get the phase of the pressure. Pressure measurements are automatically taken by means of a two channel fast-Fourier transform dynamic signal analyzer board, type NI-4551B. Both the cross spectrum and the auto spectra were simultaneously obtained at each θ_i.

A total of 256 spectra have been taken to generate the averaged spectrum finally assigned to θ_i. Thus, for a given frequency, the root-mean-square (rms) pressure $P_{rms}(r_0, \theta_i)$ is obtained. Pressure maps are obtained with a resolution of 10 Hz in ν and 2° in θ. The total time elapsed to get a pressure map is about 3 h. Two separated measurements were performed. The one without sample allows one to obtain the sound pressure of the external beam, $P^0_{rms}(r_0, \theta, \nu)$. Here, the sound amplification (SA) along the circle surrounding the sample will be presented:

$$SA(r_0, \theta, \nu)(dB) = 20 \log_{10} \left(\frac{|P_{rms}(r_0, \theta, \nu)|}{|P^0_{rms}(r_0, \theta, \nu)|} \right) \tag{6.1.19}$$

Figure 6.7 plot the SA maps corresponding to the two high symmetry directions of the hexagonal lattice ΓX and ΓJ, respectively, with respect to the impinging wave, for $\theta = \theta°$. Three main phenomena are noticeable in these maps. First, both maps show a wavy background that is produced by the interference between incident and scattered waves. Second, at large enough frequencies, SAs are shown along certain directions that are related to diffraction effects produced by lattice planes. For example, sound amplification at backscattering ($\theta = 180°$) is observed in Figure 6.7(a) in the

region enclosed by the horizontal lines. This feature defines the pseudo gap produced at these frequencies by the planes (10) of the crystal lattice. Third, for large enough wavelengths the sound cannot distinguish the inner structure of the cluster, and consequently, the map obtained for the cluster oriented along the ΓX direction is the same as that obtained along the ΓJ orientation, that is, the cluster is homogeneous below these frequencies. To determine the cutoff frequency (ν_c) under the one where this phenomenon appears, we have analyzed the difference between those maps. Particularly, figure 6.7(c) shows that below $\nu_c \approx 3$ kHz both maps are practically equal.

The data provided by the experimental set up can also be analyzed to obtain the effective parameters of the cluster, once the effective radius has been defined. The data obtained is the pressure field as a function of the frequency ν and the polar angle θ. The pressure field is composed of some incident field, provided by the loudspeaker, and the scattered field by the cluster of cylinders, which is assumed to be a homogeneous cylinder whose acoustic parameters have to be determined. Then, writting $k = 2\pi\nu/c_{air}$ and as explained in chapter 2, the measured field at a radius r_0 is

$$P(k,\theta) = \sum_q \left[A_q^0(k)J_q(kr_0) + A_q(k)H_q(kr_0)\right] e^{iq\theta} \tag{6.1.20}$$

where the k-dependence of the A coefficients has been explicitly indicated.

The objective here is to obtain the quotient between the coefficients A_q and A_q^0, that is, the elements of the T matrix. The low frequency limit of these matrix elements are used to obtain the effective parameters of the cluster with the help of equations B.1.6 and B.1.10.

The first operation to be made with this field is the angular FFT, which will isolate the different q-contributions

$$P_q(k) = A_q^0(k)J_q(kr_0) + A_q(k)H_q(kr_0) \tag{6.1.21}$$

The meassurement radius r_0 is assumed to be large, so that in the above expression the assymptotic form of the Bessel and Hankel functions can be used, then

$$P_q(k) = C(k)\left[A_q^0(k)\cos(kr_0 + \Phi_q) + A_q(k)e^{ikr_0+\Phi_q}\right] \tag{6.1.22}$$

the quantity $C(k)$ can be introduced in the coefficients A, because the only

relevant quantity is the quotient betwen them. If the cos function is expanded

$$P_q(k) = \left[\frac{1}{2}A_q^0(k) + A_q(k)\right] e^{i(kr_0+\Phi_q)} + \frac{1}{2}A_q^0(k)e^{-i(kr_0+\Phi_q)} \tag{6.1.23}$$

By following the same procedure without sample, the coefficients A_q^0 could be obtained, and then use the last equation to obtain the A_q coefficients. However this is not the right way to proceed as explained below.

Let us assume that we measure the field without sample, but some experimental error might appear and the distance at which the field is meassured is not exactly r_0 but $r_0 + \epsilon_r$, then the vacuum field is

$$P_q^0(k) = \frac{1}{2}A_q^0(k)e^{ik\epsilon_r}e^{i(kr_0+\Phi_q)} + \frac{1}{2}A_q^0(k)e^{-ik\epsilon_r}e^{-i(kr_0+\Phi_q)} \tag{6.1.24}$$

With this procedure, the obtained value will not be A_q^0 but $A_q^0 e^{ik\epsilon_0}$, and the difference between the total field and the vacuum field, supposedly being the scattered field, is

$$\begin{aligned} P_q(k) - P_q^0(k) = \\ \left[\frac{1}{2}(1-e^{ik\epsilon_r})A_q^0(k) + A_q(k)\right] e^{i(kr_0+\Phi_q)} + \frac{1}{2}(1-e^{-ik\epsilon_r})A_q^0(k)e^{-i(kr_0+\Phi_q)} \\ (1-e^{ik\epsilon_r})A_q^0(k)\cos(kr_0+\Phi_q) + A_q(k)e^{i(kr_0+\Phi_q)} \end{aligned} \tag{6.1.25}$$

Note that, effectively, if ϵ_r where equal to zero, this procedure is very good. However, in our case $\epsilon_r \neq 0$ always since we cannot controll accuratelly the position of the receiver microphone, which is hanging from the ceiling and its position change when the sample is removed. Therefore, another data analysis needs to be made.

The Fourier transform of $P_q(k)$, defined as

$$\tilde{P}_q(\tau) \equiv \int_0^\infty P_q(k)e^{ik\tau}dk$$

is equal to

$$\tilde{P}_q(\tau) = \left[\frac{1}{2}\tilde{A}_q^0(\tau+r_0) + \tilde{A}_q(\tau+r_0)\right] e^{i\Phi_q} + \frac{1}{2}\tilde{A}_q^0(\tau-r_0)e^{-i\Phi_q}$$

Therefore it is expected that this function presents, for a given q, two peaks separated a distance $2r_0$ in τ-space, as shown in figure 6.8. From this

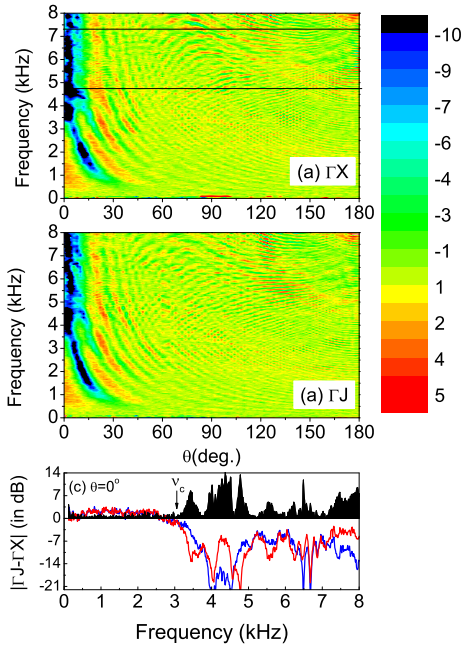

Figure 6.7: (a) Sound amplification map $SA(\nu, \theta_i)$ measured at 170 cm around the center of the cluster for the case in which the external sound wave impinging the hexagonal lattice is oriented along the ΓX direction. The horizontal lines define the bottom (4.6 kHz) and top (7.1 kHz) edges of the pseudogap associated with the acoustic crystal embedded in the cluster. (b) The corresponding map taken when the cluster is oriented along the ΓJ direction. (c) Difference (in dB) of sound pressures measured along the two high symmetry directions at forward scattering, $\theta = 0°$. The SAs along ΓX and ΓJ are represented by the red and blue lines, respectively.

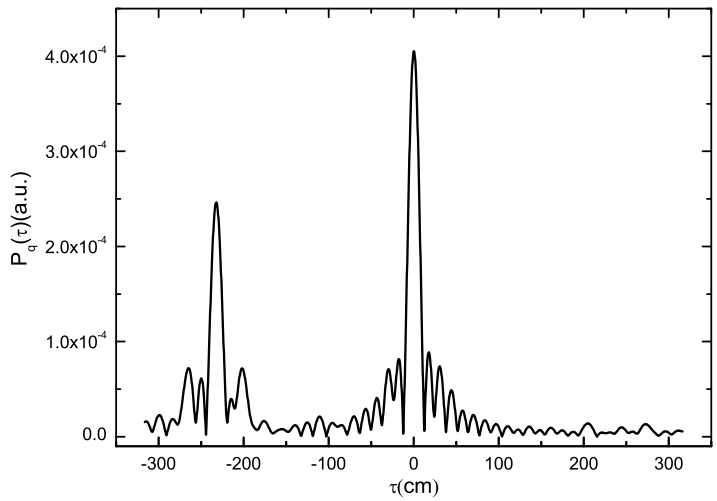

Figure 6.8: Experimental data τ-transformed corresponding to $q = 1$ (see text). Both peaks are separated a distance $2r_0 = 340cm$, which is the distance from the center of the cluster at which meassurements are made. From the

figure it is obvious that the functions can be isolated and analyzed independently, obtaining in this way the coefficients $\tilde{A}_q^0(\tau)$ and $\tilde{A}_q(\tau)$. If the inverse transform is computed, these coefficients allows to obtain the T matrix elements. The result is shown in figure 6.9. From the low frequency limit the effective parameters are obtained.

The parameters of the homogenized cluster experimentally determined from equations (B.1.6) and (B.1.10) are represented in figure 6.1.8. They have been obtained by considering $D = 39cm$, which has been established from the condition of f conservation. In absolute units, $\rho_{eff} = 1.92 \pm 0.40 kg/m^3$ and $c_{eff} = 316 \pm 17 m/s$, which roughly corresponds to those of argon gas ($\rho_{Ar} = 1.6 kg/m^3, c_{Ar} = 319 m/s$ at $25°C$). The measured parameters are slightly different to those predicted by simulations because (i) the cylinders are not long enough for the large wavelengths in which we are dealing with, and (ii) the experimental setup contains some unavoidable scattering centers that are sources of error in the data analysis.

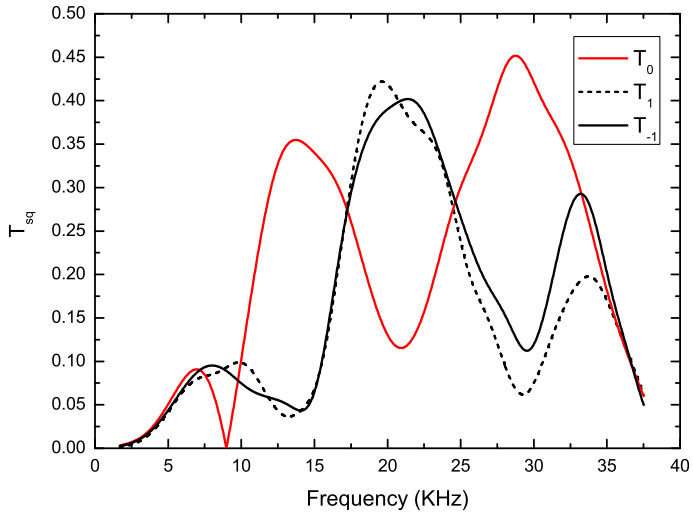

Figure 6.9: Elements corresponding to $q = 0, \pm 1$ of the T matrix obtained from the experimental data.

6.2 Small clusters and Magic Numbers

In the previous section the effective parameters were computed for a cluster having a fixed number of scatterers. However, the Δ factor computed in real space can also be used to determine the effective parameters of a cluster but now as a function of the number of cylinders in it. This is another finite-size effect that can be studied with this theory.

6.2.1 Theoretical analysis

The effective parameters have been computed for clusters consisting of $N = 2, 3, 4, \cdots$ cylinders put at the positions of a hexagonal lattice, the filling fraction of the infinite lattice being $f_{hex} = (2\pi/\sqrt{3})R_0^2/d^2$. Each successive cluster is formed from the previous one (starting from the single cylinder) by adding a cylinder, which is placed at the nearest lattice site from the cluster's center. Each cluster is compared with an effective fluid-like cylinder with radius $R_{eff} = \sqrt{N\sqrt{3}/2}d$, given by equation (6.1.1). The construction procedure is shown in figure 6.10.

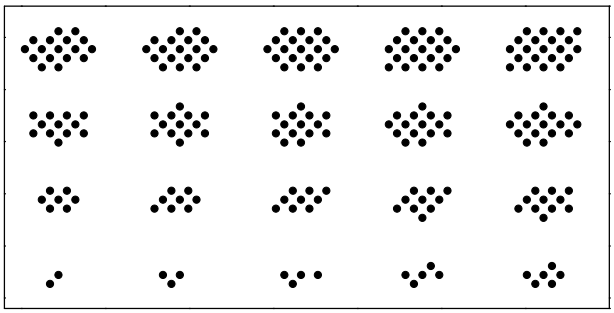

Figure 6.10: Construction of clusters by adding cylinders to the lattice site nearest to the cluster's center

Figure 6.11 plots the effective speed of sound, relative to those of the background, for two different R_0. The effective parameters oscillate in both cases as a function of the cluster size and converge to values of the corresponding infinite periodic systems. Both results show that certain magic sizes ($N = 7, 19, 37, 61, 85, 121$ and 163) have effective parameters (see figure 6.11) that are equal to those of the corresponding infinite medium. The magic clusters are schematically drawn at the top in figure 6.11.

The circular shape obtained for $N = 85, 121$, and 163 is understandable since the homogenization method is based on a comparison between T matrices of clusters and their corresponding homogenized circular cylinders, as explained in section 5.2. However, the magic sizes $N = 7, 19, 37$, and 61 indicate that the hexagonal shape gives a good representation of the sound scattering by fluid-like circular cylinders when the number of scatterers is low enough.

In order to understand the physical origin of this extraordinary phenomenon, we have analyzed the behavior of the Δ factor as a function of cluster size. Since $\widehat{M}$ in equation (B.3.12) is equal to $I - \widehat{G}$, where $\widehat{G}$ represents the multiple-scattering contribution to the scattered sound, its inverse can be approximated by:

$$\widehat{M}^{-1} = (I - \widehat{G})^{-1} \approx I + \widehat{G} + \widehat{G}\widehat{G} + \cdots \tag{6.2.1}$$

being $\widehat{G}$ an upper triangular matrix and therefore its contribution to $(\widehat{M}^{-1}_{\alpha\beta})_{11}$

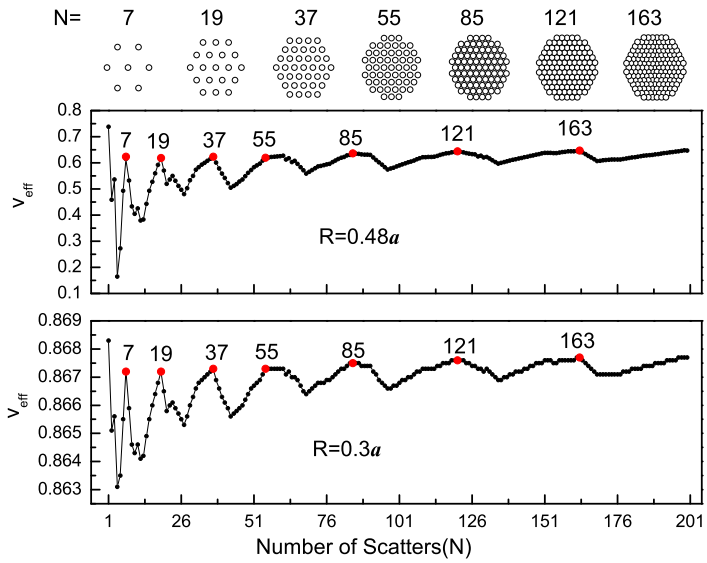

Figure 6.11: Effective speed of sound as a function of the number of cylinders.Results are shown for two different values of the cylinder's radii: R0=0.48d (upper panel) and 0.30d (lower panels), where d is the separation between cylinders. Red dots define the values that are equal to those obtained by homogenization of the infinite system. The magic clusters are schematically drawn on top.

is equal to zero. Then,

$$(\widehat{M}^{-1}_{\alpha\beta})_{11} \approx \delta_{\alpha\beta} + \sum_{\gamma}\sum_{q}(\widehat{G}_{\alpha\gamma})_{1q}(\widehat{G}_{\gamma\beta})_{q1} \tag{6.2.2}$$

where

$$(\widehat{G}_{\alpha\gamma})_{1q}(\widehat{G}_{\gamma\beta})_{q1} = \frac{R_0^4}{R_{\alpha\gamma}^2 R_{\gamma\beta}^2} e^{-2i(\theta_{\alpha\gamma}-\theta_{\beta\gamma})}(1-\delta_{\alpha\gamma})(1-\delta_{\beta\gamma}) \tag{6.2.3}$$

Now Δ can be easily cast as a summation of two terms, one (A_{2b}) containing the contribution of double-scattering events ($\alpha = \beta$) and the other (A_{3b}) containing triple-scattering events ($\alpha \neq \beta$)

$$\frac{1}{\Delta} \approx 1 + R_0^4(A_{2b} + A_{3b}) \tag{6.2.4}$$

where

$$A_{2b} \equiv \frac{1}{N}\sum_{\alpha\neq\gamma}\frac{1}{R_{\alpha\gamma}^4} \tag{6.2.5}$$

$$A_{3b} \equiv \frac{1}{N}\sum_{\alpha\neq\beta\neq\gamma}\frac{e^{-2i(\theta_{\alpha\gamma}-\theta_{\beta\gamma})}}{R_{\alpha\gamma}^2 R_{\gamma\beta}^2} \tag{6.2.6}$$

The upper panel in figure 6.12 plots A_{2b} and A_{3b}, which are both real and represent an average of the double-scattering and triple-scattering events, respectively, over the cluster size. Note that A_{3b} has minim (maxim in $-A_{3b}$) at cluster sizes corresponding to magic numbers. Moreover, these minims are enhanced when the addition of both terms is performed (lower panel). The only exception is $N = 61$ (red dashed arrow), which has a difference of less than 10% from its neighbor minimum ($N = 55$) in $A_{2b} + A_{3b}$ and none regarding their effective parameters (see figure 6.11). According to equation (6.2.6), the existence of magic numbers does not depend on the cylinder radius R_0. However, large R_0 will produce a better observability in Δ [see (6.2.4)] and thus in determining the effective parameters. It is concluded that triplescattering events are the main effect responsible for the existence of magic clusters in the homogenization of clusters to fluidlike cylinders.

An interesting application of these results is in designing metamaterials that dynamically behave as true 2D fluid-fluid composite systems. Fluid-fluid systems has been studied from the 1990s, when the existence of sonic

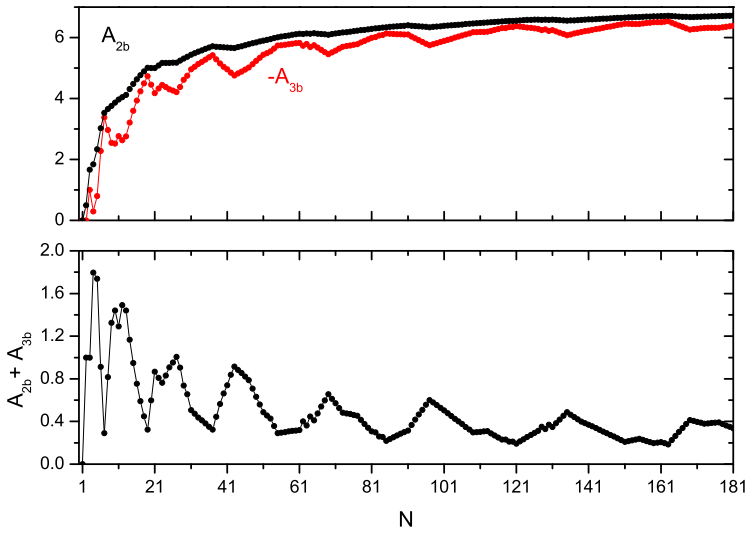

Figure 6.12: Upper panel: Behavior of the averaged double-(A_{2b}) and triple-(A_{3b}) scattering events as a function of the cluster size (see equations 6.2.5 and 6.2.6). Note that $-A_{3b}$ [red (gray) dots] has been represented for a better comparison with A_{2b}. Lower panel: The summation of both terms ($A_{2b}+A_{3b}$) shows minima at the magic sizes. The case N=61 (dashed red arrow) is the only exception.

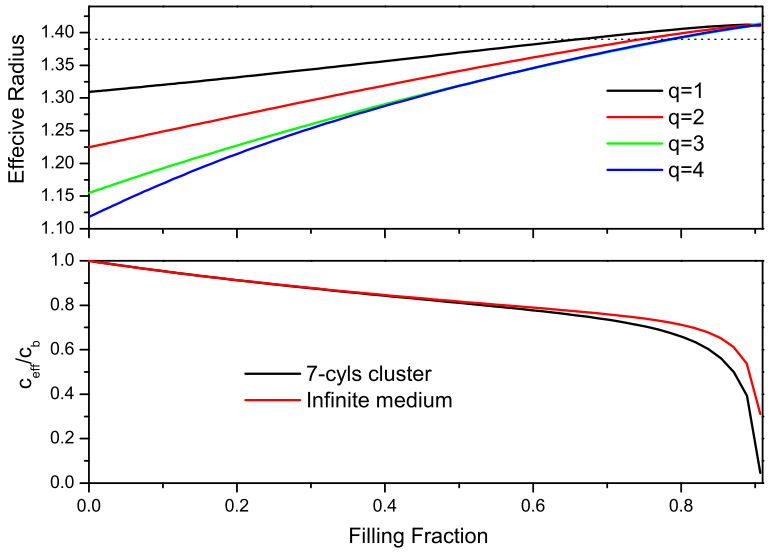

Figure 6.13: (upper panel) Effective radius for several q-values for a 7-cylinders cluster. The horizontal dotted line corresponds to the theoretical value given by (5.2.8).(lower panel) Effective speed of sound for the 7-cylinders cluster (black line) compared with that of the infinite lattice (red line). The agreement is evident in almost all the filling fractions, though there is a small deviation for high filling fractions.

bands and band gaps was derived for the simple one-dimensional fluid model [Dow92]. More recently, a 2D fluid-fluid structure consisting of a square lattice of water cylinders in a mercury background was suggested to observed negative refraction [ZL04]. Obviously, the practical realization of these structures has not been reported yet. However, below we use the smaller magic cluster as building unit to demonstrate that composite systems dynamically behaving as true 2D fluid-fluid systems are now possible.

First, let us assume that the $N = 7$ magic cluster (figure 6.10) are made of rigid cylinders such that $R_0/d = 1/3$,($f = 0.403$). The homogenization theory predicts that this cluster dynamically responds like a circular fluid-like cylinder of radius $R_{eff} = 1.39d$, and parameters $\rho_{eff} = 2.34\rho_b$, $c_{eff} = 0.843c_b$. Also, let us consider that both the magic clusters and the fluid-like

cylinders are placed at the positions of a hexagonal lattice with parameter $a = 5d$. In terms of a, $R_{eff} = 0.278a$. Figure **??** presents a comparison between the reflectance calculated for a five-layer-thick slab made of $N = 7$ magic cluster as building blocks and that obtained for a similar slab made of fluid-like cylinders with acoustical parameters equal to those obtained by homogenization of the magic cluster. The simulation shows that both reflectances are identical in a wide range of frequencies. For frequencies above $a/\lambda = 1$, the graphs start to differ slightly, and above $a/\lambda = 1.6$ the graphs are completely different.

Then, for frequencies $a/\lambda = 1.5$ and above the impinging sound distinguishes the inner structure of the cluster. This cutoff frequency represents a wavelength $\lambda \approx 3.1d$, which is consistent with the value obtained in the previous section.

6.2.2 Experimental verification

To verify the theoretical predictions previously reported, we built a sample by using 40-cm-long ceramic cylinders of 2 mm radius (R_0). The separation between cylinders in the magic clusters is 6 mm (d), and the clusters are arranged on a hexagonal lattice with lattice constant 30 mm (a). The sample defines an acoustic slab five rows thick that contains ten clusters in each row. The size of this sample is large enough to expect a fair comparison between measurements and multiple-scattering simulations [SHCSD03]. Also, since the cylinders are made of alumina material ($\rho_{cyl} = 3860kg/m3$), their huge acoustic impedance relative to air makes them practically impenetrable to sound, and the rigid approach ($\rho_{cyl} = \infty$) employed in the simulations is justified. Phase-delay and reflectance measurements on the sample were performed in an anechoic chamber.

To measure the phase delay $\Delta\Phi$, we used a setup consisting of a loudspeaker and two microphones [RCSP$^+$99]. The microphones are located at each side of the sample, each one put at an equal distance $d_1 = d_2 = 10cm$ from its corresponding surface. The wave number inside the crystal $k(\nu)$ can be determined from $\Delta\Phi$ through the equation [RCSP$^+$99, RI98]

$$\Delta\Phi = k_0(d_1 + d_2) + k(\nu)L, \tag{6.2.7}$$

where $L(= 13cm)$ is the thickness of the crystal, and k_0 is the wave number

of the impinging wave traveling in air; i.e., $k_0 = 2\pi\nu/c_{air}$, and the measured $c_{air} = 344 \pm 9m/s$. The left panel in figure 6.14 shows the measured $k(\nu)$ folded into the first Brillouin zone and the band structure calculated along the direction ΓX of a hexagonal lattice of fluid cylinders with acoustic parameters obtained from the homogenization of that infinite lattice.

The reflectance $\mathcal{R}$ of the slab is measured by using two microphones put in front of the slab (at a distance of 7 cm from its surface) separated from each other by $\ell = d_2 - d_1 = 1.1cm$. The reflection coefficient is [CB80]

$$r = e^{-2ikd_1} \frac{S_{11} - S_{12}e^{ik\ell}}{S_{11} - S_{12}e^{-ik\ell}} \tag{6.2.8}$$

where d_1 (d_2) is the distance from microphone 1 (2) to the crystal, surface and the quantities S_{11} and S_{12} are the autospectrum in microphone 1 and the cross spectrum between the microphones, respectively. The measured $\mathcal{R} = |r|^2$ is plotted as a function of frequency and compared with that calculated by multiple-scattering theory in the right panel of figure 6.14. For frequencies lying in the band gap, the experimental reflectance obtained is larger than 1, due to multiple reflections between the loudspeaker and the crystal, and it disappears when the crystal is slightly rotated. The bandgap center, which is at $\nu \approx 6kHz$, fairly corresponds to the reduced frequency $a/\lambda \approx 0.55$ determined by multiplescattering simulations. Let us point out that this value corresponds to a wavelength that in terms of d(the separation between cylinders in the magic cluster) is five times lower than that expected for a uniform lattice with lattice period d.

6.3 Summary

In this chapter the formulas derived in chapter 5 have been applied to obtain the effective parameters for several circular clusters of rigid cylinders. The method has also been applied to study disordering effects in the lattice, showing that the effective parameters deviated from that of the ordered lattice only for large lling fractions. It can be concluded that the method here reported is a useful tool to design acoustic metamaterials with prexed acoustic parameters, which can be used to fabricate refractive devices or new structures able to demonstrate fundamental properties of composite uids.

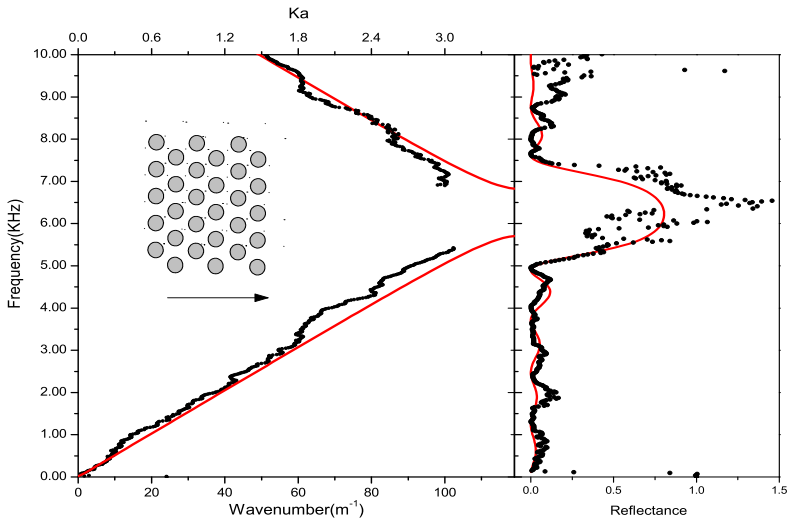

Figure 6.14: Left: Sonic band structure of the acoustic slab schematically drawn in the inset. The structure calculated by multiple, scattering theory (red solid line) is compared with the one obtained by phase-delay measurement (black dots). Right: Reflectance calculated (red solid line) and measured (black dots). The calculations assume that the slab is made of fluid-like cylinders with parameters determined by homogenization of the smallest magic cluster (N=7).

Also, experimental evidence of the existence of 2D magic clusters has been reported, showing that they dene a kind of acoustic metamaterial with fluidlike properties. Moreover, from the analysis of the sound scattering by magic clusters it has been concluded that its existence is a pure geometrical phenomenon and thus of a general nature. Therefore a similar phenomenon is expected to occur for any wave process, such as scattering of electromagnetic waves by clusters of dielectric rods.

This chapter is based on:

1. Daniel Torrent, Andreas Håkansson, Francisco Cervera, and José Sánchez-Dehesa. *Homogenization of two-dimensional clusters of rigid rods in air*. Physical Review Letters, 96(20):204302, 2006.

2. Daniel Torrent and José Sánchez-Dehesa. *Effective parameters of clusters of cylinders embedded in a nonviscous fluid or gas*. Physical Review B (Condensed Matter and Materials Physics), 74(22):224305, 2006.

3. Daniel Torrent and José Sánchez-Dehesa. *Evidence of two-dimensional magic clusters in the scattering of sound*. Physical review. B, Condensed matter and materials physics, 75(24):241404–, 2007.

Chapter 7

Designing Acoustic Metamaterials

It has been shown that two-dimensional arrays of rigid or fluidlike cylinders in a fluid or a gas define, in the limit of large wavelengths, new class of acoustic materials non existing in nature that can be called like "acoustic metamaterials". The effective parameters (sound velocity and density) of these metamaterials can be tailored up to a certain limit. This section goes a step further by considering arrays of solid cylinders in which the elastic properties of cylinders are taken into account. It is shown that both effects broaden the range of acoustic parameters available for designing metamaterials. As a potential application of the proposed metamaterials, gradient index lens are presented and optimized for airborne sound (i.e. a sonic Wood lens) whose functionality are demonstrated by multiple scattering simulations.

7.1 Phase diagrams and acoustic metamaterials

The homogenization method can be also applied to clusters made of solid cylinders and, therefore, the full elastic properties of cylinders are taken into account. It is shown here that these clusters lead to effective isotropic media in which sound travels with a speed that can be larger or smaller than that of the surrounding medium depending on the elastic parameters and the filling fraction of the cylinders in the lattice. Moreover, phase diagrams are

introduced to establish (in the ρc-plane) the metamaterial properties as a function of the elastic parameters of cylinders and its filling fraction in the corresponding sonic crystal.

In chapter 5 was shown that the elements $\widehat{T}_{00}$ and $\widehat{T}_{11}$ are enough to characterize the homogenization of sonic crystals based on fluid or elastic cylinders. It has been also shown that $\widehat{T}_{00}$ and $\widehat{T}_{11}$ elements of a solid cylinder are equal to those of a fluid-like cylinder with sound speed given by

$$c_a \equiv \sqrt{c_\ell^2 - c_t^2} \tag{7.1.1}$$

where c_ℓ and c_t are, respectively the longitudinal and transversal velocities of the actual elastic cylinder. Therefore, the effective parameters of sonic crystals made of 2D binary solid(cylinders)fluid(background) composites can be obtained from the general expressions already reported for 2D fluidfluid composites in chapter 5.

In what follows, it will be discussed the behavior (in the homogenization limit) of c_{eff}, the effective velocity of sound propagating in a sonic crystal consisting of a square distribution of solid cylinders in water as a function of the filling fraction f . In regards to the effective mass density, ρ_{eff}, its behavior is monotonic between that of the background ρ_b at $f = 0$ and a final ρ_{CP} (that approaches that of the solid, ρ_a) at the condition of close-packing, $f = f_{CP}$. This behavior is of little interest and will not be discussed here.

Hereafter, an over-lined variable denotes the corresponding quantity normalized to that of the background; for example, $\bar{\rho} \equiv \rho/\rho_b$ and $\bar{c} \equiv c/cb$.

In brief, at long wavelengths, a 2D array of elastic cylinders embedded in a fluid or a gas defines an acoustic metamaterial in which sound travels with a speed c_{eff} determined by ((5.2.20)):

$$\frac{1}{\overline{c}_{eff}^2} = \left[\frac{f}{\overline{\rho}_a \overline{c}_a^2} + (1-f)\right] \cdot \frac{\overline{\rho}_a(\Delta + f) + (\Delta - f)}{\overline{\rho}_a(\Delta - f) + (\Delta + f)}, \tag{7.1.2}$$

where c_a is the fluid-like speed of sound of the solid cylinder defined in (7.1.1) and the Δ factor, as explained before, contains information about the material parameters of cylinders, their positions in the 2D space and their mutual interaction. As in the case of 2D fluidfluid composites, the value of Δ is different from 1 only for large f.

Figure 7.1 plots the three possible behaviors expected for c_{eff} as a function of f. When the cylinders are made of lead (Pb), c_{eff} is always lower

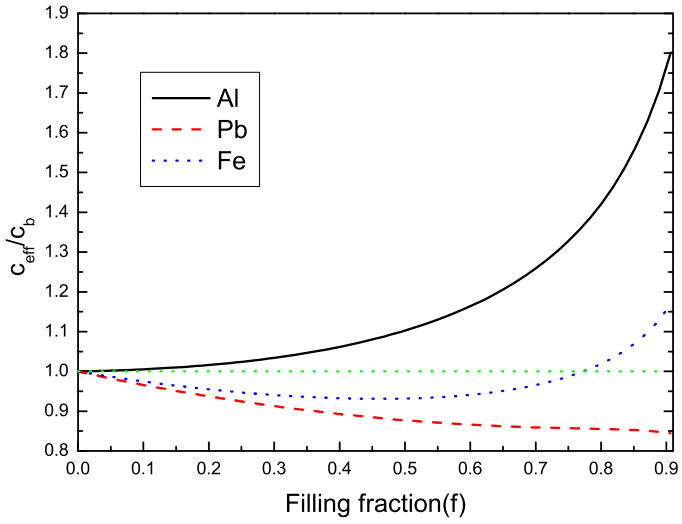

Figure 7.1: Speed of sound in a 2D acoustic metamaterial consisting on a square configuration of solid cylinders in water. The calculated effective sound speed, c_{eff}, relative to that of water, c_b is plotted as a function of the filling fraction, f. Three different behaviors are possible when f increases: (1) a continuous decreasing of velocity as in the case of Pb, (2) a continuous increasing of velocity as in the case of aluminum (Al), and (3) an initial decreasing that with increasing f becomes in a velocity larger than the background as for iron (Fe) cylinders. The horizontal dashed line is a guide for the eye that defines the condition $c_{eff} = c_b$.

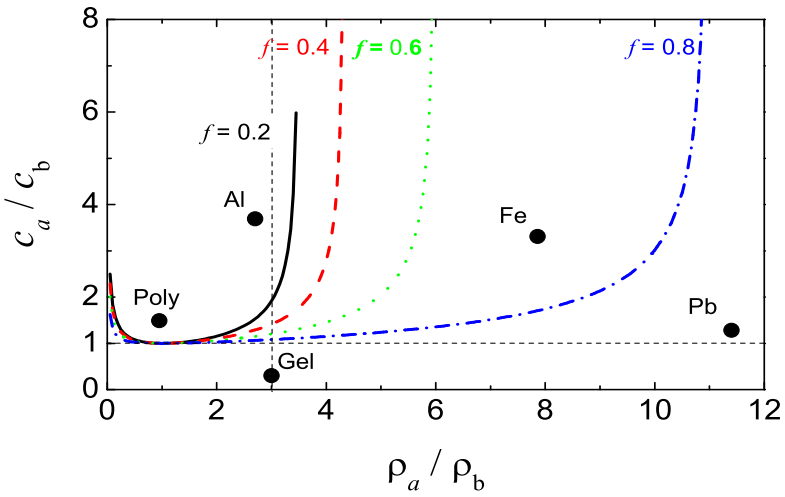

Figure 7.2: $c\rho$ phase diagram of acoustic metamaterials based on sonic crystals made of a square configuration of one single component full elastic cylinders. For the given fraction of volume occupied by the cylinders in the lattice (f), the corresponding color line separates the region where the metamaterial has a speed of sound relative to that of the background ($\overline{c}_{eff}$) lower than one (upper-left region) or higher than one (bottom-right region). The symbols plot the parameters of several solid materials. It can be concluded that, for example, the propagation of sound in metamaterials based on lead (Pb) or aerogel (Gel) cylinders will always take place at a speed lower than that of the background, while those using Aluminum (Al) or polyethylene (Pol) will be larger than in the background. However, for the case of iron (Fe) both behaviors could be possible, being the behavior depending of the filling fraction of the corresponding lattice. The horizontal (vertical) dashed line is a guide for the eye and defines the condition c_a=1 ($\rho_a = 3$)

than one; a behavior similar to that found for rigid cylinders, and it is due to the huge acoustic impedance of Pb relative to that of water. However, for the Al case, c_{eff} is always higher than one due to the low ratio of acoustic impedances Z_a/Z_b. Finally, the case of iron (Fe) cylinders is an intermediate case; c_{eff} is lower than one for low f and higher than 1 for f large enough. The parameters of the elastic materials employed in the calculations are listed in table 7.1.

As explained above, a variety of behaviors is expected for c_{eff} depending on the material composition of cylinders and their filling fraction in the SC. This phenomenon motivates the introduction of some kind of phase diagrams for 2D elastic-fluid composites. It turns out that the condition $c_{eff} > 1$ leads to the following relation (assuming $\Delta = 1$) between the cylinder's fluidlike speed of sound, c_a, its density ρ_a and f

$$\overline{c}_a^2 > \frac{1}{\overline{\rho}_a} \cdot \frac{(1-f)+(1+f)\overline{\rho}_a}{(3-f)-(1-f)\overline{\rho}_a} \tag{7.1.3}$$

The color lines in figure 7.2 represent the separation between the two possible 'phases' of the metamaterial according to the value of c_{eff} (higher or lower than 1). They are plotted for four different f in the $\rho_a c_a$-plane. It is shown that these lines are always above the region $c_a = 1$, which means that c_{eff} cannot obtain a value higher than one if c_a is lower than that of the surrounding medium.

Note that all the lines become vertical in the limit

$$\overline{\rho}_a \to \frac{3-f}{1-f} \tag{7.1.4}$$

Thus, $c_{eff} < 1$ when $c_a \geq 3$ and $\rho_a \geq (3-f)/(1-f)$. In more general terms, it can be said that lines associated to a given f separate the region in which the metamaterial behaves with $c_{eff} > 1$ (upper-left region) from the one in which $c_{eff} < 1$ (lower-right region).

The black dots in figure 7.2, represent the elastic properties of several materials commonly used in building sonic crystals. According to their positions in the $\rho_a c_a$-plane, it is concluded that:

1. sonic crystals made of Pb or Gel will always result in metamaterials with $c_{eff} < 1$,

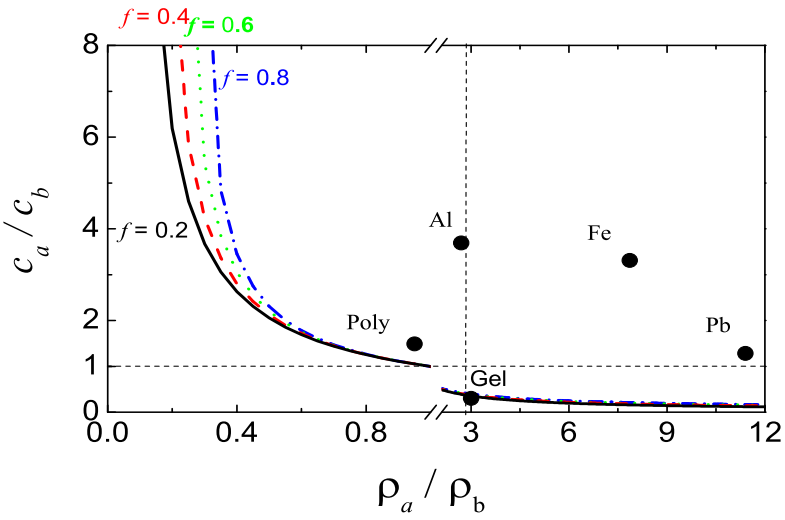

Figure 7.3: $c\rho$ phase diagram of acoustic metamaterials based on sonic crystals made of a square configuration of one single component elastic cylinders. For the given filling fraction, f, the corresponding color line separates the region where the metamaterial has an acoustic impedance relative to that of the background ($\overline{Z}_{eff}$) larger than one (upper-right region) or smaller than one (bottom-left region).

Table 7.1: Parameters of the elastic materials studied in this work. The density, ρ_a, and the fluidlike velocity, $c_a = \sqrt{c_\ell^2 - c_t^2}$, are normalized to those of water. However, the parameters for the silica aerogel (last column) are normalize to air.

	Poly	Al	Fe	Pb	Gel
$\overline{\rho}_a$	0.95	2.70	7.86	11.40	3.00
$\overline{c}_a$	1.74	3.69	3.31	1.28	0.30

2. if the cylinders in the SC are made of Al or polyethylene (Poly), their associated metamaterials will always have $c_{eff} > 1$ and

3. for cylinders made of Fe, the behavior of c_{eff} depends on f , as was already shown in figure 7.1.

The possibility of having metamaterials with matching of impedance with the embedded background is being looking at in many fields because of its potential application in novel devices. For example, in the field of optics a thin-film metamaterial with such a property has been recently discovered [XSK$^+$07]. Also, it is known that anti-reflective nanostructures have been naturally developed to enhance the photon collection efficiency of the visual system in animals [FN01]. If such an anti-reflective effect occurs in acoustics, the transmittance at the interface between the metamaterial and background will be equal to one, although sound propagates with different speed in each medium. This property is of paramount importance in order to make useful acoustic devices like, for example, high-efficient ultrasonics transducers or powerful sonic lenses that collect all the impinging sound.

Figure 7.4 plots the corresponding phase diagram for Z_{eff}. The color lines represent the condition of matching of impedances, $Z_{eff} = 1$, for several values of f . The condition Z_{eff} is very restrictive and is very difficult to achieve for common elastic materials in bulk, only the silica Gel (a material difficult to handle) almost satisfies this condition. The acoustic are plotted as black dots in figure 7.3 and are obtained from the acoustic values given in table 7.1. Note that figure 7.3 shows that the condition Z_{eff} could be achieved by 2D sonic crystal only if the solid cylinders are made of materials having the same property (i.e. $Z_a \approx 1$). However, now will be demonstrated that this drawback can be overcome by using metamaterials based on a two

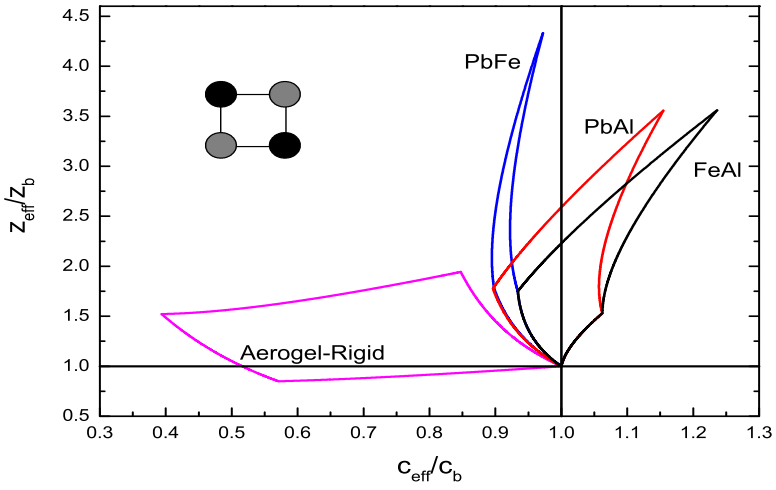

Figure 7.4: Zc phase diagram of acoustic metamaterials based on sonic crystals made of square arrangements of two types of solid cylinder in a background. A square lattice configuration like that displayed in the inset generates an isotropic metamaterial. The range of available relative acoustic impedances, Z_{eff}, and sound speed, c_{eff} in the given background are defined by the area enclosed by lines with equal colors. The calculations corresponding to combinations of two metals have employed water as the background. instead, the mixture of aerogel and rigid cylinders are embedded in air. Note that the mixtures of aerogel and rigid cylinders lead to metamaterials that perfectly match the air impedance. The horizontal (vertical) thin line is a guide for the eye and defines the condition $\overline{Z}_{eff}$ =1 ($\overline{c}_{eff} = n_{eff}^{-1}$ =1).

component sonic crystal.

Let us consider mixtures of two different elastic cylinders of radii R_1 and R_2, respectively, that are arranged in a square configuration of side a (see inset in figure 7.4). The respective filling fractions are $f_1 = \pi R_1^2/(2a2)$ and $f_2 = \pi R_2^2/(2a2)$. If their fluidlike parameters (see section 2) are ρ_1, B_{a1} and ρ_2, B_{a2}, the resulting metamaterial has parameters determined from:

$$\zeta_{eff} = \zeta_1 f_1 + \zeta_2 f_2, \tag{7.1.5}$$

$$\eta_{eff} = \eta_1 f_1 + \eta_2 f_2, \tag{7.1.6}$$

where $\zeta_i \equiv (1 - B_b/B_{ai})$ and $\eta_i \equiv (\rho_i - \rho_b)/(\rho_i + \rho_b)$, for $i = 1, 2$. Moreover, $\zeta_{eff} \equiv (1 - B_b/B_{eff})$ and $\eta_{eff} \equiv (\rho_{eff} - \rho_b)/(\rho_{eff} + \rho_b)$. From these expressions:

$$\frac{1}{B_{eff}} = \frac{1-f}{B_b} + \frac{f_1}{B_{a1}} + \frac{f_2}{B_{a2}}, \tag{7.1.7}$$

$$\rho_{eff} = \frac{1 + f_1\eta_1 + f_2\eta_2}{1 - f_1\eta_1 - f_2\eta_2}\rho_b, \tag{7.1.8}$$

$$c_{eff} = \sqrt{\frac{B_{eff}}{\rho_{eff}}}, \tag{7.1.9}$$

f being the total volume fraction occupied by both cylinders, $f = f_1 + f_2$.

The question now is, could these metamaterials accomplish the criterion of impedance matching with the surrounding background? To answer this question, let us look at figure 7.4 where the effective impedance Z_{eff} is plotted against c_{eff} for several sonic crystals made of pairs of selected materials. The calculations involving two types of metal cylinders (PbFe, PbAl and FeAl) are embedded in water while the sonic crystals made of Gel and rigid cylinders are in air. Results have been obtained under the approach $\Delta = 1$. On such a Zc diagram, each point on a curve obtained for a certain value f , which has associated a corresponding f_1 and f_2, represents a possible metamaterial. The various curves obtained by changing f_1 and f_2 define an area enclosed by the parametric lines $Z_{eff}(f_1, f_2)$ and $c_{eff}(f_1, f_2)$. Since the larger cylinders considered have radii $R_i = a/2$, the four corners of a selected area correspond to values $(f_1 = 0, f_2 = \pi/8)$, $(f_1 = \pi/8, f_2 = \pi/8)$, $(f_1 = \pi/8, f_2 = 0)$ and $(f_1 = 0, f_2 = 0)$. The last one is always centered at the point $(1, 1)$ in the phase diagram. Note that only the combination of Gel

and rigid cylinders in air leads to a metamaterial that passes through the line $Z_{eff} = 1$. In other words, only this composite system is able to create a metamaterial with perfect matching of impedance with the background, which is air. Moreover, note that this remarkable property is accomplished in a broad range of filling fractions (f_1, f_2), which opens the possibility of having metamaterials transparent to airborne sound but with different refractive index.

The reflectance of a ten-layer slab made of a mixture of Gel cylinders ($f_1 = 0.015$) and rigid cylinders ($f_2 = 0.141$) put in a square lattice is shown in the lower panel of figure 7.5 as an example. The slab is oriented along the diagonal direction of the square lattice (i.e. along the ΓM direction); layer planes with the same type of cylinders alternate with a separation of $a/\sqrt{2}$. Note how the reflectance is almost zero or negligible in a broad range of frequencies below the first bandgap. This structure is one of many possible ones that accomplish the condition $Z_{eff} = 1$ in figure 7.4. As a comparison, the cases of slabs with the same number of layers but with one single type of cylinders, rigid or aerogel, have also been plotted. Note that for the mixture, the zero-reflectance condition is accomplished for a broad range of wavelengths; i.e., for $\lambda \geq 4a[\omega a/(2\pi c_b) \leq 0.25]$, which is the cutoff for the validity of the homogenization.

The phenomenon described above is of paramount importance because it can be used, for example, to design anti-reflective acoustic coatings, which would be similar to those recently developed for optics [XSK+07] and to build highly effective sonic lenses. Particularly, the next section shows that gradient-index sonic lenses are possible thanks to the predicted acoustic transparency (zero-reflectance) of some compound metamaterials.

7.2 Gradient index lens

Acoustical refractive devices for airborne sound similar to those existing for optical lightwaves are not possible because solid materials are not transparent to sound waves. Also, since the sound speed of solids is larger than in air, a converging lens would have a concave rather than a lenticular shape. However, when dealing with arrays of hard scatterers embedded in air (which act as a low reflective medium at large enough wavelengths) the incident

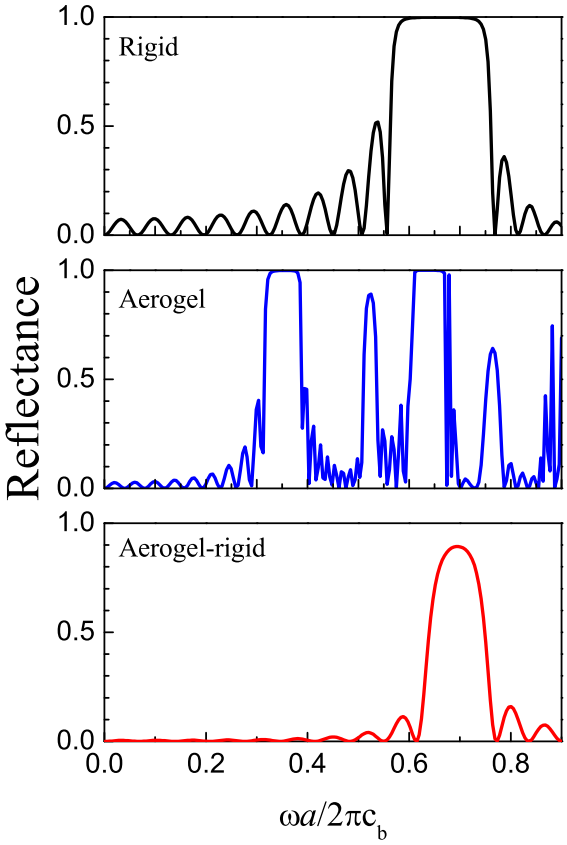

Figure 7.5: Reflectance of three different ten-layer slab of cylinders distributed in a square lattice of lattice period a embedded in air and oriented along the ΓM direction. The slabs are made of rigid cylinders (top panel), aerogel cylinders (middle panel) and a mixture of both (lower panel). Note how the mixture has a negligible reflectance for low frequencies.

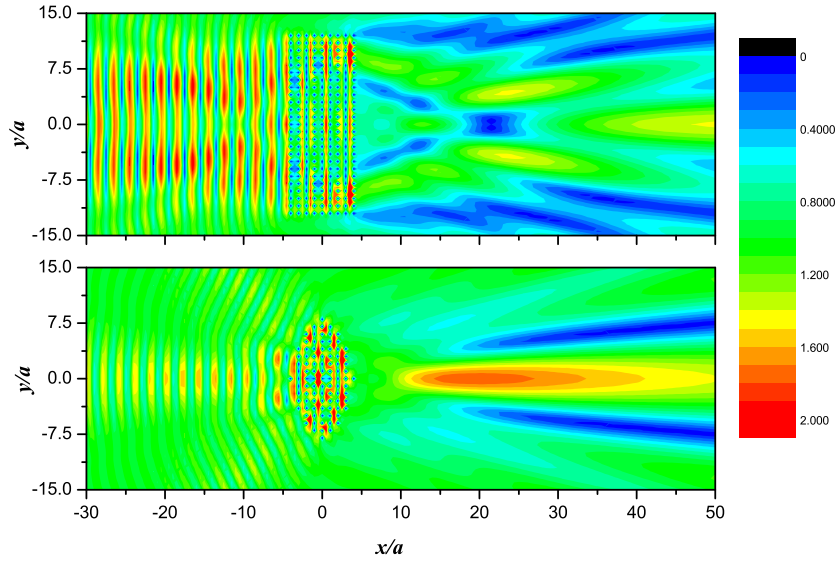

Figure 7.6: Comparison between the acoustic field scattered by a finite rectangular slab (upper panel) and a circular lens (lower panel). The focusing effect is evident in the second case, but strong diffracting effects are present in both situations.

sound wave and the scattered waves are superimposed in such a way that the sound propagates at a reduced speed. Thus, Meyer and Neumann [EG72] were aware of these two effects and constructed a converging lens by using disks as scatterers. More recently, Cervera and coworkers [CSSP$^+$01] reported a full demonstration of the focusing effect by using circular-shaped cylinders as scatterers.

In figure 7.6 can be shown the difference between the field scattered by a simple rectangular slab and a curved slab. The focusing effect is evident for the case of the curved lens, though there are some diffracting effects in both situations.

The zero-reflectance property of aerogel-rigid mixed lattices described before can be used, for example, in the construction of high effective lenticular-shaped sonic lenses by employing the procedure in [CSSP$^+$01].

However, thanks to the fact that the acoustic refractive index of the SC can be tailored without loosing the zero-reflectance property, here we present the design of a gradient-index sonic lens whose functionality is based on the same effect already applied in optics [W78].

This novel acoustic device fully exploits the powerful properties of metamaterials based on arrays of aerogel and rigid cylinders analyzed in the previous section.

Probably the most interesting type of gradient index lens is one for which the variation in refractive index exhibits cylindrical symmetry about the lens axis, i.e. n varies only as a function of the perpendicular distance to the lens axis. For the simplest case, where the ends of the cylinder are planes perpendicular to the axis, the lens is referred to as a Wood lens, after the original inventor. As in the more general case of optics, we proposed here a sonic Wood lens with a parabolic variation of the acoustic refractive index (see left panel in figure 7.8), thus

$$n_{eff}(y_\ell) = n^0_{eff} - (n^0_{eff} - 1)y^2_\ell/(h/2)^2, \tag{7.2.1}$$

where n^0_{eff} is the refractive index on the lens axis, h is the total length on the perpendicular direction to the lens axis (i.e. $y-$axis), and y_ℓ defines the positions along the $y-$axis of the cylinders.

In figure 7.7 the comparison between the focusing effect of a curved lens and a gradient index lens is plotted. The gradient index lens has the ad-

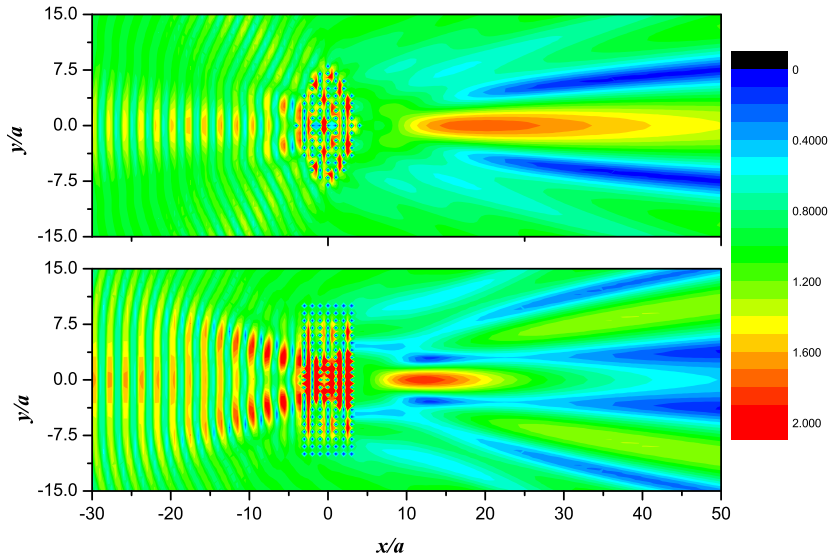

Figure 7.7: Comparison between the focusing effect of a circular lens (upper panel) and a gradient index lens (lower panel). Both systems can focus sound on the right hand side, but the geometry simplification in the gradient index lens is evident.

vantage of geometry simplification, because it is not always possible to cut a square slab with circular shape due to the discrete nature of the lattice.

The designed lens is nine layers thick and consists of twenty rows of cylinders ($h/2$ =$10a$) in the vertical direction with decreasing values of their radii, R_i. Maximum values correspond to the axial row (y_ℓ =0), where R_1 =$0.2a$ (rigid), R_2 =$0.3a$ (aerogel) and n_{eff} =1.31. Minimum values are achieved in the upper and lower rows ($y_\ell = \pm 10a$), where R_i =0 and $n_{eff}^{(}0)$ =1. The radius of a given type of cylinders at any given row y_ℓ is determined by solving (7.1.5) and (7.1.6) under the condition $Z_{eff} = 1$, which gives the following set of coupled linear equations:

$$\zeta_1 f_1 + \zeta_2 f_2 = 1 - n_{eff}(y_\ell) \tag{7.2.2}$$

$$\eta_1 f_1 + \eta_2 f_2 = -\frac{1-n_{eff}(y_\ell)}{1+n_{eff}(y_\ell)}, \tag{7.2.3}$$

from which R_1 and R_2 are obtained.

The focusing effect of the proposed lens is shown in the right panel of figure 7.8 for the case of a wavelength λ =$4a$. The simulation has been performed by the multiple scattering method developed in [SHCSD03,GY03], where no viscosity effects are taken into account. This lens outperforms that of broadband lenticular-shaped lens based on rigid cylinders [CSSP$^+$01, GY03]. Thus, the ten layer proposed lens obtains a maximum intensity of 8.8 dB at the focal point while the lenticular-shaped lens get only 6.6 dB by using nineteen layer thick lens.

7.3 Summary

This chapter has shown that a great variety of acoustic metamaterials can be designed by using SC consisting of 2D arrangements of solid cylinders in a uid or gas. Also, for the case of two component cylinders, it has been introduced Zc phase diagrams that have allowed to nd metamaterials with perfect matching of impedance with air.

As an application, it has been reported a sonic Wood lens in which a parabolic variation of the refractive index is achieved by changing the cylinders radii in the direction perpendicular to the lens axis. Its focusing property

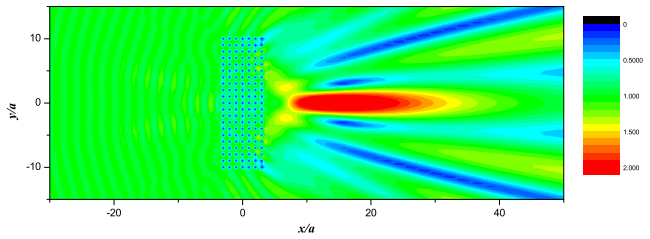

Figure 7.8: Sound focusing by a transparent acoustic gradient index lens. The condifion $Z_{eff} = 1$ has been imposed through all the surface and all the acoustic energy is located around the focus of the lens.

has been demonstrated by multiple scattering simulations and it outperforms the functionality of other lenses previously reported.

In summary, this chapter shows that isotropic acoustic metamaterials with a broad range of possible parameters are now possible by simple means.

This chapter is based on:

1. Daniel Torrent and José Sánchez-Dehesa. *Acoustic metamaterials for new two-dimensional sonic devices*. New Journal of Physics, 9(9):323, 2007.

Chapter 8

Anisotropic fluids and acoustic cloaking

Here the anisotropic properties of periodic media already reported in Chapter 5 are analyzed. First, basic 2D lattices are studied and wave propagation through this media is analyzed. Finally, the problem of acoustic cloaking of objects is analyzed and solved with 1D periodic acoustic media.

8.1 Anisotropic fluids

We see that anisotropy in (5.1.15) comes from factor Γ, which is given in (5.1.13). The main contribution to the anisotropy Γ comes from $\Gamma^{(0)}$ [see (B.2.30)]. The value of $\Gamma^{(0)}$ given in (B.2.30) allows to introduce the so called parameter of anisotropic strength A_Γ, which is defined as:

$$A_\Gamma \equiv \left| \sum_{h \neq 0} \frac{J_3(Q_h R_{min})}{Q_h^3} e^{-2i\theta_h} \right|, \tag{8.1.1}$$

A_Γ is here analyzed as a function of the ratio a_2/a_1 and the angle ϕ (see section 3.3).

Figure 8.1 plot A_Γ for several values of the ratio a_2/a_1 as a function of the angle between lattice vectors. The calculation predict that large anisotropy in sound speed and mass density should be expected for the lattices where this A_γ takes large values. The predictions are corroborated by the results obtained for c_{eff} and ρ_{eff} as it is shown below.

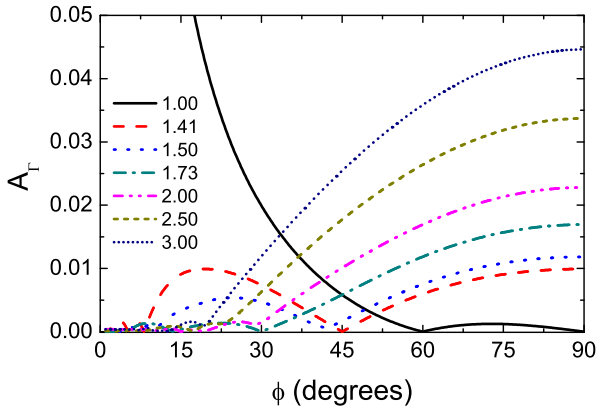

Figure 8.1: Anisotropy factor, A_Γ, which is defined in 8.1.1, for several values of the ratio, a_2/a_1, as a function of the angle, ϕ, between lattice vectors. Anisotropy disappears for the 2D isotropic lattices (square and hexagonal) corresponding to parameters described in Table 1.

8.1.1 Effective speed of sound

The strength of anisotropic effects predicted by A_Γ is analyzed in figure 8.2, where the diagonal elements of the sound speed tensor, $\sqrt{\bar{c}^2_{xx}}$ and $\sqrt{\bar{c}^2_{yy}}$, are plotted for the case of rigid cylinders in three different anisotropic lattices and compared with the corresponding results for the hexagonal lattice, which is isotropic. Note that the maximum possible value for R_a, which is determined by the touching condition between neighboring cylinders, depends of the lattice geometry. It is seen in figure 8.2 that the more anisotropic behavior corresponds to the case $a_2 = 2a_1$ and $\phi = 75^o$, which has the larger value of A_Γ (see figure 8.1).

Isotropic lattices

The case of isotropic lattices deserves special attention because results has been published by two different research teams [KAG03, MLWS06]. The solution for this case is easily obtained from matrix (5.1.14) by introducing the isotropy condition, that is Γ =0. After straightforward manipulations,

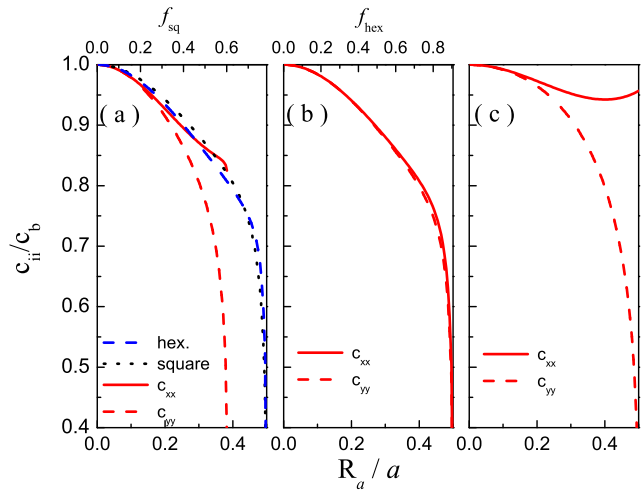

Figure 8.2: Diagonal components of the speed of sound tensor, $\sqrt{(c_{ii}/c_b)^2}$ as a function of the cylinder radius, R_a for the three anisotropic lattices: (a) $a_2 = a_1$, $\phi = 45^o$; (b) $a_2 = a_1$, $\phi = 75^o$; (c)$a_2 = 2a_1$, $\phi = 75^o$. Results for the isotropic lattices (hexagonal and square) are also depicted in (a) for comparison. The filling fraction f for the square (sq) and hexagonal (hex) lattices are also shown to emphasize that f is determined by R_a and the symmetry of the lattice.

the secular equation can be cast in:

$$det\begin{vmatrix} \Delta-\eta\frac{\bar{c}_{eff}^2}{1-\bar{c}_{eff}^2}f & i\eta\frac{\bar{c}_{eff}}{1-\bar{c}_{eff}^2}f & \eta\frac{1}{1-\bar{c}_{eff}^2}f \\ -i\zeta\frac{\bar{c}_{eff}}{1-\bar{c}_{eff}^2}f & 1-\zeta\frac{\bar{c}_{eff}^2}{1-\bar{c}_{eff}^2}f & i\zeta\frac{\bar{c}_{eff}}{1-\bar{c}_{eff}^2}f \\ \eta\frac{1}{1-\bar{c}_{eff}^2}f & -i\eta\frac{\bar{c}_{eff}}{1-\bar{c}_{eff}^2}f & \Delta-\eta\frac{\bar{c}_{eff}^2}{1-\bar{c}_{eff}^2}f \end{vmatrix} = 0. \tag{8.1.2}$$

The analytical solution of this equation is:

$$\bar{c}_{eff}^2 = \frac{\Delta - f\eta}{\Delta + f\eta}\cdot\frac{1}{1+f\zeta}, \tag{8.1.3}$$

This solution contains relevant terms of multiple scattering interaction that has been forgotten in the solution given by Mei and coworkers [MLWS06], who were also working in the framework of multiple scattering theory. Particularly, ours results reduced to those in [MLWS06] when we impose in (8.1.3) the condition $\Delta = 1$. In other words, when its is assumed that multiple scattering interactions are neglected. However, it has been shown by us [THCSD06,TSD06] that this condition is only valid at low filling fractions. The parameter Δ is the responsible of the abrupt decreasing of speed of sound when the filling fraction approaches the condition of close-packing as shown in figure 8.2. This behavior that is not shown in figure 1 of [MLWS06]. Our results fully agree with those found in Krokhin *et al.*, which used a plane wave expansion (see figure 1 in [KAG03]).

Wave propagation

Wave propagation in this type of materials is complex and it should be studied in a separated work, however it can be introduced here looking at the so called refractive index ellipsoid, which here we introduced in acoustics in a manner similar to that in optics:

$$n_{eff}(\theta) = \frac{1}{\sqrt{c_{eff}^2(\theta)}} \tag{8.1.4}$$

Two index ellipsoids have been plotted in polar coordinates in Figs. 8.3 and 8.4 for two different anisotropic lattices and for several values of cylinder's radius R_a. In Fig.8.3 must be note that the principal axis are rotated 22.5° with respect to the $x-$axis of the lattice. However, it is remarkable how

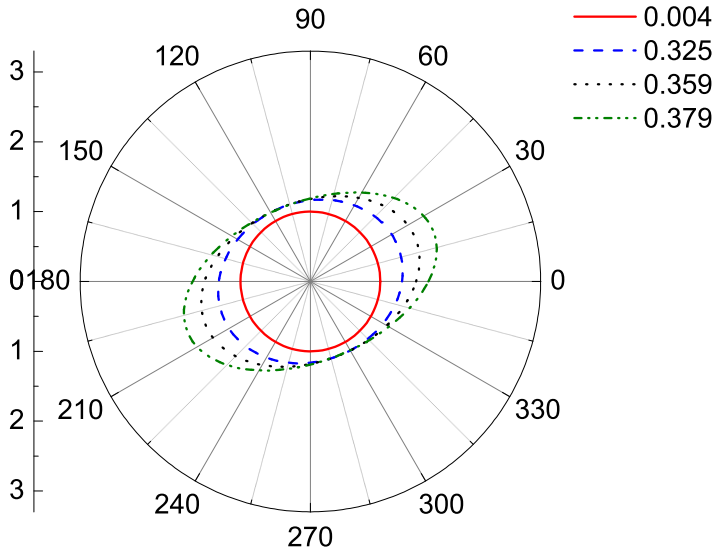

Figure 8.3: Index ellipsoid $n_{eff}(\theta)$ for the anisotropic lattice defined by $a_2 = a_1$ and $\phi = 45^o$ (see figure for several values of cylinder radius in reduced units, R_a/a. Note that the ellipsoid longer axis follows the direction that bisects the angle $\phi = 22.5^o$.

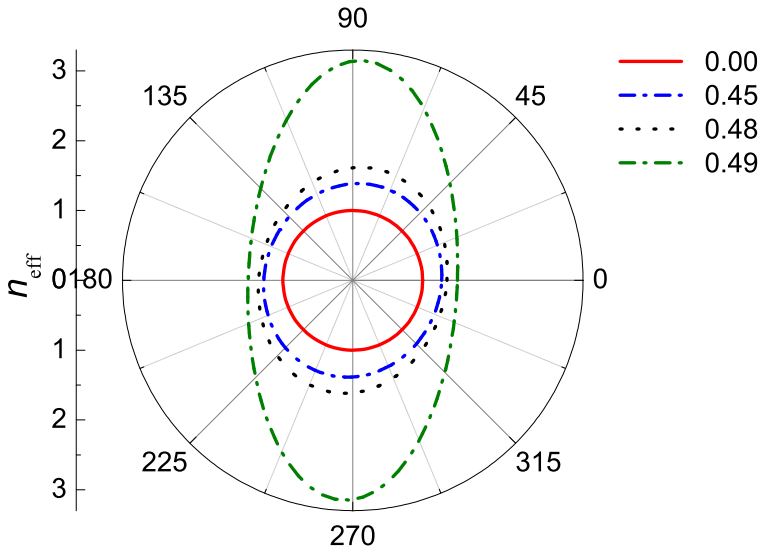

Figure 8.4: Index ellipsoid $n_{eff}(\theta)$ for the anisotropic lattice defined by $a_2 = 2a_1$ and ϕ =30° and for several cylinder radius R_a. Note how the rotation of the principal axis depends of R_a (i.e., it is a function of the lattice filling fraction).

for the lattice studied in Fig.8.3 the principal axis are slightly rotated with respect to the $xy-$axis, and more important the tilted angle depends on the filling fraction of the lattice. The wave propagation will respond to the index ellipsoid, in such a way that slow propagation is expected along the direction defined by the longer side of the ellipsoid and faster propagation will take place along the direction defined by the smaller side of ellipsoid.

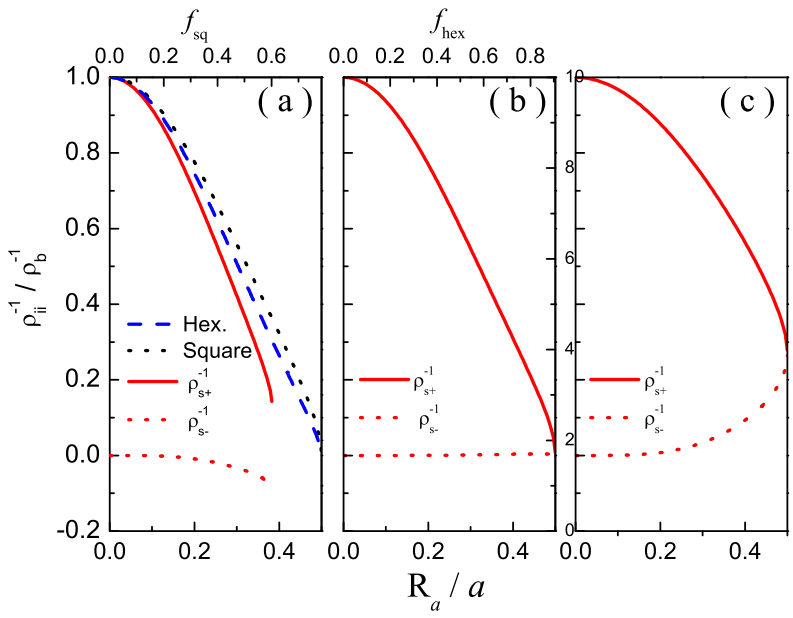

Figure 8.5: Reciprocal of the effective density tensor as a function of the radius of cylinders in reduced units (R_a/a) for three different anisotropic lattices: (a) $a_2 = a_1$, $\phi = 45^o$; (b) $a_2 = a_1$, $\phi = 75^o$; (c)$a_2 = 2a_1$, $\phi = 75^o$. Results for the 2D isotropic lattices (hexagonal and square) are also shown in (a) comparison.

8.1.2 Effective Mass Density

With the expressions derived above, the reciprocal density tensor are derived from $\rho_{eff}^{-1}(\theta) = c_{eff}^2(\theta)/B_{eff}$, see equation (1.2.32):

$$\rho_{s+}^{-1} = \frac{|\Delta|^2 - |\Gamma|^2 - f^2\eta^2}{(\Delta + f\eta)(\Delta^* + f\eta) - |\Gamma|^2} \tag{8.1.5}$$

$$\rho_{s-}^{-1} = -\frac{2f\eta|\Gamma|\cos\Phi_\Gamma}{(\Delta + f\eta)(\Delta^* + f\eta) - |\Gamma|^2} \tag{8.1.6}$$

$$\rho_{a+}^{-1} = \frac{2f\eta|\Gamma|\sin\Phi_\Gamma}{(\Delta + f\eta)(\Delta^* + f\eta) - |\Gamma|^2} \tag{8.1.7}$$

It is important to note that the reciprocal density tensor (and the effective density) does not depend on the bulk modulus of background and cylinder. In other words, the effective density only depends on the lattice structure, its filling fraction and the density of cylinders relative to the background. The elastic nature of cylinders will be only present in the effective density for high filling fractions, where the higher orders of the T matrix will be present in both the Δ and Γ factors.

Isotropic lattices

For the case of isotropic lattices the effective density already given in (8.1.3) can be also cast in:

$$\overline{c}_{eff}^2 = \frac{1}{\rho_{eff}} \cdot \frac{B_a}{fB_b + (1-f)B_a}, \tag{8.1.8}$$

in which:

$$\rho_{eff} = \frac{\rho_a(\Delta + f) + \rho_b(\Delta - f)}{\rho_a(\Delta - f) + \rho_b(\Delta + f)}\rho_b, \tag{8.1.9}$$

and the second factor is the effective bulk modulus B_{eff} given in (5.1.22). It can be demonstrated that for low enough f (i.e., Δ =1) the expression 8.1.9 reduces to that obtained by Berryman [Ber92] for the dimensionality parameter $d = 2$ [see also equation (2) in [MLWS06]].

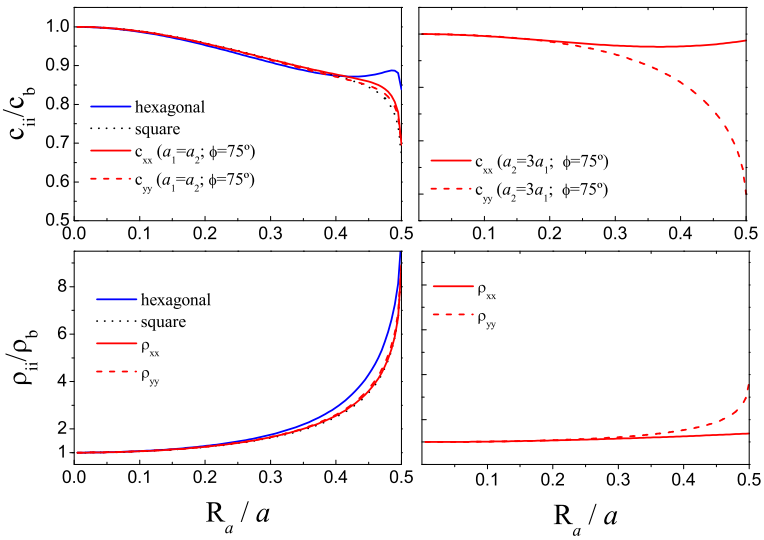

Figure 8.6: Effective parameters for 2D arrays of lead (Pb) cylinders embedded in water for the two isotropic lattices (hexagonal and square) and two different anisotropic lattices.

8.1.3 Effective Parameters for lattices of elastic cylinders

When the ratio between acoustic impedances of cylinders and background Z_a/Z_b is not large enough the condition of rigid cylinders (i.e. $\rho = \infty$) is not valid and the sound propagation inside the cylinders has to be taken into account. This is the usual case when working with solid cylinders embedded in water. Therefore, the full elastic properties of cylinders must be considered in the corresponding T matrix. As a consequence, the effective parameters of metamaterials based on solid cylinders embedded in a fluid, like water, present a rich variety of behavior depending of the ratio Z_a/Z_b, the lattice topology and the fraction of volume (f) occupied by the cylinders in the corresponding lattice. As example of typical behaviors encountered, figures 8.6, 8.7, 8.8 represent the cases of cylinders made of lead (Pb), iron (Fe) and aluminum (Al), respectively, embedded in water. Results are shown for the two 2D isotropic lattices (square and hexagonal) and two anisotropic lattices. As anisotropic lattice we have studied one ($a_1 = a_2$ and ϕ =75^o) characterized by a very small anisotropic strength parameter (A_Γ =0.001) and another ($a_1 = 3a_2$ and ϕ =75^o) in which this parameter is more than one order of magnitude larger (A_Γ =0.042).

Results for the slightly anisotropic lattice (A_Γ =0.001) in left panels of figures 8.6, 8.7, and 8.8 show that the values of their effective parameters are in between of those calculated for the hexagonal (ϕ =60^o) and square (ϕ =90^o) lattices and the difference between diagonal elements is very small. Results for the strong anisotropic lattice are depicted in the right panels of the same figures. They show that diagonal elements show appreciable differences that increase with cylinder's radius and should be observable in acoustic experiments. Also note that the difference between diagonal elements decreases with decreasing density. Therefore, we can concluded that in order to observe strong anisotropic effects in lattices of solid cylinders embedded in a fluid, we have to select a lattice with a large value of A_Γ made of cylinders with a density as large as possible in comparison with that of the fluid background.

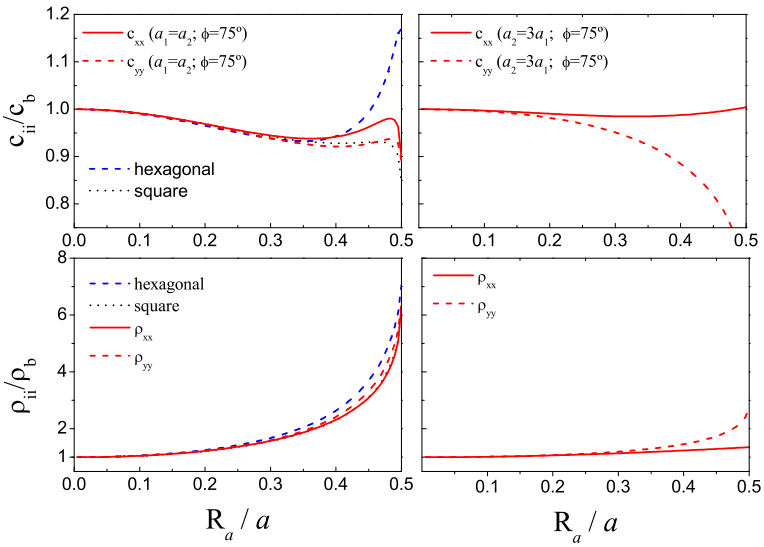

Figure 8.7: Effective parameters for 2D arrays of iron (Fe) cylinders embedded in water for the two isotropic lattices (hexagonal and square) and two different anisotropic lattices.

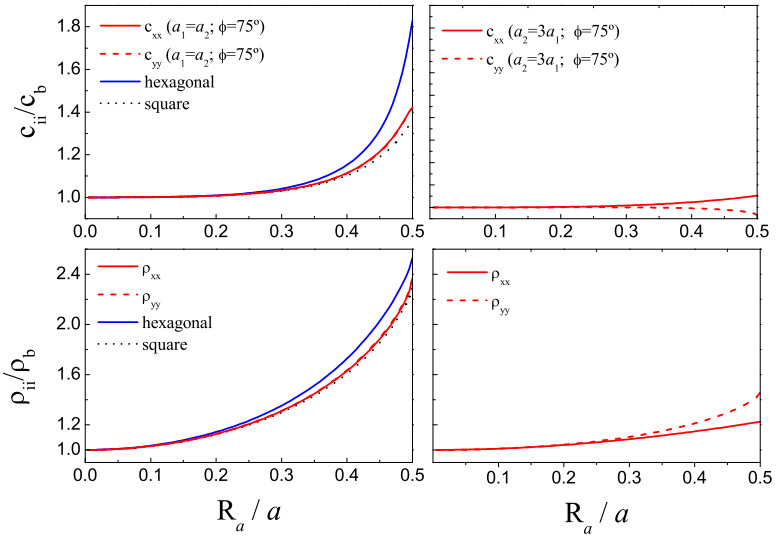

Figure 8.8: Effective parameters for 2D arrays of aluminum (Al) cylinders embedded in water for the two isotropic lattices (hexagonal and square) and two different anisotropic lattices.

8.2 Acoustic cloaking

In a recent work by Cummer and Schurig [Cum07] was predicted that acoustic cloaking is possible in a two-dimensional (2D) geometry by means of a cloak made of an acoustic material having a strong mass anisotropy not existing in nature. This result in acoustics follows a previous analogous result discovered by Pendry *et al.* [Pen06] in electromagnetism by using a material with equivalent requirements for the permitivity and permeability tensor components. However, while the electromagnetic (EM) cloaking has been experimentally demonstrated by using a metamaterial specially designed [Sch06], its acoustic counterpart has not been demonstrated yet. Moreover, the demonstration for the acoustic cloaking is still waiting for some proposal of engineered material (metamaterial) that accomplishes the requirements on mass anisotropy predicted in [Cum07].

In this regards, the work by Milton *et al.* [Mil06] describes conceptually how the mass anisotropy could be possible by spring loaded masses. Besides, a recent advance in the physical realization of metamaterial with mass density anisotropy has been performed by these authors by demonstrating that such uncommon property can be made possible by using non-symmetric lattices of solid cylinders [TSD08].

In this section an acoustic cloak that could be physically realizable is presented. In brief, the proposed cloak is based on a multilayered structure consisting of two layers with the same thickness and made of two different acoustic isotropic metamaterials. These metamaterials are built with sonic crystals (i.e., periodic arrays of sonic scatterers) based on two types of elastic cylinders that have to accomplish certain requirements on their mass density and effective sound speed. Numerical experiments based on multiple scattering method are present to support the exact performance of the proposed cloak.

8.2.1 The acoustic cloak: a proposal

The solution reported by Cummer and Schurig for the acoustic cloaking in [Cum07] requires a fluid material with an anisotropic density and a scalar bulk modulus. Moreover, these parameters must be dependent on the radial

distance to the hidden object. The predicted functional form is

$$\frac{\rho_r}{\rho_b} = \frac{r}{r-R_1}, \tag{8.2.1a}$$

$$\frac{\rho_\theta}{\rho_b} = \frac{r-R_1}{r}, \tag{8.2.1b}$$

$$\frac{B}{B_b} = \left(\frac{R_2-R_1}{R_2}\right)^2 \frac{r}{r-R_1}, \tag{8.2.1c}$$

where R_1 and R_2 are the inner and outer radii of the cloaking shell, B is the bulk modulus of the shell, ρ_r and ρ_θ are the components of the diagonal mass density tensor, and the quantities with subscript b are those of the surrounding background that is a fluid or a gas. Materials with such uncommon properties does not exist in nature and, therefore, some engineered material should be introduced to accomplish them.

In the previous section it has been shown that, in the low frequency limit, arrangements of cylinders in non-symmetric lattices leads to acoustic metamaterials with anisotropic mass density and scalar bulk modulus, as required by equations (8.2.1).

The lattices considered in that section are single-cylinder lattices and, as a consequence, when the mass density of the cylinder is larger (smaller) than that of the background, the effective mass density tensor is always larger (smaller) than that of the background. This is an important drawback because in conditions (8.2.1) one component of the mass density tensor is the reciprocal of the other and consequently the radial (angular) component of the mass tensor is always larger (smaller) than that of the background.

Therefore, a material having certain mass density in the radial direction and its reciprocal along the tangential direction cannot be engineered by using the theory developed so far. However, we suggest below a path to get the actual realization of such property by using periodic structures.

We arrive to the solution here proposed by exploring the possibility of building anisotropic materials based on sonic crystals with two types of materials cylinders, following a combination of two approaches previously introduced. Unfortunately, the practical realization of conditions (8.2.1) was impossible to achieve because of the limitation imposed by the close packing condition of the lattice. Therefore, in a natural way, we conclude that a multilayered structure made of two materials overcome such problem and give a

solution to accomplish the required conditions. It is interesting to note that an approach similar to this was also proposed to get EM cloaking [Hua07]. However, while the EM cloak only verifies a reduced set of the conditions imposed for EM cloaking, the one reported here exactly matches the conditions for acoustic cloaking.

Let us consider a cloaking shell consisting of a multilayered structure that is made of alternating layers of materials of type 1 and 2. For any periodic system the bulk modulus (in the homogenization limit) does not depend of the type (isotropic or anisotropic) of lattice; in fact, it has been shown in chapter 5 that the effective bulk modulus at large wavelength, B_{eff}, can be determined by simply doing a volume average of its reciprocal. This volume average, for a one-dimensional multilayered system of materials 1 and 2, becomes in

$$\frac{1}{B_{eff}} = \frac{1}{d_1 + d_2}\left[\frac{d_1}{B_1} + \frac{d_2}{B_2}\right] \tag{8.2.2}$$

where B_1 (B_2) is the bulk modulus of material 1 (2) and d_1 (d_2) is the length of layer 1 (2).

To obtain the tensor associated to the effective speed of sound we need to calculate first the dispersion relation $K(\omega)$ of the system; i.e., the wavenumber as a function of the frequency. This calculation is very simple by following a procedure explained in textbooks like [Tre],

$$\cos K_x d = \cos k_{1x} d_1 \cos k_{2x} d_2 - \frac{1}{2}\left[\frac{\rho_1 k_{2x}}{\rho_2 k_{1x}} + \frac{\rho_2 k_{1x}}{\rho_1 k_{2x}}\right] \sin k_{1x} d_1 \cos k_{2x} d_2 \tag{8.2.3}$$

where

$$K_{ix}^2 = \frac{\omega^2}{c_i^2} - K_y^2, \tag{8.2.4}$$

for $i = 1, 2$

The effective speed of sound is defined (in the low frequency limit) as the ratio between the angular frequency ω and the wave number K. This ratio can be obtained by making a power expansion of the trigonometric functions up to second power of their arguments. It is easy to show that the effective speed of sound tensor that follows is

$$c_\perp^2 = B_{eff}\frac{d_1 + d_2}{d_1\rho_1 + d_2\rho_2} \tag{8.2.5a}$$

$$c_\parallel^2 = B_{eff}\frac{d_1^2 + d_2^2 + d_1 d_2(\rho_1/\rho_2 + \rho_2/\rho_1)}{(d_1 + d_2)(d_1\rho_1 + d_2\rho_2)} \tag{8.2.5b}$$

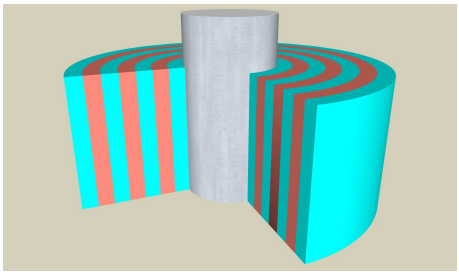

Figure 8.9: Schematic view of the cloaking shell. It consists of a circular-shaped multilayered structure made of two different materials of the same thicknesses.

where $c_\perp$ and $c_\parallel$ define the diagonal components of the speed tensor for the propagation along the perpendicular and parallel directions, respectively, to the layered system.

From the equations above the reciprocal density tensor can be identified as the ration between the speed tensor and the effective bulk modulus. If $d_1 = d_2 = d/2$ and $\rho_2/\rho_b = \rho_b/\rho_1$ the reciprocal mass density tensor becomes

$$\frac{\rho_\perp^{-1}}{\rho_b^{-1}} = \frac{2}{\rho_1/\rho_b + \rho_b/\rho_1} \tag{8.2.6a}$$

$$\frac{\rho_\parallel^{-1}}{\rho_b^{-1}} = \frac{\rho_1/\rho_b + \rho_b/\rho_1}{2} \tag{8.2.6b}$$

This structure satisfies the conditions (8.2.1); i.e., $\rho_\perp/\rho_b = \rho_b/\rho_\parallel$. Moreover, the component of the mass density tensor along the perpendicular direction is always larger than one, as also required by the first of equations (8.2.1).

Now, we have to determine the materials properties of media 1 and 2. If material 1 is selected as the high density material, from (8.2.6b) the dependence of ρ_1 as a function of r is

$$\rho_1(r) = \rho_r(r) + \sqrt{\rho_r^2(r) - \rho_b^2} = \frac{r + R_1\sqrt{2r/R_1 - 1}}{r - R_1}\rho_b \tag{8.2.7}$$

The bulk modulus of both materials must also depend on the radial distance. To accomplish this condition, one possibility is assuming that both materials have the same speed of sound c_1. Therefore, the dependence of

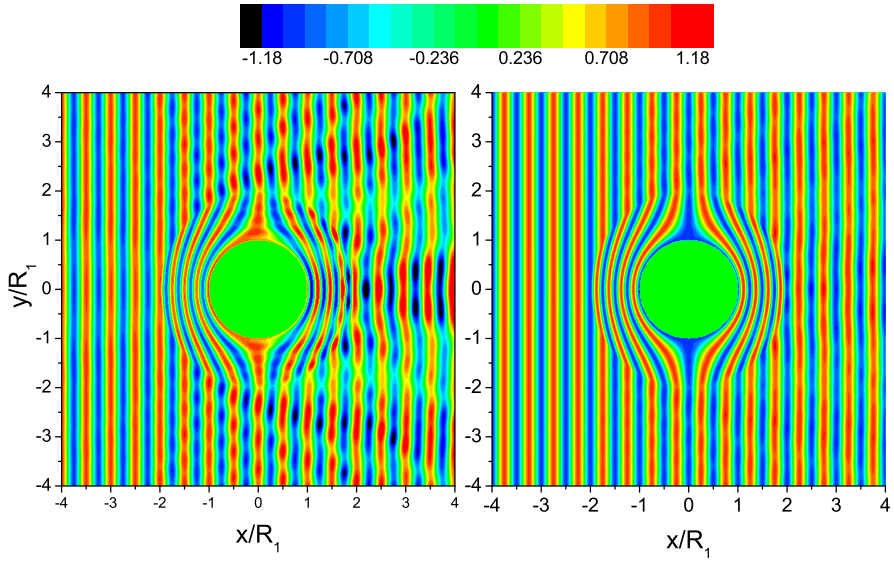

Figure 8.10: Pressure map for a planar wave incident on a rigid cylindrical scatterer surrounded by a multilayered acoustic shell made of 50 layers (left panel) and 200 layers (right panel. The radius of the shell is two times the radius of the core ($R_2 = 2R_1$). The wavelength of the incident field is $\lambda = R_1/2$.

this quantity as a function of r can be obtained by inserting $B_1 = \rho_1 c_1^2$ and $B_2 = \rho_2 c_1^2$ into equations (8.2.1) and (8.2.2)

$$c_1(r) = \sqrt{\frac{B^* \rho_r}{\rho_b^2}} = \frac{R_2 - R_1}{R_2} \frac{r}{r - R_1} c_b \tag{8.2.8}$$

Equations (8.2.7) and (8.2.8) define the properties of medium 1 while those for medium 2 are derived from them as explained above:

$$\rho_2(r) = \rho_b^2/\rho_1 = \frac{r - R_1}{r + R_1\sqrt{2r/R_1 - 1}} \rho_b \tag{8.2.9a}$$

$$c_2(r) = c_1(r) = \frac{R_2 - R_1}{R_2} \frac{r}{r - R_1} c_b \tag{8.2.9b}$$

The proposed cloak is schematically shown in figure 1, where the 1D structure is transformed into a circular-shaped shell that it is expected to cloak a rigid core placed in its interior.

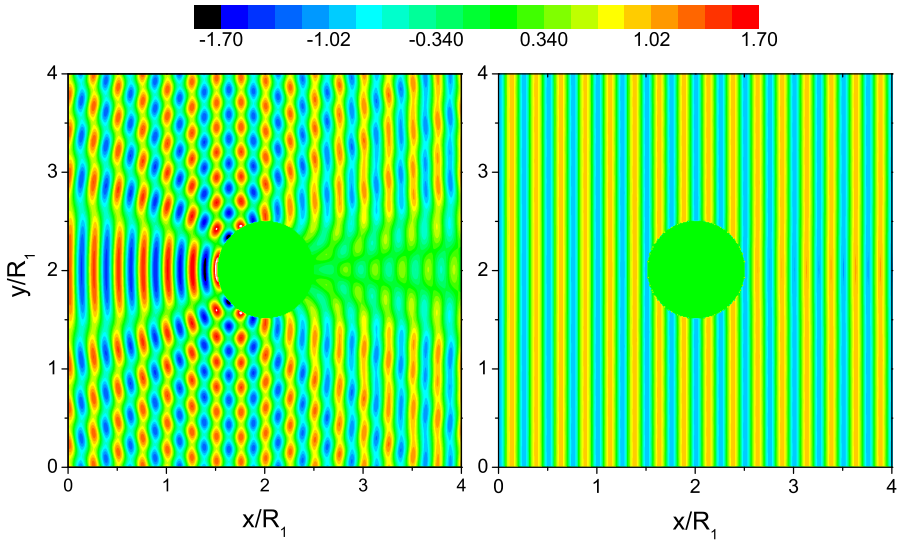

Figure 8.11: Left panel:Pressure map for a planar wave incident on a rigid cylindrical scatterer of radius R_1. Right panel: Map corresponding to the same scatterer surrounded by a extremely thin cloak shell ($R_2 - R_1$ =$0.01R_1$) made of 200 layers. The wavelength of the incident field is $\lambda = R_1/2$.

To check the functionality of the multilayered cloak we have performed multiple scattering simulations by using the method developed in [Cai04, CSD08].

Maps of the acoustic pressure at a time instant are represented by the real part of the complex amplitude p and are shown in figure 8.2.1 for the case of a rigid core of radius R_1 that is placed inside a multilayered shell of radius $R_2 = 2R_1$. The full structure is submitted to an acoustic field of wavelength $\lambda = R_1/2$. The performance of two different shells are depicted in figure 2 where the left panel corresponds to a shell made of 50 layers and the right panel to one composed of 200 layers, where each layer of thickness d is composed o two alternative layers of thickness of material 1 and 2, respectively; i.e., $d = d_1+d_2 = d/2+d/2$. The cloaking effect is evident in both representations, but that corresponding to 200 layers is can be considered like perfect. These results can be compared with the case of the rigid cylinder with no cloak that is represented in the left panel of figure 3, where the incident wave is strongly scattered by the cylinder. On the other hand, in the right panel of figure 3 is depicted the acoustic cloaking by a extremely thin cloak, its thickness being two order of magnitude smaller than the hidden cylinder, but it is also made of 200 layers. This result is very promising because it indicates the possibility of building cloaks as thiner as the available technology allows.

Now, it is also interesting to analyze the cloaking effect as a function of the number of layers employed in the fabrication of the cloak. The resulting behavior is important in order to simplify as much as possible the fabrication of the cloaking shell. We have studied the backscattered field as a typical parameter characterizing the cloak's performance and it is represented (in a logarithmic scale) in figure 4 as a function of the frequency for different number of layers. It is remarkable in figure 4 that only 50 layers are able to reduce in more than one order of magnitude (for a wide range of frequencies) the back scattered field in comparison with that for the corresponding naked rigid cylinder. Other interesting cases like a penetrable and a void regions are not reported here but we expect results analogous to those already published [Cai07].

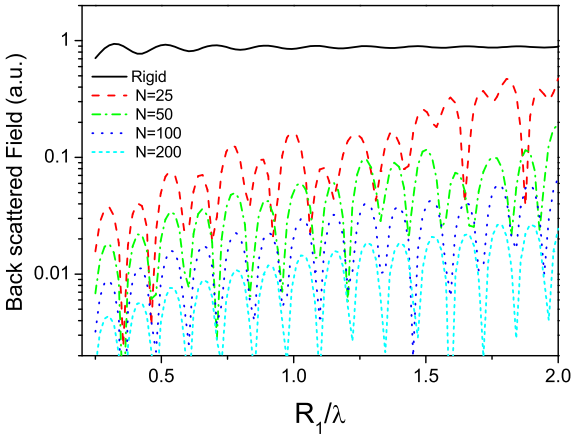

Figure 8.12: Frequency response of the back scattered pressure for a rigid cylinder surrounded by a cloaking shell consisting of a multilayered structure as described in figure 1. N is the number of layers in the structure. The case of the bare rigid cylinder without the shell is also represented (black line).

8.2.2 Building the layers of the cloak: a feasible approach

It has been shown above that the acoustic cloak can be exactly realized by using a set of N layers, each one made of one isotropic metamaterial of type 1 and another of type 2, their acoustic parameters being described by conditions (8.2.7), (8.2.8), and (8.2.9).

This section is devoted to show that the requested metamaterials 1 and 2 can be actually realized by those introduced by these authors in previous works. Particularly, we have shown that sonic crystals are a class of metamaterials that dynamically behaves (in the homogenization limit) as true fluidlike materials whose properties can be tailored with practically no limitation. For example, for sonic crystal made of only one type of component the acoustic parameters of the homogenized acoustic metamaterial basically depend on the filling fraction of the lattice [THCSD06, TSD06]. More recently, we have shown [TSD07] that sonic crystals made of two material cylinders increase the possibilities of metamaterial design. Here, we have used the

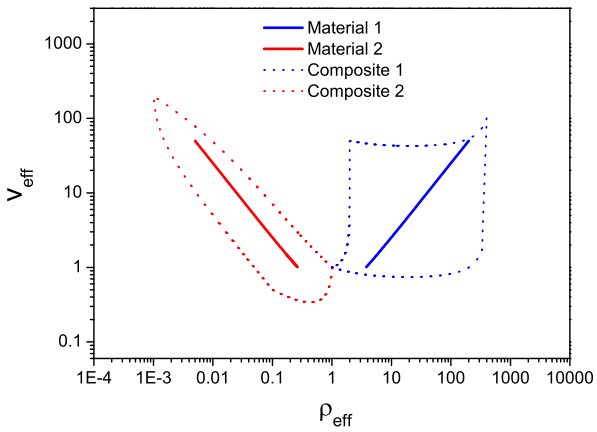

Figure 8.13: Phase diagram showing that the acoustic properties for materials 1 and 2 can be satisfied with only two different materials. The continuous line represents the range of values for materials 1 and 2. The dotted lines enclosed the area representing the range of values that is possible to obtain with the corresponding two-component sonic crystal.

last approach to design the acoustic properties needed in the layers of the cloaking shell.

For instance, let us assume that metamaterials 1 and 2 are going to be made of two types of cylinders with acoustic parameters: $(\rho_{1\alpha}, c_{1\alpha})$ and $(\rho_{1\beta}, c_{1\beta})$ for metamaterial 1, and $(\rho_{2\alpha}, c_{2\alpha})$, and $(\rho_{2\beta}, c_{2\beta})$ for metamaterial 2. The parameters of metamaterials 1 and 2 can be tailored with the filling fractions $f_{1\alpha}, f_{1\beta}, f_{2\alpha}$ and $f_{2\beta}$ of the components involved in their fabrication. Thus,

$$\frac{1}{B_1} = \frac{1-f_{1\alpha}-f_{1\beta}}{B_b} + \frac{f_{1\alpha}}{B_{1\alpha}} + \frac{f_{1\beta}}{B_{1\beta}} \tag{8.2.10}$$

$$\eta_1 = \eta_{1\alpha} f_{1\alpha} + \eta_{1\beta} f_{1\beta} \tag{8.2.11}$$

$$\frac{1}{B_2} = \frac{1-f_{2\alpha}-f_{2\beta}}{B_b} + \frac{f_{2\alpha}}{B_{2\alpha}} + \frac{f_{2\beta}}{B_{2\beta}} \tag{8.2.12}$$

$$\eta_2 = \eta_{2\alpha} f_{2\alpha} + \eta_{2\beta} f_{2\beta} \tag{8.2.13}$$

where $\eta_i = (\rho_i - \rho_b)/(\rho_i + \rho_b)$

In figure 5 we have represented the so called phase diagram [TSD07] of the

Table 8.1: Acoustic parameters of the materials forming the composites. The third column reports the effective velocity of the elastic cylinder $c = \sqrt{c_\ell^2 - c_t^2}$, where c_ℓ and c_t are the longitudinal and transversal velocities, respectively

Material	ρ/ρ_b	c/c_b
1α	400	100
1β	2	50
2α	0.1	0.5
2β	0.001	200

metamaterial that can be obtained by using composites made of two component sonic crystals. This diagram has be obtained by considering cylinders made of materials whose parameters are reported in Table 8.1. Lines of the same color enclose the area in which a metamaterial with parameters (ρ_{eff}, c_{eff}) are available by just changing the filling fraction of the materials employed in the composite. For instance, the area enclosed by the blue lines define the range of parameter that can be tailored using materials 1α and 1β in the composition of metamaterial 1. Within this area, the blue straight line represents the variation in (ρ_{eff}, c_{eff}) needed by material 1 in order to accomplish the cloaking by the multilayered structure. In other words, the conditions for material 1 given by (8.2.7) and (8.2.8) can be fully accomplished by using materials 1α and 1β in Table 8.1. For the case of material 2, the red straight line in figure 5 represent the range of variation requested for cloaking. The set of materials in Table 8.1 selected to get the acoustic metamaterials needed is the construction of the cloaking shell are just one possibility. In order to make the cloak real a more appropriate set should be chosen to match the availability of materials in nature.

We should point out that the present proposal can be extended to the case of acoustic cloaking in three dimensions, where the parameter conditions of the cloaking shell have been recently reported [Che07, Cum08]. By using an analogous development, we can foresee that the corresponding shell could be made of multilayers of two different isotropic metamaterials, which might consist of spheres of different solid materials.

8.3 Summary

In this chapter numerical calculations of anisotropic acoustic parameters have been presented for relevant examples like the case of rigid cylinders in air and some elastic cylinders embedded in water. Wave propagation through these systems has also been analyzed.

Also,it has been shown that acoustic cloaking shells are possible by means of multilayered structures made with two types of acoustic isotropic metamaterials whose acoustic parameters should change as a function of the distance from the layer to the center of the shell. The practical realization of the required radial dependence can be achieved by using homogenized 2D sonic crystals having two full elastic cylinders per unit cell.

The parameters of the sonic crystal needed to get the cloaking eect can be obtained thought a phase diagram analysis of the selected materials used in the cylinders.

This chapter is based on:

1. Daniel Torrent and José Sánchez-Dehesa. *Anisotropic mass density by two-dimensional acoustic metamaterials.* New Journal of Physics, 10, 2008.

2. Daniel Torrent and José Sánchez-Dehesa. *Acoustic Cloaking in two dimensions: a feasible approach.* New Journal of Physics, (to be published).

Chapter 9

Concluding remarks

In this chapter the main results are summarized and the work that has to be done is explained. It is shown that although this work has solved several interesting problems many others are derived.

9.1 Conclusions

It is evident that the long wavelength behaviour of sonic crystals is a open field with many applications. Both ordered and disordered systems can now be studied, showing that the disordering effects does not alter the parameters of the effective medium, which means that practical realization of the purposed devices is not very sensitive to small fabrication defects.

Althoug acoustic waves was the main application of sonic crystals in the low frequency limit, it has been shown how these type of devices can be improved, and how many others, like gradient index devices, can also be built.

It has been also shown that fully transparent acoustic devices are possible, hardly improving the efficacy of these devices.

Probably the most impressive device described in this work is the acoustic cloaking shell. It is clear that the invisibility in acoustic can be achieved with sonic crystals. Although the solution reported here is still too much theoretical, it is evident that multilayered systems are in the correct way to finally build the shell.

9.2 Future Work

The results of the present work suggest that refractive devices should be possible with a wide range of design possibilities. However, experimental work has been secundary in this work, and one step further should be done in order to really know how far refractive devices can arrive. Then, the next point in this field should be done in the experimental part.

But in the theoretical part there are some fields open. First, the homogenization theory has been developed for two situations: fluid background-fluid cylinder and fluid background-elastic cylinder. It is evident that the same situations but with elastic background has to be done. And the results needs to be extrapolated to both one and threedimensional systems.

Finally, the acoustic cloaking is also a very interesting starting point for future work. Here it has been shown that it is possible to build the acoustic cloak with a multilayer of fluid-like materials. It should be seriously studied the possibility of build it with a multilayered elastic medium. That is probably the best way to physically realize this interesting phenomenon, which is very representative of what could be understood by "the full control of sound".

Appendix A

Bessel Functions

A.1 Basic relations

A.1.1 Bessel Differential Equation and Solutions

Helmholtz equation in polar coordinates is

$$\left(\frac{\partial^2}{\partial r^2}+\frac{1}{r}\frac{\partial}{\partial r}+\frac{1}{r^2}\frac{\partial^2}{\partial\theta^2}+k^2\right)\Psi=0 \tag{A.1.1}$$

this equation has a solution of the form

$$\Psi=\sum_{q=-\infty}^{\infty}\Upsilon_q(kr)e^{iq\theta}$$

where q must be integer in order to satisfy periodicity in θ. The functions $\Upsilon_q(x)$ satisfies Bessel differential equation

$$\frac{d^2\Upsilon_q}{dx^2}+\frac{1}{x}\frac{d\Upsilon_q}{dx}+(1-\frac{q^2}{x^2})\Upsilon_q=0 \tag{A.1.2}$$

regular solutions, which will be called Bessel functions are

$$J_q(x) = \sum_{n=0}^{\infty}\frac{(-1)^n}{n!(n+q)!}\left(\frac{x}{2}\right)^{q+2n} \tag{A.1.3a}$$

$$J_{-q}(x) = (-1)^q J_q(x) \tag{A.1.3b}$$

while non regular solutions, which will be called Neumann functions, are

$$Y_q(x) = \lim_{p\to q}\frac{J_p(x)\cos p\pi - J_{-p}(x)}{\sin px} \tag{A.1.4a}$$

$$Y_{-q}(x) = (-1)^q Y_q(x) \tag{A.1.4b}$$

In the present work, the so called Hankel functions are more used for the non regular solutions, and they are defined by

$$H_q(x) = J_q(x) + iY_q(x) \tag{A.1.5}$$

A.1.2 Recurrence relations

The following relations are satisfied for both the regular and non regular Bessel functions (the symbol $'$ implies derivative respect to the argument)

$$\Upsilon_{q+1}(x) = \frac{2q}{x}\Upsilon_q(x) - \Upsilon_{q-1}(x) \tag{A.1.6a}$$

$$\Upsilon'_q(x) = \frac{1}{2}\left[\Upsilon_{q-1}(x) - \Upsilon_{q+1}(x)\right] \tag{A.1.6b}$$

$$\Upsilon''_q(x) = \frac{1}{4}\left[\Upsilon_{q-2}(x) - 2\Upsilon_q(x) + \Upsilon_{q+2}(x)\right] \tag{A.1.6c}$$

A.1.3 Asymptotic forms for small arguments

For $x \to 0$ Bessel functions are simply

$$J_q(x) \approx \frac{1}{q!}\frac{x^q}{2^q}\left[1 - \frac{x^2}{4(q+1)}\right] \tag{A.1.7}$$

while Hankel functions are

$$H_q(x) \approx \begin{cases} -\frac{i(q-1)!}{\pi}\frac{2^q}{x^q} & q > 0 \\ \\ \frac{2i}{\pi}\ln x & q = 0 \end{cases} \tag{A.1.8}$$

With the above expressions it is easy to show that the asymptotic forms for the first derivatives of the Bessel functions are

$$J'_q(x) \approx \begin{cases} \frac{1}{(q-1)!}\frac{x^{q-1}}{2^q} & q > 0 \\ \\ -\frac{x}{2} & q = 0 \end{cases} \tag{A.1.9}$$

and of the Hankel functions are

$$H'_q(x) \approx \begin{cases} -\frac{iq!}{\pi}\frac{2^q}{x^{q+1}} & q > 0 \\ \\ \frac{2i}{\pi x} & q = 0 \end{cases} \tag{A.1.10}$$

another useful expansion is that of the second derivative of the Bessel function, which is

$$J_q''(x) \approx \begin{cases} \frac{1}{(q-2)!}\frac{x^{q-2}}{2^q} & q > 1 \\ -\frac{3x}{8} & q = 1 \\ \frac{1}{2}\left[\frac{x^2}{8} - 1\right] & q = 0 \end{cases} \tag{A.1.11}$$

A.1.4 Asymptotic forms for large arguments

When $x \to \infty$

$$J_q(x) \approx \sqrt{\frac{2}{\pi x}} \cos\left(x - \frac{q\pi}{2} - \frac{\pi}{4}\right) \tag{A.1.12}$$

$$Y_q(x) \approx \sqrt{\frac{2}{\pi x}} \sin\left(x - \frac{q\pi}{2} - \frac{\pi}{4}\right) \tag{A.1.13}$$

$$H_q(x) \approx \sqrt{\frac{2}{\pi x}}(-i)^q e^{-i\pi/4} e^{ix} \tag{A.1.14}$$

A.1.5 Integral Representations

Integral representation of Bessel functions are specially useful when dealing with scattering problems and lattice sums. In [MA] the following integral representation of Bessel functions is given

$$J_q(x) = \frac{1}{\pi}\int_0^\pi \cos(x\sin\tau - q\tau)d\tau = \frac{i^{-q}}{\pi}\int_0^\pi e^{ix\cos\tau}\cos(q\tau)d\tau \tag{A.1.15}$$

expressing $\cos(q\tau)$ in exponential form the integral is separated in two parts

$$J_q(x) = \frac{i^{-q}}{2\pi}\int_0^\pi e^{ix\cos\tau}e^{iq\tau}d\tau + \frac{i^{-q}}{2\pi}\int_0^\pi e^{ix\cos\tau}e^{-iq\tau}d\tau \tag{A.1.16}$$

if in the second integrand the variable of integration is replaced by $-\tau$ it is easy to show that

$$J_q(x) = \frac{i^{-q}}{2\pi}\int_{-\pi}^\pi e^{ix\cos\tau}e^{iq\tau}d\tau \tag{A.1.17}$$

The corresponding integral representation for the Neumann function is

$$Y_q(x) = \frac{1}{\pi}\int_0^{\pi} \sin(x\sin\tau - q\tau)d\tau - \frac{1}{\pi}\int_0^{\infty} \left[e^{qt} + (-1)^q e^{-qt}\right] e^{-x\sinh t}dt \tag{A.1.18}$$

It can be shown that with the above relation Hankel functions are [MA]

$$H_q(x) = \frac{1}{\pi i}\lim_{\epsilon\to\infty}\int_{-\epsilon}^{\epsilon+\pi i} e^{x\sinh t}e^{-qt}dt \tag{A.1.19}$$

replacing $t = i(\pi/2 - \tau)$ the above expression will be

$$H_q(x) = \frac{i^{-q}}{\pi}\lim_{\epsilon\to\infty}\int_{i\epsilon-\pi/2}^{-i\epsilon+\pi/2} e^{ix\cos\tau}e^{iq\tau}d\tau \tag{A.1.20}$$

This expression can be used to obtain an integral representation of a general Hankel wave

$$\begin{aligned} H_q(kr)e^{iq\theta} &= \frac{i^{-q}}{\pi}\lim_{\epsilon\to\infty}\int_{i\epsilon-\pi/2}^{-i\epsilon+\pi/2} e^{ikr\cos\tau}e^{iq(\tau+\theta)}d\tau \\ &= \frac{i^{-q}}{\pi}\lim_{\epsilon\to\infty}\int_{i\epsilon-\pi/2+\theta}^{-i\epsilon+\pi/2+\theta} e^{ikr\cos(\tau-\theta)}e^{iq\tau}d\tau \end{aligned} \tag{A.1.21}$$

The presence in the integration limits of the variable θ can be deleted taken a different path of integration. It can be shown by means of Cauchy's that the above integral is equivalent to

$$H_q(kr)e^{iq\theta} = \frac{i^{-q}}{\pi}\int_C e^{i\boldsymbol{k}_\tau\cdot\boldsymbol{r}}e^{iq\tau}d\tau \tag{A.1.22}$$

where $\boldsymbol{k}_\tau = k(\cos\tau, \sin\tau)$ and C is a path from $z_0 = i\infty - \pi/2$ to $z_f = -i\infty + \pi/2$ if $\cos\theta \geq 0$ and from $z_0 = i\infty + \pi/2$ to $z_f = -i\infty + 3\pi/2$ if $\cos\theta \leq 0$.

This last expression will be especially useful when analyzing the response of the infinite line of cylinders.

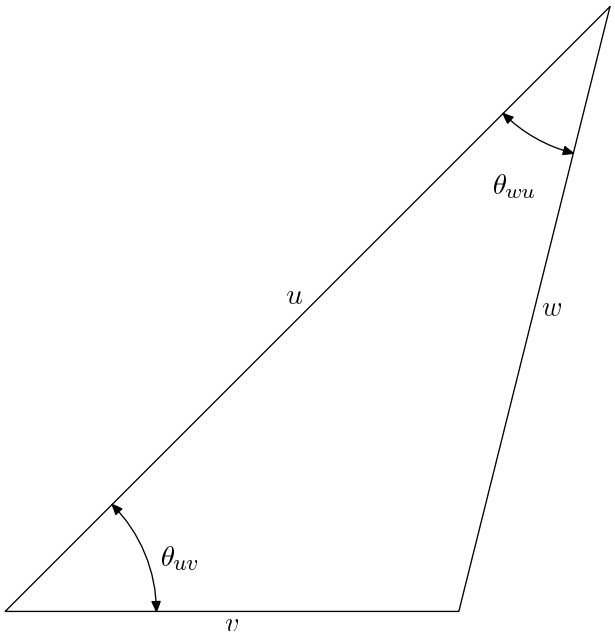

Figure A.1: Angle and distance definitions for Graf's addition theorem.

A.2 Addition Theorem

A.2.1 Two Dimensional Case

Graf's addition theorem allows change the reference frame of the Bessel functions. The theorem asserts that

$$\Upsilon_s(w)e^{is\theta_{wu}} = \sum_q \Upsilon_{s+q}(u)J_q(v)e^{iq\theta_{uv}} \quad , \quad v < u \tag{A.2.1}$$

where $\Upsilon_r(\cdot)$ can be both a Bessel or a Hankel function and the quantities u, v, w, θ_{wu} and θ_{uv} are defined in figure A.1

In the multiple scattering derivation of section 3.1 the objective is to express the quantity

$$H_s(kr_\beta)e^{is\theta_\beta} \tag{A.2.2}$$

in the reference frame of the cylinder α. From the multiple scattering geometry of figure 3.1 it is clear that the triangle involved in the change is the triangle defined by the vectors $\mathbf{r}_\alpha, \mathbf{r}_\beta$ and $\mathbf{R}_{\alpha\beta}$. It is important to relate this triangle with the triangle $\widehat{uvw}$.

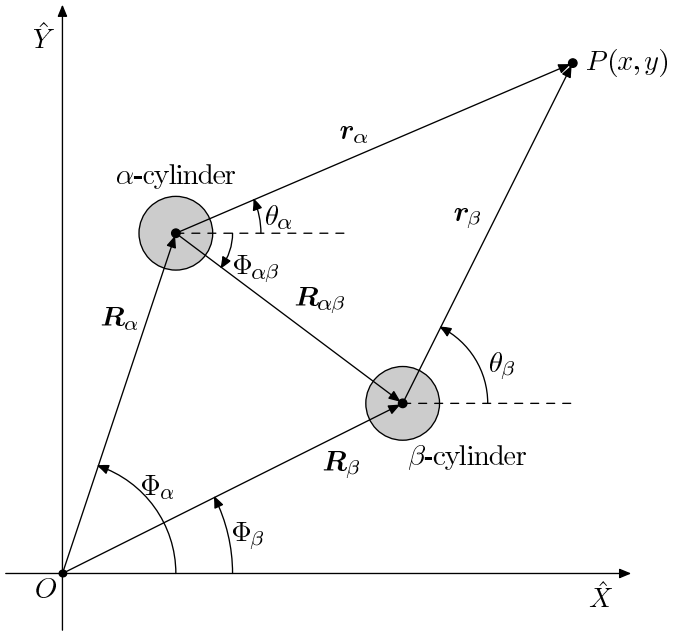

Figure A.2: Figure of section 3.1

It is obvious from figure A.2 that $w = r_\beta$, because is the variable of the function to be expanded. Because this change of reference frame is necessary to apply boundary conditions, in the new frame r_α will be equal to the cylinder radius, and then it will be always smaller than $R_{\alpha\beta}$, that is

$$r_\alpha < R_{\alpha\beta} \tag{A.2.3}$$

so it is possible to identify $v = r_\alpha$ and $u = R_{\alpha\beta}$. The angle θ_{wu} is then the angle between the r_β and $R_{\alpha\beta}$ segments, which is $\Phi_{\beta\alpha} - \theta_\beta$. Finally, the angle θ_{uv} is then the angle between the r_α and $R_{\alpha\beta}$ segments, that is $\theta_{uv} = \theta_\alpha - \Phi_{\alpha\beta}$. With this assignment Graf's theorem is

$$H_s(kr_\beta)e^{is\Phi_{\beta\alpha}}e^{-is\theta_\beta} = \sum_q H_{s+q}(kR_{\alpha\beta})J_q(kr_\alpha)e^{iq\theta_\alpha}e^{-iq\Phi_{\alpha\beta}} \tag{A.2.4}$$

or

$$H_s(kr_\beta)e^{is\theta_\beta} = (-1)^s e^{is\Phi_{\beta\alpha}} \sum_q H_{-s+q}(kR_{\alpha\beta})J_q(kr_\alpha)e^{iq\theta_\alpha}e^{-iq\Phi_{\alpha\beta}} \tag{A.2.5}$$

figure 3.1 shows as well that $\Phi_{\beta\alpha} = \pi + \Phi_{\alpha\beta}$, so that

$$H_s(kr_\beta)e^{is\theta_\beta} = \sum_s H_{q-s}(kR_{\alpha\beta})e^{i(s-q)\Phi_{\alpha\beta}}J_q(kr_\alpha)e^{iq\theta_\alpha} \tag{A.2.6}$$

A.2.2 Three Dimensional Case

The coefficients for the translation of the spherical wave functions are given by

$$g^{(h)}_{lml'm'}(\mathbf{R}) = \sum_L (-1)^{(l-l'-L)/2} 4\pi C_{lml'm'LM} h_L(kR) Y_{LM}(\mathbf{R}) \tag{A.2.7}$$

with $M = m - m'$ and

$$C_{lml'm'LM} = \frac{(-1)^{m'}}{\sqrt{4\pi}} \sqrt{(2l'+1)(2l+1)(2L+1)} \times \begin{pmatrix} l & l' & L \\ 0 & 0 & 0 \end{pmatrix} \begin{pmatrix} l & l' & L \\ m & -m' & M \end{pmatrix} \tag{A.2.8}$$

for the linear chain of bubbles $\mathbf{R}_\alpha = \alpha a \hat{\mathbf{z}}$, then the spherical harmonic Y_{LM} equals to zero whenever M be diferent fo zero,and is equal to 1 or $(-1)^L$ depending on the sphere being in the positive or negative part of the z axis.But $M = 0$ implies $m = m'$, so that

$$g^{(h)}_{lml'm}(\mathbf{R}) = \sum_L (-1)^{(l-l'-L)/2} 4\pi C_{lml'mL0} h_L(kR) (\pm)^L \tag{A.2.9}$$

and then we can define

$$\tilde{g}^{(h)}_{lml'm}(ka) = \sum_{\beta \neq 0} g^{(h)}_{lml'm}(\mathbf{R}_\beta) = \sum_L (1 + (-1))^L (-1)^{(l-l'-L)/2} 4\pi C_{lml'mL0} S_L(ka) \tag{A.2.10}$$

it is clear that only the odd values of L contributes to the sum, so that

$$\tilde{g}^{(h)}_{lml'm}(ka) = 8\pi (-1)^{(l-l')/2} \sum_{n=|l-l'|/2}^{|l+l'|/2} (-1)^n C_{lml'm(2n)0} S_{2n}(ka) \tag{A.2.11}$$

A.3 Lattice Sums

A.3.1 Lattice Sums for the Linear Array of Cylinders

Complete Lattice Sums

When studying the transmission and reflection of sound waves by infinite slabs the following quantity appears in several situations

$$S_q^c(ka, \sin\theta_0, \boldsymbol{r}, \boldsymbol{R}_l) = \sum_{\alpha=-\infty}^{\infty} e^{i\alpha ka \sin\theta_0} H_q(kr_\alpha^l) e^{iq\theta_\alpha^l} \tag{A.3.1}$$

where from figure A.3 it is clear that

$$\boldsymbol{r}_\alpha^l = \boldsymbol{r} - \boldsymbol{R}_l - \boldsymbol{R}_\alpha^l \tag{A.3.2}$$

note that the vector $\boldsymbol{R}_\alpha^l$ is simply the position vector of the α-cylinder relative to the origin in the infinite line, that is

$$\boldsymbol{R}_\alpha^l = a\alpha\hat{\boldsymbol{y}} \tag{A.3.3}$$

then

$$\boldsymbol{r}_\alpha^l = \boldsymbol{r} - \boldsymbol{R}_l - a\alpha\hat{\boldsymbol{y}} \tag{A.3.4}$$

this sums converges very slowly, so that for practical computation another expression must be found. But the interest of find another expression is not only for numerical purposes but for understand the physical meaning of the sum.

The derivation will use the integral representation of Hankel functions given in (A.1.22)

$$e^{i\alpha ka \sin\theta_0} H_q(kr_\alpha^l) e^{iq\theta_\alpha^l} = \frac{i^{-q}}{\pi} \int_C e^{i\boldsymbol{k}_\tau \cdot \boldsymbol{r}_\alpha^l} e^{i\alpha ka \sin\theta_0} e^{iq\tau} d\tau \tag{A.3.5}$$

where the integration path C is a line from $z_0 = -i\infty + \pi/2 + (\pi)$ to $z_f = i\infty - \pi/2 + (\pi)$ if $x_\alpha^l = x - x_l > 0 (< 0)$. Note that the phase factor $e^{i\alpha ka \sin\theta_0}$ can be introduced in the integrand.

The argument of the exponential function in the integrand can be expressed as

$$\boldsymbol{k}_\tau \cdot \boldsymbol{r}_\alpha^l = \boldsymbol{k}_\tau \cdot (\boldsymbol{r} - \boldsymbol{R}_l) - \alpha ka \sin\tau \tag{A.3.6}$$

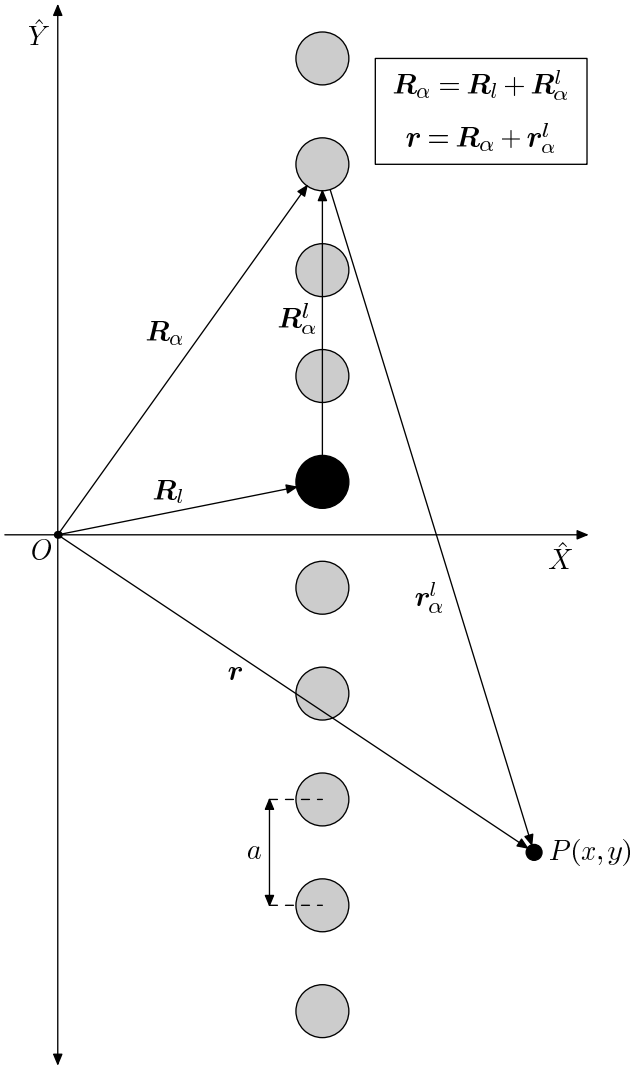

Figure A.3: Geometry of the infinite line

so that

$$e^{i\alpha ka\sin\theta_0}H_q(kr_\alpha^l)e^{iq\theta_\alpha^l}=\frac{i^{-q}}{\pi}\int_C e^{i\boldsymbol{k}_\tau\cdot(\boldsymbol{r}-\boldsymbol{R}_l)}e^{i\alpha ka(\sin\theta_0-\sin\tau)}e^{iq\tau}d\tau \tag{A.3.7}$$

When performing the sum in α the integral and the sum operators commutes, then the sum operator will act only in the exponential factor dependent on α,

$$\sum_{\alpha=-\infty}^{\infty}e^{i\alpha ka\sin\theta_0}H_q(kr_\alpha^l)e^{iq\theta_\alpha^l}=\frac{i^{-q}}{\pi}\int_C e^{i\boldsymbol{k}_\tau\cdot(\boldsymbol{r}-\boldsymbol{R}_l)}\sum_{\alpha=-\infty}^{\infty}e^{i\alpha ka(\sin\theta_0-\sin\tau)}e^{iq\tau}d\tau \tag{A.3.8}$$

The infinite series in the integrand can be expressed as a Dirac comb

$$\sum_{\nu=-\infty}^{\infty}\delta(t-\nu T)=\frac{1}{T}\sum_{\alpha=-\infty}^{\infty}e^{2\pi\alpha t/T} \tag{A.3.9}$$

then

$$\sum_{\alpha=-\infty}^{\infty}e^{i\alpha ka(\sin\theta_0-\sin\tau)}=\frac{2\pi}{ka}\sum_{\nu=-\infty}^{\infty}\delta(\sin\theta_0-\sin\tau-\frac{2\pi\nu}{ka}) \tag{A.3.10}$$

in order to use the Dirac delta properties it is necessary to convert the integral in the complex plane in an integral in the range $(-\infty,\infty)$. To do that, the change

$$\sin\tau=t\quad d\tau=\pm\frac{dt}{\sqrt{1-t^2}} \tag{A.3.11}$$

has to be made. The $\pm$ sign comes from the square root in the denominator. This sign is positive (negative) when $x-x_l$ is positive (negative). With this change of variable, when $\tau\to-i\infty+\pi/2$, which means that $x-x_l>0$, the variable t goes to

$$\lim_{\tau\to-i\infty+\pi/2}t=\lim_{\epsilon\to\infty}\frac{e^{i\pi/2}e^{\epsilon}-e^{-i\pi/2}e^{-\epsilon}}{2i}=\infty \tag{A.3.12}$$

and for the lower limit

$$\lim_{\tau\to i\infty-\pi/2}t=\lim_{\epsilon\to\infty}\frac{e^{-i\pi/2}e^{-\epsilon}-e^{i\pi/2}e^{\epsilon}}{2i}=-\infty \tag{A.3.13}$$

When $x-x_l<0$ the limits of integration in the complex plane have to be displaced a quantity π in the real axis. In this case the limits of the

new variable t change to $(\infty, -\infty)$, but the square root in (A.3.11) takes a negative sign, then it is possible to exchange the integration limits. The result is that the in both situations the integral takes the same form.

Once this change has been made, the integral is along the real axis and in the interval $(-\infty, \infty)$

$$\sum_{\alpha=-\infty}^{\infty} e^{i\alpha ka\sin\theta_0} H_q(kr_\alpha^l) e^{iq\theta_\alpha^l} = \frac{2i^{-q}}{ka} \sum_{\nu=-\infty}^{\infty} \int_{-\infty}^{\infty} e^{i\boldsymbol{k}_t^{\pm}\cdot(\boldsymbol{r}-\boldsymbol{R}_l)} \delta(\sin\theta_0 - t - \frac{2\pi\nu}{ka}) e^{iq\tau(t)} \frac{dt}{\sqrt{1-t^2}} \quad \text{(A.3.14)}$$

The vector $\boldsymbol{k}_t^{\pm}$ is a function of the parameter t of the form

$$\boldsymbol{k}_t^{\pm} = k(\cos\tau, \sin\tau) = k(\pm\sqrt{1-t^2}, t) \quad \text{(A.3.15)}$$

where the sign $\pm$ is, as explained before, the same of $x - x_l$. In the same way, the quantity $e^{iq\tau(t)}$ is

$$e^{iq\tau(t)} = [\cos\tau + i\sin\tau]^q = \left[\pm\sqrt{1-t^2} + it\right]^q \quad \text{(A.3.16)}$$

The presence of the Dirac delta function in the integrand makes it possible to integrate the function, yielding

$$S_q^c(ka, \sin\theta_0, \boldsymbol{r}, \boldsymbol{R}_l) = \sum_{\alpha=-\infty}^{\infty} e^{i\alpha ka\sin\theta_0} H_q(kr_\alpha^l) e^{iq\theta_\alpha^l} = \frac{2i^{-q}}{ka} \sum_{\nu=-\infty}^{\infty} \frac{e^{iq\tau_\nu}}{|\cos\tau_\nu|} e^{i\boldsymbol{k}_\nu^{\pm}\cdot(\boldsymbol{r}-\boldsymbol{R}_l)} \quad \text{(A.3.17)}$$

where the complex angle τ_ν is defined from

$$\sin\tau_\nu = \sin\theta_0 + \frac{2\pi\nu}{ka}, \quad \nu = 0, \pm1, \pm2, \cdots \quad \text{(A.3.18a)}$$

$$\cos\tau_\nu = \pm\sqrt{1-\sin^2\tau_\nu} \quad \text{(A.3.18b)}$$

Incomplete Lattice Sums

The incomplete lattice sum is defined as

$$S_q^i(ka, \sin\theta_0) = \sum_{\alpha=1}^{\infty} e^{i\alpha ka\sin\theta_0} H_q(\alpha ka) \quad \text{(A.3.19)}$$

now the integral form of Hankel function given by equation A.1.20 will be used

$$H_q(x) = \frac{i^{-q}}{\pi} \lim_{\epsilon \to \infty} \int_{i\epsilon - \pi/2}^{-i\epsilon + \pi/2} e^{ix\cos\tau} e^{iq\tau} d\tau \tag{A.3.20}$$

If the following change of variable is performed

$$\sin\tau = e^{-i\pi/4} t \quad d\tau = \frac{e^{-i\pi/4} dt}{\sqrt{1+it^2}} \tag{A.3.21}$$

the lattice sum will be

$$S_q^i(ka, \sin\theta_0) = \sum_{\alpha=1}^{\infty} \frac{i^{-q} e^{-i\pi/4}}{\pi} \int_{-\infty}^{\infty} e^{i\alpha ka\sqrt{1+it^2}} e^{i\alpha ka\sin\theta_0} \frac{\left[\sqrt{1+it^2} + ite^{-i\pi/4}\right]^q}{\sqrt{1+it^2}} dt \tag{A.3.22}$$

the sum commutes again with the integral operator and will be expressed as

$$\lim_{M\to\infty} \sum_{\alpha=1}^{M} e^{i\alpha ka\sqrt{1+it^2}} e^{i\alpha ka\sin\theta_0} = \lim_{M\to\infty} e^{ika\sqrt{1+it^2}} e^{ika\sin\theta_0} \frac{1 - e^{iMka\sqrt{1+it^2}} e^{iMka\sin\theta_0}}{1 - e^{ika\sqrt{1+it^2}} e^{ika\sin\theta_0}} \tag{A.3.23}$$

It is easy to show that

$$\lim_{M\to\infty} e^{iMka\sqrt{1+it^2}} = 0 \tag{A.3.24}$$

for that, note that the number $z = 1 + it^2$ has its imaginary part positive, so that this number can be put in the form $z = re^{i\theta}$, where $\theta \in [0, \pi]$. It means that the number $\sqrt{1+it^2}$ can be expressed in the form

$$\sqrt{1+it^2} = r^{1/2}(\cos(\theta/2) + i\sin(\theta/2)) \tag{A.3.25}$$

then

$$\lim_{M\to\infty} e^{iMka\sqrt{1+it^2}} = \lim_{M\to\infty} e^{iMkar^{1/2}\cos(\theta/2)} e^{-Mkar^{1/2}\sin(\theta/2)} = 0 \tag{A.3.26}$$

due to the fact that $\sin(\theta/2)$ is always positive.

Then the final form for the lattice sum is

$$S_q^i(ka, \sin\theta_0) = \frac{i^{-q}e^{-i\pi/4}e^{ika\sin\theta_0}}{\pi}\int_{-\infty}^{\infty}\frac{e^{ika\sqrt{1+it^2}}\left[\sqrt{1+it^2}+ite^{-i\pi/4}\right]^q}{\sqrt{1+it^2}\left[1-e^{ika\sqrt{1+it^2}}e^{ika\sin\theta_0}\right]}dt \quad \text{(A.3.27)}$$

The above expression can be easily computed numerically and is more suitable for numerical calculations than the direct sum.

Application to the Infinite Slab

With the above result it is possible to calculate the lattice sums appearing in section 3.2

$$(\mathcal{G}_{lm})_{rs} \equiv \sum_{\beta=-\infty}^{\infty}(G_{0\beta}^{lm})_{rs}e^{i\beta ka\sin\theta_0} \quad \text{(A.3.28a)}$$

with $(G_{0\beta}^{lm})_{rs}$ given by equation 3.1.7

$$(G_{0\beta}^{lm})_{rs} = \sum_q (1-\delta_{0\beta})(T_l)_{rq}H_{q-s}(kR_{0\beta}^{lm})e^{i(s-q)\theta_{0\beta}^{lm}} \quad \text{(A.3.28b)}$$

here $(T_l)_{rq}$ is the T matrix of the cylinders laying along line l, and the vector $\boldsymbol{R}_{0\beta}$ is the vector that has its origin in the central cylinder of the line l and its end in the β cylinder of line m, that is

$$\boldsymbol{R}_{0\beta} = \boldsymbol{R}_m - \boldsymbol{R}_l + \beta a\hat{\boldsymbol{y}} \quad \text{(A.3.29)}$$

when $l \neq m$ the $\delta_{0\beta}$ function is redundant, because the β cylinder of the line m will never be equal to the 0 cylinder, which here stands for the central cylinder of line l, then, commuting the sums in q and β

$$(\mathcal{G}_{lm})_{rs} = \sum_q (T_l)_{rq}\sum_{\beta=-\infty}^{\infty}H_{q-s}(kR_{0\beta}^{lm})e^{i(s-q)\theta_{0\beta}^{lm}}e^{i\beta ka\sin\theta_0} \quad \text{(A.3.30)}$$

taken into account that $H_{q-s}(\cdot) = (-1)^{q-s}H_{s-q}(\cdot)$ the above expression can be related with the complete lattice sums as

$$(\mathcal{G}_{lm})_{rs} = \sum_q (T_l)_{rq}(-1)^{q-s}S_{s-q}^c(ka, \sin\theta_0, \boldsymbol{R}_m, \boldsymbol{R}_l) \quad \text{(A.3.31)}$$

For the case $l = m$ the delta function implies that the sum in β has to be taken excluding the $\beta = 0$ term

$$(\mathcal{G}_{ll})_{rs} = \sum_q (T_l)_{rq}(-1)^{q-s} \sum_{\substack{\beta=-\infty \\ \beta\neq 0}}^{\infty} H_{s-q}(kR^{ll}_{0\beta}) e^{i(s-q)\theta^{ll}_{0\beta}} e^{i\beta ka \sin\theta_0} \tag{A.3.32}$$

Note that $R^{ll}_{0\beta} = \beta a$ and $\theta^{ll}_{0\beta} = \pm\pi/2$, where the sign is positive for β positive and negative for β negative. Then the Hankel function inside the sum can be transformed

$$H_{s-q}(kR^{ll}_{0\beta}) e^{i(s-q)\theta^{ll}_{0\beta}} = H_{s-q}(\beta ka) i^{s-q} (-1)^{\beta/|\beta|} \tag{A.3.33}$$

and

$$\sum_{\substack{\beta=-\infty \\ \beta\neq 0}}^{\infty} H_{s-q}(\beta ka) i^{s-q} (-1)^{\beta/|\beta|} e^{i\beta ka \sin\theta_0} =$$

$$i^{s-q} \sum_{\beta=1}^{\infty} H_{s-q}(\beta ka) \left[e^{i\beta ka \sin\theta_0} + (-1)^{s-q} e^{-i\beta ka \sin\theta_0} \right] =$$

$$i^{s-q} \left[S_{s-q}(ka, \sin\theta_0) + (-1)^{s-q} S_{s-q}(ka, -\sin\theta_0) \right] \tag{A.3.34}$$

then the final result is

$$(\mathcal{G}_{ll})_{rs} = \sum_q (T_l)_{rq}(-i)^{q-s} \left[S^i_{s-q}(ka, \sin\theta_0) + (-1)^{s-q} S^i_{s-q}(ka, -\sin\theta_0) \right] \tag{A.3.35}$$

A.3.2 Lattice Sums for the Band Structure

The lattice sums for the band structure are used in the same form that appear in [NR94], and no demonstration will be given because in this paper the notation is very similar to the present one. The only incise will be done is about a mistake that appears there and must be fixed for a correct convergence of the sums.

Given a lattice defined by the vectors

$$\boldsymbol{R}_\beta = n_1 \boldsymbol{a}_1 + n_2 \boldsymbol{a}_2 \tag{A.3.36}$$

and some Bloch wave vector $\boldsymbol{K}$, the lattice sum is defined as

$$S_q^H(k,\boldsymbol{K}) \equiv \sum_{\beta\neq 0} H_q(kR_{0\beta})e^{iq\theta_{0\beta}}e^{i\boldsymbol{K}\cdot\boldsymbol{R}_\beta} \tag{A.3.37}$$

the following identity is proved in [NR94]

$$S_q^H(k,\boldsymbol{K}) = S_q^J(k,\boldsymbol{K}) + iS_q^Y(k,\boldsymbol{K}) \tag{A.3.38}$$

where

$$S_q^J(k,\boldsymbol{K}) = -\delta_{0q} \tag{A.3.39}$$

and

$$\begin{aligned} S_q^J(k,\boldsymbol{K})J_{q+1}(kR_{\min}) = \\ -\left[Y_1(kR_{\min}) + \frac{2}{\pi kR_{\min}}\right]\delta_{0q} \\ -4i^q\frac{k}{V_d}\sum_h \frac{J_{q+1}(G_hR_{\min})}{G_h(G_h^2-k^2)}e^{iq\theta_h} \end{aligned} \tag{A.3.40}$$

where the vector $\boldsymbol{G}_h$ is composed by the addition of the Block wave vector $\boldsymbol{K}$ and the reciprocal lattice vectors $\boldsymbol{b}_1$ and $\boldsymbol{b}_2$ defined in equations (3.3.18), that is

$$\boldsymbol{G}_h = \boldsymbol{K} + h_1\boldsymbol{b}_1 + h_2\boldsymbol{b}_2 \tag{A.3.41}$$

A.3.3 Lattice Sums for the Linear Chain of Spheres

The lattice sum of the linear chain can be expressed in terms of elementary functions.These lattice sums are

$$\begin{aligned} S_l(ka) = \sum_{\alpha=1}^{\infty} h_l(ka\alpha) = \\ \sum_{\alpha=1}^{\infty} i^{-l}\frac{e^{ika\alpha}}{ika\alpha}\sum_{\nu=0}^{l}\frac{(l+\nu)!}{\nu!(l-\nu)!}\left(\frac{i}{2ka\alpha}\right)^{\nu} = \sum_{\nu=0}^{l}\frac{i^{\nu-l-1}}{2^\nu}\frac{(l+\nu)}{\nu!(l-\nu)!}\sigma_\nu(ka) \end{aligned} \tag{A.3.42}$$

so the sum to calculate is

$$\sigma_\nu(x) = \sum_{s=1}^{\infty}\frac{e^{ixs}}{s^{\nu+1}} \tag{A.3.43}$$

for $\nu = 0$ and the Taylor series of $\ln(1+z)$ we have

$$\sigma_0(x) = \sum_{s=1}^{\infty} \frac{e^{ixs}}{s} = -\ln(1-e^{ix}) = \frac{i}{2}(\pi - x) - \ln|2\sin\frac{x}{2}| \tag{A.3.44}$$

but

$$\ln\sin z = \ln z + \sum_{q=1}^{\infty} \frac{(-1)^q 2^{2q-1} B_{2q}}{q(2q)!} z^{2q} \tag{A.3.45}$$

then

$$\sigma_0(x) = \frac{i}{2}(\pi - x) - \ln x - \sum_{q=1}^{\infty} \frac{(-1)^q B_{2q}}{2q(2q)!} x^{2q} \tag{A.3.46}$$

and it is possible to show that

$$\sigma_\nu(x) = i\int_0^x \sigma_{\nu-1}(x')dx' + \sum_{s=1}^{\infty} \frac{1}{s^{\nu+1}} \tag{A.3.47}$$

Defining the operator

$$\mathcal{L}f(x) \equiv i\int_0^x f(x')dx' \tag{A.3.48}$$

we arrive to

$$\sigma_\nu(x) = \mathcal{L}^\nu \sigma_0(x) + \sum_{\mu=0}^{\nu-1} \mathcal{L}^\mu \zeta(\nu+1-\mu) \tag{A.3.49}$$

it can be shown that

$$\mathcal{L}^\nu x^\mu = \frac{\mu! i^\nu}{(\nu+\mu)!} x^{\nu+\mu} \tag{A.3.50}$$

and that

$$\mathcal{L}^\nu \ln x = \frac{i^\nu}{\nu!} x^\nu (\ln x - \sum_{\mu=1}^{\nu} \frac{1}{\mu}) \tag{A.3.51}$$

and then we arrive to

$$\begin{aligned}\sigma_\nu(x) = \frac{i^\nu}{\nu!} x^\nu \Bigg[\frac{i}{2}(\pi - x/(\nu+1)) - \ln x + \sum_{\mu=1}^{\nu} 1/\mu - \\ \sum_{\mu=1}^{\infty} \frac{(-1)^\mu \nu! B_{2\mu}}{2\mu(2\mu+\nu)!} x^{2\mu} \Bigg] \\ + \sum_{\mu=0}^{\nu-1} \frac{i^\mu \zeta(\nu+1-\mu)}{\mu!} x^\mu\end{aligned} \tag{A.3.52}$$

The infinite sum

$$\sum_{\mu=1}^{\infty} \frac{(-1)^{\mu}\nu! B_{2\mu}}{2\mu(2\mu+\nu)!} x^{2\mu} \tag{A.3.53}$$

converges provided that $x < 2\pi$,that is, for $x = ka$ the sum will converge always that

$$a < \lambda \tag{A.3.54}$$

which is the diffraction limit. In the present work this limit is not taken into account, so that the previous expression for the lattice sum will be enough to describe all the phenomenon described here.

Appendix B

Long wavelength behavior

The homogenization theory developed in the present work is based in the long wavelength behavior of the scattering properties of the acoustic systems. Before present the theory it is necessary some mathematical preliminaries, which are the long wavelength behavior of the functions involved in the scattering and multiple scattering of sound waves by elastic and fluid cylinders.

B.1 Long wavelength behavior of the T Matrices

B.1.1 The fluid cylinder

The T matrix of a fluid cylinder is given in equation 2.3.8

$$T_q = -\frac{\rho_q J_q'(kR_a) - J_q(kR_a)}{\rho_q H_q'(kR_a) - H_q(kR_a)} \tag{B.1.1}$$

where

$$\rho_q = \frac{\rho_a v_a}{\rho_b v_b} \frac{J_q(k_a R_a)}{J_q'(k_a R_a)} \tag{B.1.2}$$

In the appendix A the asymptotic expression of the Bessel functions for small arguments are given. These are the expressions which will be used here to analyze the long wavelength limit of the T matrix, because when $\lambda \to \infty$ the wavenumber k goes to zero.

For $q = 0$, as $J_0'(\cdot) = -J_1(\cdot)$, the element ρ_q when $k_a \to 0$ will be

$$\rho_0 = -\frac{\rho_a v_a}{\rho_b v_b}\frac{J_0(k_a R_a)}{J_1(k_a R_a)} \approx -\frac{\rho_a v_a}{\rho_b v_b}\frac{2}{k_a R_a} \tag{B.1.3}$$

then the numerator of the T matrix will be

$$\frac{\rho_a v_a^2}{\rho_b v_b^2} - 1 \tag{B.1.4}$$

The denominator of the T matrix is formed by two terms with different k-dependence in the $k \to 0$ limit. The term $\rho_0 H_1(kR_a)$ is proportional to $1/k^2$, while the term $H_0(kR_a)$ is proportional to $\ln kR_a$, so that the dominant term will be the first one

$$\rho_0 H_1(kR_a) \approx \frac{\rho_a v_a^2}{\rho_b v_b^2}\frac{4i}{\pi R_a^2 k^2} \tag{B.1.5}$$

then the asymptotic form of the T_0 element will be

$$T_0 \approx \frac{i\pi R_a^2}{4}\left[\frac{\rho_b v_b^2}{\rho_a v_a^2} - 1\right] k^2 \tag{B.1.6}$$

For $q > 0$ the element ρ_q will be

$$\rho_q \approx \frac{\rho_a v_a}{\rho_b v_b}\frac{k_a R_a}{q} \tag{B.1.7}$$

and it is easy to verify that the numerator of the T matrix is

$$\rho_q J_q'(kR_a) - J_q(kR_a) \approx \frac{k^q R_a^q}{q! 2^q}\left[\frac{\rho_a}{\rho_b} - 1\right] \tag{B.1.8}$$

while the denominator is

$$\rho_q H_q'(kR_a) - H_q(kR_a) \approx \frac{i(q-1)! 2^q}{\pi k^q R_a^q}\left[\frac{\rho_a}{\rho_b} + 1\right] \tag{B.1.9}$$

then the asymptotic form of the T_q elements will be

$$T_q \approx \frac{i\pi R_a^{2q}}{4^q}\frac{1}{q!(q-1)!}\frac{\rho_a - \rho_b}{\rho_a + \rho_b}k^{2q} \tag{B.1.10}$$

note that from equation 2.3.8 it is easy to show that

$$T_{-q} = T_q \tag{B.1.11}$$

then the asymptotic form is also valid for $q < 0$ but expressing q in absolute value.

B.1.2 The elastic cylinder

For the elastic cylinder the expressions are more complex than for the fluid one, although the final result, as will be shown, is very similar. The difference between both types of cylinders is the factor ρ_q. The corresponding expression for the elastic cylinder is given in equation (2.4.23)

$$\rho_q = \frac{G_q}{I_q} \tag{B.1.12}$$

being G_q

$$G_q = \frac{2iq\mu_a F_q}{R_a^2}\left[J_q(k_t R_a) - k_t R_a J_q'(k_t R_a)\right] - k_l^2\left[\lambda_a J_q(k_l R_a) - 2\mu_a J_q''(k_l R_a)\right] \tag{B.1.13}$$

and I_q

$$I_q = \rho_b k c_b^2\left[-k_l J_q'(k_l R_a) + \frac{iq}{R_a} F_q J_q(k_t R_a)\right] \tag{B.1.14}$$

the factor F_q appearing in the above equations is

$$F_q = \frac{2iq}{k_t^2 R_a^2}\left[\frac{J_q(k_l R_a) - k_l R_a J_q'(k_l R_a)}{J_q(k_t R_a) + 2J_q''(k_t R_a)}\right] \tag{B.1.15}$$

For the case $q = 0$ the factor F_q equals to zero, then the factors G_0 and I_0 are

$$G_0 \approx -(\lambda_a + \mu_a)k_l^2 \tag{B.1.16}$$

$$I_0 \approx \frac{k\rho_b c_b^2 R_a^2}{2} k_l^2 \tag{B.1.17}$$

and the term ρ_0 will be

$$\rho_0 \approx -\frac{\lambda_a + \mu_a}{\rho_b c_b^2}\frac{2}{kR_a} \tag{B.1.18}$$

Proceeding as in the previous section, the final asymptotic form of the T_0 element will be

$$T_0 \approx \frac{i\pi R_a^2}{4}\left[\frac{\rho_b c_b^2}{\lambda_a + \mu_a} - 1\right] k^2 \tag{B.1.19}$$

This element is equal to that of the fluid cylinder but defining the fluid-like bulk modulus as

$$B_a = \lambda_a + \mu_a \tag{B.1.20}$$

which is the area bulk modulus derived from the elasticity equations in two dimensions [Tho85].

Due to the presence of the second derivative of the Bessel functions, the $q = 1$ case has to be studied independently. For this case, the numerator of the F_q factor will be, in the long wavelength limit

$$J_1(k_l R_a) - K_l R_a J_1'(k_l R_a) \approx \frac{k_l^3 R_a^3}{8} \tag{B.1.21}$$

the cubic term k_l^3 appears due to the cancellation of the first terms in the Taylor series of $J_1 - xJ_1'$. The denominator has a special form for $q = 1$

$$J_1(k_t R_a) + 2J_1''(k_t R_a) = -\frac{1}{2} J_1(k_t R_a) \tag{B.1.22}$$

then it is easy to show that for $k \to 0$

$$F_1 \approx -i \frac{c_t^3}{c_l^3} \tag{B.1.23}$$

Similar terms appear in the quantity G_q for $q = 1$, leading to

$$G_1 \approx -\frac{1}{2}(\lambda_a + \mu_a) R_a k_l^3 \tag{B.1.24}$$

the factor I_q can be expressed as

$$I_1 = \frac{1}{2} \rho_b c_b^2 (c_t^2 - c_l^2) \frac{k^2}{c_l^3} \tag{B.1.25}$$

so that ρ_q will be

$$\rho_1 = \frac{\rho_a}{\rho_b} R_a k \tag{B.1.26}$$

this factor has the same form for both the fluid and the elastic cylinder, then the asymptotic form for the T_1 element will be the same as in the fluid case

$$T_1 = \frac{i\pi R_a^2}{4} \frac{\rho_a - \rho_b}{\rho_a + \rho_b} k^2 \tag{B.1.27}$$

For $q > 1$, the F_q factor is

$$F_q \approx -i \frac{c_t^q}{c_l^q} \left[1 + \frac{k^2 R_a^2}{4(q-1)} \left(\frac{1}{c_t^2} - \frac{1}{c_l^2} \right) \right] \tag{B.1.28}$$

The presence of the Bessel function in the factor G_q induces to think that the lower order of this factor will be q, but the addition of all the factors proportionals k^q equals to zero, because to order k^q

$$\frac{2iq\mu_a F_q}{R_a^2}\left[J_q(k_t R_a) - k_t R_a J_q'(k_t R_a)\right] \approx -\frac{2\mu_a}{(q-2)!R_a^2}\left[\frac{k_l R_a}{2}\right]^q \tag{B.1.29}$$

and this term cancels with the other one in G_q, corresponding to the second derivative of the Bessel function

$$2\mu_a k_l^2 J_q''(k_l R_a) \approx \frac{2\mu_a}{(q-2)!R_a^2}\left[\frac{k_l R_a}{2}\right]^q \tag{B.1.30}$$

so that the lower order of the G_q factor is $q+2$. This factor will be divided by the I_q one, whose lower order again seems to be $q+1$ but, as before, this term cancels and the corresponding one is $q+3$, it happens because inside the brackets in

$$I_q = \rho_b k c_b^2\left[-k_l J_q'(k_l R_a) + \frac{iq}{R_a}F_q J_q(k_t R_a)\right] \tag{B.1.31}$$

the terms corresponding to k^q cancels, so the lower order is $q+2$ multiplied by the factor outside the brackets, resulting in a term of the form $\approx k^{q+3}$.

These asymptotic forms makes that the quantity ρ_q be

$$\rho_q = \widehat{\rho}_q \frac{1}{k} \tag{B.1.32}$$

where $\widehat{\rho}_q$ is some k-independent quantity. When this expression is placed in the T matrix, the numerator becomes

$$\rho_q J_q'(kR_a) - J_q(kR_a) \approx \widehat{\rho}_q J_q'(kR_a)/k \tag{B.1.33}$$

and the denominator

$$\rho_q H_q'(kR_a) - H_q(kR_a) \approx \widehat{\rho}_q H_q'(kR_a)/k \tag{B.1.34}$$

when dividing these two expressions the factor $\widehat{\rho}_q$ disappears, and with it all the information about the physical properties of the cylinder, being the resulting asymptotic form equal to that of the rigid cylinder

$$T_q \approx \frac{i\pi R_a^{2q}}{4^q}\frac{1}{q!(q-1)!}k^{2q} \tag{B.1.35}$$

Then it is obvious that in the limit $\mu_a \to 0$ the fluid cylinder is not recovered for the elements such that $q > 1$. To recover the fluid cylinder, the limit $\mu_a \to 0$ has to be made before the limit $k \to 0$, then the expression for the ρ_q factor is the same than that of the fluid cylinder.

B.1.3 The anisotropic fluid cylinder

For an anisotropic fluid cylinder the elements of the T matrix are defined by the equation

$$\sum_k H_{sk} T_{kq} = -J_{sq} \tag{B.1.36}$$

In the present work, as will be shown later, only the asymptotic form of the element T_{00} will be required, so that for $q = 0$

$$\sum_k H_{sk} T_{k0} = -J_{s0} \tag{B.1.37}$$

but

$$N_{0s} = \frac{i^{-s}}{2\pi} \int_0^{2\pi} e^{is\tau} d\tau = \delta_{s0} \tag{B.1.38}$$

$$M_{0s} = -\frac{i^{-s}}{2\pi} k^2 \frac{R_0}{2} \int_0^{2\pi} \frac{\rho_{rr}^{-1}}{v^2} e^{is\tau} d\tau = -k^2 \frac{R_0}{2B_0} \delta_{0s} \tag{B.1.39}$$

then

$$H_{00} = -1 \tag{B.1.40}$$

$$J_{00} = \frac{i\pi R_0^2}{4} \left[\frac{1}{B_0} - 1 \right] k^2 \tag{B.1.41}$$

and the low order term of the T_{00} element is

$$T_{00} = \frac{i\pi R_0^2}{4} \left[\frac{1}{B_0} - 1 \right] k^2 \tag{B.1.42}$$

if the bulk modulus of the background is different than one

$$T_{00} = \frac{i\pi R_0^2}{4} \left[\frac{B_b}{B_0} - 1 \right] k^2 \tag{B.1.43}$$

B.2 Long wavelength behavior of the band structure

The band structure of a periodic medium is linear in the low frequency limit, i.e. $k \to 0 (\omega \to 0)$. The slope of this line determines the effective speed of

sound of the equivalent homogeneous medium. The effective speed of sound is defined then as

$$c_{eff} = \lim_{\omega \to 0} \frac{\omega}{|\boldsymbol{K}(\omega)|} = c_b \lim_{k \to 0} \frac{k}{|\boldsymbol{K}(k)|} \tag{B.2.1}$$

where c_b is the background speed of sound. To simplify the notation, hereafter the quantity the relative effective speed of sound will be denoted just by c, then

$$c \equiv \frac{c_{eff}}{c_b} = \lim_{k \to 0} \frac{k}{|\boldsymbol{K}(k)|} \tag{B.2.2}$$

To study this limit, it is better to define the frequency-normalized coefficients $\widehat{A}_q$ such that

$$\widehat{A}_q \equiv A_q k^{-|q|-\delta_{0q}} \tag{B.2.3}$$

as we are now interested only in lattice of circular cylinders, the T matrix becomes now diagonal, then the equation for this normalized coefficients becomes

$$\widehat{A}_q - T_q \sum_s S^H_{s-q} k^{|s|+\delta_{s0}-|q|-\delta_{q0}} \widehat{A}_s = 0 \tag{B.2.4}$$

and then the matrix M is now

$$M_{qs} = \delta_{qs} - T_q S^H_{s-q} k^{|s|+\delta_{s0}-|q|-\delta_{q0}} \tag{B.2.5}$$

As shown in the previous sections, the elements of the T matrix has the same asymptotic dependence for both the elastic and the fluid cylinder, then the elements of this matrix can be expressed, in the low frequency limit, as

$$T_q = \widehat{T}_q k^{2|q|+2\delta_{q0}} \tag{B.2.6}$$

where the quantity $\widehat{T}_q$ is independent of k. In this limit

$$T_q S^H_{s-q} k^{|s|+\delta_{s0}-|q|-\delta_{q0}} \approx i\widehat{T}_q S^Y_l k^{|s|+|q|+\delta_{s0}+\delta_{q0}} \tag{B.2.7}$$

and then the equation for the dispersion relation becomes $\det \widehat{M} = 0$, with

$$\widehat{M}_{qs} = \delta_{qs} - i\widehat{T}_q \lim_{k \to 0} S^Y_{s-q} k^{|s|+|q|+\delta_{s0}+\delta_{q0}} \tag{B.2.8}$$

Now will be shown that the above limit can be expressed in terms of the effective speed of sound, therefore the secular equation for the band structure will become a secular equation to determine this speed of sound.

The limit needs to be computed in three steps:

- The diagonal terms $s = q$
- The terms such tat $s > q$
- The terms such tat $s < q$

B.2.1 Diagonal terms $q = s$

To determine the asymptotic form for the diagonal terms

$$\widehat{M}_{qq} = 1 - i\widehat{T}_q \lim_{k\to 0} S_0^Y k^{2|q|+2\delta_{q0}} \tag{B.2.9}$$

the asymptotic form of the S_0 element must be computed, being

$$S_0^Y k^{2|q|+2\delta_{q0}} = \\ -\frac{4}{V_d}\left[\frac{k}{J_1(kR_{\min})}\frac{J_1(KR_{\min})}{K(K^2-k^2)} + \frac{k}{J_1(kR_{\min})}\sum_{h\neq 0}\frac{J_1(G_hR_{\min})}{G_h^3}\right] k^{2|q|+2\delta_{q0}} \tag{B.2.10}$$

Then for this element only the first term will contribute to the matrix, so that

$$S_0^Y k^{2|q|+2\delta_{q0}} = -\frac{4}{V_d}\frac{k^{2|q|+2\delta_{q0}}}{K^2-k^2} \tag{B.2.11}$$

only those terms with $q = 0, \pm 1$ will be different than zero, with the previous definition of the effective speed of sound these terms are

$$\widehat{M}_{00} = 1 - f\left[\frac{B_b}{B_a} - 1\right]\frac{c^2}{1-c^2} \tag{B.2.12}$$

$$\widehat{M}_{11} = 1 - f\left[\frac{\rho_a - \rho_b}{\rho_a + \rho_b}\right]\frac{c^2}{1-c^2} = \widehat{M}_{-1-1} \tag{B.2.13}$$

$$\widehat{M}_{qq} = 1 \quad ;\forall |q| \geq 2 \tag{B.2.14}$$

These expressions are valid for both the elastic and the fluid array of cylinders.

B.2.2 $s > q$ terms

To calculate these elements the lattice sum will be split into two separate terms,

$$S_{s-q}^Y k^{|q|+|s|+\delta_{q0}+\delta_{s0}} = S_{s-q}^c + S_{s-q}^G \tag{B.2.15}$$

where

$$S^c_{s-q} = \\ -\frac{4}{V_d} i^{s-q} \frac{k}{J_{s-q+1}(kR_{\min})} \frac{J_{s-q+1}(KR_{\min})}{K(K^2-k^2)} e^{i(s-q)\theta_0} k^{|q|+|s|+\delta_{q0}+\delta_{s0}} \quad \text{(B.2.16)}$$

and

$$S^G_{s-q} = \\ -\frac{4}{V_d} i^{s-q} \frac{k}{J_{s-q+1}(kR_{\min})} \sum_{h\neq 0} \frac{J_{s-q+1}(G_h R_{\min})}{G_h^3} e^{i(s-q)\theta_h} k^{|q|+|s|+\delta_{q0}+\delta_{s0}} \quad \text{(B.2.17)}$$

for $k \to 0$ and using the asymptotic expression for the Bessel functions

$$S^c_{s-q} = -\frac{4}{V_d} i^{s-q} \frac{k^{|q|+|s|+\delta_{q0}+\delta_{s0}}}{c^{s-q}} \frac{1}{K^2-k^2} e^{i(s-q)\theta_0} \quad \text{(B.2.18)}$$

and

$$S^G_{s-q} = \\ -\frac{4}{V_d} i^{s-q} 2^{s-q+1} (s-q+1)! \frac{k^{|q|+|s|+\delta_{q0}+\delta_{s0}}}{k^{s-q} R_{\min}^{s-q+1}} \sum_{h\neq 0} \frac{J_{s-q+1}(G_h R_{\min})}{G_h^3} e^{i(s-q)\theta_h} \quad \text{(B.2.19)}$$

Only those terms with no dependence with k will survive to the limit, that is, for the factor $S^c_{s-q} \neq f(k)$ will be required that

$$|q| + |s| + \delta_{q0} + \delta_{s0} = 2 \to (q,s) = (0,1), (-1,0), (-1,1) \quad \text{(B.2.20)}$$

and for the factor $S^G_{s-q} \neq f(\omega)$ we will have

$$|q| + |s| + \delta_{q0} + \delta_{s0} - s + q = 0 \to s > 0, q < 0 \quad \text{(B.2.21)}$$

therefore the contributions to the matrix will be

$$S^c_{s-q} = -\frac{4}{V_d} i^{|s|+|q|} \frac{c^2}{c^{|s|+|q|}} \frac{1}{1-c^2} e^{i(|s|+|q|)\theta_0}, |qs| \leq 1, s > q \quad \text{(B.2.22)}$$

and

$$S^G_{s-q} = -\frac{4}{V_d R_{\min}^{|s|+|q|+1}} i^{|s|+|q|} 2^{|s|+|q|+1} (|s|+|q|+1)! \times \\ \sum_{h\neq 0} \frac{J_{|s|+|q|+1}(G_h)}{G_h^3} e^{i(|s|+|q|)\theta_h}, s > 0, q < 0 \quad \text{(B.2.23)}$$

and the matrix $\widehat{M}_{qs}$ is

$$\widehat{M}_{qs} = \delta_{qs} - i\widehat{T}_q S^Y_{s-q} \tag{B.2.24}$$

B.2.3 $q > s$ terms

In this case, knowing that $S^Y_{s-q} = S^Y_{-(q-s)} = S^{Y*}_{(q-s)}$, and, by remembering that $i\widehat{T}_q$ is a real number, it is found that

$$\widehat{M}_{qs} = \delta_{qs} - i\widehat{T}_q S^Y_{s-q} = \delta_{qs} - i\widehat{T}_q (S^Y_{q-s})^* = \delta_{qs} - (i\widehat{T}_q S^Y_{q-s})^* \tag{B.2.25}$$

B.2.4 Final form of $\widehat{M}$

In theory the matrix M is a infinite size matrix, but in practice the number of functions to use are limited to $Q_{\max}$. Defining the quantity Q as

$$Q = 2(Q_{\max} - 1) \tag{B.2.26}$$

The $\widehat{M}$ matrix have the block form

$$\widehat{M} = \begin{pmatrix} A_{3\times 3} & B_{3\times Q} \\ C_{Q\times 3} & D_{Q\times Q} \end{pmatrix} \tag{B.2.27}$$

where

$$A = \begin{pmatrix} 1 - f\eta\frac{c^2}{1-c^2} & if\eta\frac{c}{1-c^2}e^{-i\theta} & f\eta\frac{e^{-2i\theta}}{1-c^2} + \Gamma^{(0)} \\ -if\zeta\frac{c}{1-c^2}e^{i\theta} & 1 - f\zeta\frac{c^2}{1-c^2} & if\zeta\frac{c}{1-c^2}e^{-i\theta} \\ f\eta\frac{e^{2i\theta}}{1-c^2} + \Gamma^{(0)*} & -if\eta\frac{c}{1-c^2}e^{i\theta} & 1 - f\eta\frac{c^2}{1-c^2} \end{pmatrix} \tag{B.2.28}$$

here has been assumed that the filling fraction f is

$$f = \frac{\pi R_a^2}{V_d} \tag{B.2.29}$$

and the anisotropy factor has bee defined as

$$\Gamma^{(0)} = 48\eta f \sum_{h\neq 0} \frac{J_3(G_h)}{G_h^3 R_{\min}^3} e^{-2i\theta_h} \tag{B.2.30}$$

the quantity η is

$$\eta = \frac{\rho_a - \rho_b}{\rho_a + \rho_b} \tag{B.2.31}$$

and

$$\zeta = \frac{B_b}{B_a} - 1 \tag{B.2.32}$$

The matrix D is

$$D = \begin{pmatrix} I & D_{q>s} \\ D_{q<s} & I \end{pmatrix} \tag{B.2.33}$$

with

$$D_{q<s}|_{qs} \equiv D_{-qs} = \\ -8i^{s+q}2^{s-q}\frac{(s+q+1)!}{q!(q-1)!}\frac{R_a^{2(q-1)}}{R_{\min}^{s+q+1}} f\eta^e \sum_{h\neq 0} \frac{J_{s+q+1}(G_h R_{\min})}{G_h^3} e^{i(s+q)\theta_h} \tag{B.2.34}$$

and

$$D_{q>s}|_{qs} \equiv D_{q-s} = (D_{-qs})^* \tag{B.2.35}$$

here $\eta^e = \eta$ for fluid cylinders and $\eta^e = 1$ for elastic cylinders.

For the B and C matrices it is found that

$$B = \begin{pmatrix} O & B_{1-s} \\ O & O \\ B_{-1s} & O \end{pmatrix} \tag{B.2.36}$$

$$B_{-1s} = 4i^{s+1}2^s(s+2)!\frac{f\eta}{R_{\min}^{s+2}} \sum_{h\neq 0} \frac{J_{s+2}(G_h R_{\min})}{G_h^3} e^{i(s+1)\theta_h} \tag{B.2.37}$$

$$B_{1-s} = (B_{-1s})^* \tag{B.2.38}$$

$$C = \begin{pmatrix} O & O & C_{q-1} \\ C_{-q1} & O & O \end{pmatrix} \tag{B.2.39}$$

$$C_{-q1} = \\ -16i^{q+1}2^{-q}\frac{(q+2)!}{q!(q-1)!}\frac{R_0^{2(q-1)}}{R_{min}^{q+2}} f\eta^e \sum_{h\neq 0} \frac{J_{q+2}(G_h R_{\min})}{G_h^3} e^{i(1+|q|)\theta_h} \tag{B.2.40}$$

$$C_{q-1} = (C_{-q1})^* \tag{B.2.41}$$

Some properties of the matrix elements of $BD^{-1}C$ are necesary to express them in a more symmetric form. These elements are

$$BD^{-1}C\big|_{kl} = \sum_s \sum_q B_{ks} D_{sq}^{-1} C_{ql} \tag{B.2.42}$$

It is easy to verify, with the definitions of the matrices B and C, that

$$BD^{-1}C\big|_{0l} = BD^{-1}C\big|_{k0} = 0, \forall k, l \tag{B.2.43}$$

and that the diagonal terms are, for $k = l = 1$

$$BD^{-1}C\big|_{11} = \sum_s \sum_q B_{1s} D^{-1}_{sq} C_{q1} = \sum_{s>1} \sum_{q>1} B_{1-s} D^{-1}_{-s-q} C_{-q1} \tag{B.2.44}$$

and for $k = l = -1$

$$BD^{-1}C\big|_{-1-1} = \sum_s \sum_q B_{-1s} D^{-1}_{sq} C_{q-1} = \sum_{s>1} \sum_{q>1} B_{-1s} D^{-1}_{sq} C_{q-1} = \sum_{s>1} \sum_{q>1} B^*_{1-s} D^{-1}_{sq} C^*_{-q1} \tag{B.2.45}$$

while, from the definition of the D^{-1} matrix, it is shown that

$$\sum_s D_{ls} D^{-1}_{sq} = \sum_{s>0} D_{-ls} D^{-1}_{sq} = \delta_{lq} \tag{B.2.46}$$

and

$$\sum_s D_{ls} D^{-1}_{-s-q} = \sum_{s>0} D_{l-s} D^{-1}_{-s-q} = \delta_{l-q} = \sum_{s>0} D^*_{-ls} D^{-1}_{-s-q} = \delta_{-l-q} = \delta_{lq} \tag{B.2.47}$$

then it is obvious that

$$D^{-1}_{sq} = D^{-1*}_{-s-q} \tag{B.2.48}$$

which implies that

$$BD^{-1}C\big|_{11} = BD^{-1}C\big|^*_{-1-1} \equiv \Delta' \tag{B.2.49}$$

Proceeding in the same way

$$BD^{-1}C\big|_{1-1} = BD^{-1}C\big|^*_{-11} \equiv \Gamma' \tag{B.2.50}$$

Therefore, the final form of matrix $BD^{-1}C$ is

$$BD^{-1}C = \begin{pmatrix} \Delta' & 0 & \Gamma' \\ 0 & 0 & 0 \\ \Gamma'^* & 0 & \Delta'^* \end{pmatrix} \tag{B.2.51}$$

B.3 Long wavelength behavior of the Effective T Matrix

For the effective T matrix defined in equation (4.1.9),

$$T_{pt}^{\text{eff}} = \sum_{\alpha,\beta} \sum_{q,r,s} J_{p-q}(kR_\alpha) e^{(q-p)\Phi_\alpha} (M_{\alpha\beta}^{-1})_{qr} (T_\beta)_{rs} J_{t-s}(kR_\beta) e^{i(t-s)\Phi_\beta} \quad \text{(B.3.1)}$$

the lower order terms can be obtained from the dominant terms of each of the four elements which form it. The asymptotic form of the first term containing Bessel functions is simply

$$J_{p-q}(kR_\alpha) e^{i(q-p)\Phi_\alpha} \approx (\widehat{J}_\alpha)_{pq} k^{|p-q|} \quad \text{(B.3.2)}$$

being

$$(\widehat{J}_\alpha)_{pq} \equiv \frac{\sigma_{p-q}^{p-q}}{|p-q|!} \left[\frac{R_\alpha}{2}\right]^{|p-q|} e^{i(q-p)\Phi_\alpha} \quad \text{(B.3.3)}$$

the sign function σ_n^m is defined as follows

$$\sigma_n^m = \begin{cases} 1 & \text{if} \quad n \geq 0 \\ (-1)^m & \text{if} \quad n < 0 \end{cases} \quad \text{(B.3.4)}$$

the above result is valid for the other term appearing in the expression for T^{eff}, but now note the difference in the phase factor

$$J_{t-s}(kR_\beta) e^{i(s-t)\Phi_\beta} \approx (\widehat{J}_\beta)_{ts}^* k^{|t-s|} \quad \text{(B.3.5)}$$

Here all the cylinders of the cluster are circular and identical, only in chapter 6 will be considered the case of different cylinders, therefore from now on the matrix $(T_\beta)_{rs}$ will be simply $T_r \delta_{rs}$, being the asymptotic form

$$T_r \approx \widehat{T}_r k^{2|r|+2\delta_{r0}} \quad \text{(B.3.6)}$$

the quantity $\widehat{T}_r$ depends, as explained in sections B.1.1 and B.1.2 , on the type of cylinder (elastic or fluid).

The asymptotic form of the matrix $(M_{\alpha\beta}^{-1})_{qr}$ is more complex, because there is no an explicit form for this matrix, but can be obtained from its definition

$$\sum_r \boldsymbol{M}_{qr}^{-1} \boldsymbol{M}_{rs} = \delta_{qs} \boldsymbol{I} \quad \text{(B.3.7a)}$$

$$\sum_r \boldsymbol{M}_{qr} \boldsymbol{M}_{rs}^{-1} = \delta_{qs} \boldsymbol{I} \quad \text{(B.3.7b)}$$

where the greek subindex has been omitted because is not relevant in the following discussion.

The asymptotic form of the M matrix is

$$\boldsymbol{M}_{rs} = \delta_{rs}\boldsymbol{I} - \widehat{\boldsymbol{G}}_{rs}k^{2|r|+2\delta_{r0}-|r-s|} \tag{B.3.8}$$

where

$$(\widehat{G}_{\alpha\beta})_{rs} = \widehat{T}_r\sigma_{r-s}^{r-s}(|r-s|-1)!\frac{1}{i\pi}\left[\frac{2}{r_{\alpha\beta}}\right]^{|r-s|} e^{i(s-r)\theta_{\alpha\beta}}(1-\delta_{rs})(1-\delta_{\alpha\beta}) \tag{B.3.9}$$

the term δ_{rs} appears because when $r = s$, the asymptotic form of G matrix has a factor of the form $\approx \boldsymbol{I}k^2 \ln k$, which is lower than the factor $\boldsymbol{I}$. With this definition, multiplying equations B.3.7a and B.3.7b by $k^{|s|-|q|}$ and defining a new matrix

$$\widehat{\boldsymbol{M}}_{qr}^{-1} \equiv \boldsymbol{M}_{qr}^{-1}k^{-|q|+|r|} \tag{B.3.10}$$

equations (B.3.7a) and (B.3.7b) take the form

$$\sum_r \widehat{\boldsymbol{M}}_{qr}^{-1}\left[\delta_{rs}\boldsymbol{I} - \widehat{\boldsymbol{G}}_{rs}k^{|r|+|s|+2\delta_{r0}-|r-s|}\right] = \delta_{qs}\boldsymbol{I} \tag{B.3.11a}$$

$$\sum_r \left[\delta_{qr}\boldsymbol{I} - \widehat{\boldsymbol{G}}_{qr}k^{|q|+|r|+2\delta_{q0}-|q-r|}\right]\widehat{\boldsymbol{M}}_{rs}^{-1} = \delta_{qs}\boldsymbol{I} \tag{B.3.11b}$$

in these equations k appears rised to a number which is always bigger than or equal to zero, so when $k \to 0$ all terms will disappear except those which k be rised to zero, so the inverse of the matrix

$$\widehat{\boldsymbol{M}}_{qs} = \begin{cases} \delta_{qs}\boldsymbol{I} - \widehat{\boldsymbol{G}}_{qs} & \text{if} \quad qs \leq 0 \wedge q \neq 0 \\ \delta_{qs}\boldsymbol{I} & \text{if} \quad qs > 0 \vee q = 0 \end{cases} \tag{B.3.12}$$

is the matrix $\widehat{\boldsymbol{M}}_{qr}^{-1}$. Note that both the matrix $\widehat{\boldsymbol{M}}_{qs}$ and $\widehat{\boldsymbol{M}}_{qr}^{-1}$ are independent of k and then

$$\boldsymbol{M}_{qr}^{-1} = \widehat{\boldsymbol{M}}_{qr}^{-1}k^{|q|-|r|} \tag{B.3.13}$$

is the asymptotic form of the matrix M^{-1}.

Finally, the asymptotic form of the effective T matrix is

$$T_{pt}^{\text{eff}} = \sum_{\alpha,\beta}\sum_{r,q}(\widehat{J}_\alpha)_{pq}(\widehat{M}_{\alpha\beta}^{-1})_{qr}\widehat{T}_r(\widehat{J}_\beta)_{tr}^* k^{|p-q|}k^{|q|-|r|}k^{2|r|+2\delta_{r0}+|t-r|} \tag{B.3.14}$$

the lower oder terms of this equations will be those which $|p-q|+|q| = |p|$ and $|r|+|t-r|+2\delta_{r0} = |t|+2\delta_{t0}$, these conditions limits the possible values which can take r and q in the definition of $\widetilde{T}_{pt}$. These values defines, respectively, the sets $\mathcal{R}$ and $\mathcal{Q}$, then

$$T^{\text{eff}}_{pt} = \widehat{T}^{\text{eff}}_{pt} k^{|p|+|t|+2\delta_{t0}} \tag{B.3.15}$$

where

$$\widehat{T}^{\text{eff}}_{pt} = \sum_{r,q\in\mathcal{R},\mathcal{Q}} \sum_{\alpha,\beta} (\widehat{J}_\alpha)_{pq} (\widehat{M}^{-1}_{\alpha\beta})_{qr} \widehat{T}_r (\widehat{J}_\beta)^*_{tr} \tag{B.3.16}$$

Appendix C

Publications

C.1 International Journals

1. Daniel Torrent, Andreas Håkansson, Francisco Cervera, and José Sánchez-Dehesa. *Homogenization of two-dimensional clusters of rigid rods in air.* Physical Review Letters, 96(20):204302, 2006.

2. Daniel Torrent and José Sánchez-Dehesa. *Effective parameters of clusters of cylinders embedded in a nonviscous fluid or gas.* Physical Review B (Condensed Matter and Materials Physics), 74(22):224305, 2006.

3. Daniel Torrent and José Sánchez-Dehesa. *Evidence of two-dimensional magic clusters in the scattering of sound.* Physical review. B, Condensed matter and materials physics, 75(24):241404–, 2007.

4. Andreas Hkånsson, Daniel Torrent, Francisco Cervera, and José Sánchez-Dehesa. *Directional acoustic source by scattering acoustical elements.* Applied physics letters, 90(22):224107–, 2007.

5. Daniel Torrent and José Sánchez-Dehesa. *Acoustic metamaterials for new two-dimensional sonic devices.* New Journal of Physics, 9(9):323, 2007.

6. Daniel Torrent and José Sánchez-Dehesa. *Anisotropic mass density by two-dimensional acoustic metamaterials.* New Journal of Physics, 10, 2008.

7. Daniel Torrent and José Sánchez-Dehesa. *Acoustic Cloaking in two dimensions: a feasible approach.* New Journal of Physics, (Accepted, to be published in June 2008).

C.2 International Meetings and Conferences

1. Daniel Torrent, Andreas Håkakansson and José Sánchez-Dehesa. *Sound attenuation by lattices of rigid elliptic cylinders.* 149th Meeting Acoustical Society of America, Vancouver (Canada),2005.

2. Daniel Torrent and José Sánchez-Dehesa. *Effective parameters of periodic and random distributions of rigid cylinders in air.* 152nd Meeting Acoustical Society of America, Honolulu (Hawaii), 2006.

3. José Sánchez-Dehesa, Helios Sanchis-Alepuz, Yuri A. Kosevich and Daniel Torrent. *Acoustic analogue of electronic Bloch oscillations and Zener tunneling.* 152nd Meeting Acoustical Society of America, Honolulu (Hawaii), 2006.

4. Francisco Cervera, Daniel Torrent, Suitberto Cabrera, José Sánchez-Dehesa. *Acoustical properties of two-dimensional sonic crystals.* 152nd Meeting Acoustical Society of America, Honolulu (Hawaii), 2006.

5. José Sánchez-Dehesa, Yuri A. Kosevich and Daniel Torrent. *Theoretical prediction of super-radiant modes in ideal and distorted hexagonal clusters of twodimensional.* 151st Meeting Acoustical Society of America, Rhode Island, 2006.

6. Daniel Torrent, Andreas Håkansson, Francisco Cervera, and José Sánchez-Dehesa. *Homogenization of two-dimensional clusters of rigid rods in air.* 151st Meeting Acoustical Society of America, Rhode Island, 2006.

7. José Sánchez-Dehesa and Daniel Torrent. *Homogenization of Sonic Crystals: Results and Applications.* III International Physics Congress. 30th Anniversary Department for Physics Research, Hermosillo, Mexico,2007. (**Invited Talk**)

8. Daniel Torrent, Andreas Håkakansson, Francisco Cervera and José Sánchez-Dehesa. *Homogenization of two-dimensional fluid-fluid and solid-fluid composites*. International Congress on Ultrasonics 2007, Vienna, 2007.

9. Helios Sanchis-Alepuz, Daniel Torrent, Francisco Cervera and José Sánchez-Dehesa. *Acoustic Bloch oscillations and Zener tunneling in sonic superlattices*. International Congress on Ultrasonics 2007, Vienna, 2007.

10. José Sánchez-Dehesa and Daniel Torrent *Homogenization of Two-Dimensional Clusters of Cylinders Embedded in Fluid and Gases*. 9th US National Congress on Computational Mechanics, San Francisco, USA, 2007.(**Invited Talk**)

11. José Sánchez-Dehesa and Daniel Torrent *A gradient index sonic lens based on acoustic metamaterials*. 154th Meeting Acoustical Society of America, New Orleans, Louisiana (USA), 2007.

12. Daniel Torrent and José Sánchez-Dehesa *Anisotropic dynamical mass density by two-dimensional arrays of solid cilinders in air*. 154th Meeting Acoustical Society of America, New Orleans, Louisiana (USA), 2007.

Bibliography

[Ber80] James G. Berryman. Long-wavelength propagation in composite elastic media i. spherical inclusions. *The Journal of the Acoustical Society of America*, 68(6):1809–1819, 1980.

[Ber92] James G. Berryman. Single-scattering approximations for coefficients in biot's equations of poroelasticity. *The Journal of the Acoustical Society of America*, 91(2):551–571, 1992.

[Cai04] Liang-Wu Cai. Multiple scattering in single scatterers. *The Journal of the Acoustical Society of America*, 115(3):986–995, 2004.

[Cai07] LW Cai. Analysis of cummerschurig acoustic cloaking. *New journal of physics*, 9(12):450, 2007.

[CB80] J. Y. Chung and D. A. Blaser. Transfer function method of measuring in-duct acoustic properties. i. theory. *The Journal of the Acoustical Society of America*, 68(3):907–913, 1980.

[Che07] H Chen. Acoustic cloaking in three dimensions using acoustic metamaterials. *Applied physics letters*, 91(18):183518–, 2007.

[CSD08] Liang-Wu Cai and José Sánchez-Dehesa. *The Journal of the Acoustical Society of America*, (to be published), 2008.

[CSSP+01] F. Cervera, L. Sanchis, J. V. Sánchez-Pérez, R. Martínez-Sala, C. Rubio, F. Meseguer, C. López, D. Caballero, and J. Sánchez-Dehesa. Refractive acoustic devices for airborne sound. *Phys. Rev. Lett.*, 88(2):023902, Dec 2001.

[Cum07] Cummer. One path to acoustic cloaking. *New journal of physics*, 9, 2007.

[Cum08] SA Cummer. Scattering theory derivation of a 3d acoustic cloaking shell. *Physical review letters*, 100(2):024301–, 2008.

[Dow92] Jonathan P. Dowling. Sonic band structure in fluids with periodic density variations. *The Journal of the Acoustical Society of America*, 91(5):2539–2543, 1992.

[EG72] Meyer E and Neumann E G. *Physical Applied Acoustics*. New York: Academic, 1972.

[FN01] Land M F and Nilsson. *Animal Eyes*. Oxford University Press, 2001.

[GY03] Bikash C. Gupta and Zhen Ye. Theoretical analysis of the focusing of acoustic waves by two-dimensional sonic crystals. *Physical Review E (Statistical, Nonlinear, and Soft Matter Physics)*, 67(3):036603, 2003.

[HC05] Xinhua Hu and C. T. Chan. Refraction of water waves by periodic cylinder arrays. *Physical Review Letters*, 95(15):154501, 2005.

[Hua07] Y Huang. Electromagnetic cloaking by layered structure of homogeneous isotropic materials. *Optics express*, 15(18):11133–11141, 2007.

[KAG03] A. A. Krokhin, J. Arriaga, and L. N. Gumen. Speed of sound in periodic elastic composites. *Physical Review Letters*, 91(26):264302, 2003.

[LL] L.D. Landau and E.M Lifshitz. *Theory of Elasticity*.

[MA] Irene A.Stegun Milton Abramowitz. *Handbook of Mathematical Functions*.

[Mil06] G Milton. On cloaking for elasticity and physical equations with a transformation invariant form. *New journal of physics*, 8, 2006.

[MLWS06] Jun Mei, Zhengyou Liu, Weijia Wen, and Ping Sheng. Effective mass density of fluid-solid composites. *Physical Review Letters*, 96(2):024301, 2006.

[NR94] NA Nicorovici and RCMcPhedran. Lattice sums for off-axis electromagnetic scattering by gratings. *Physical review. E, Statistical physics, plasmas, fluids, and related interdisciplinary topics*, 50(4):3143–3160, 1994.

[Pen06] J Pendry. Controlling electromagnetic fields. *Science*, 312:1780, 2006.

[RCSP+99] C. Rubio, D. Caballero, J.V. Sanchez-Perez, R. Martinez-Sala, J. Sanchez-Dehesa, F. Meseguer, and F. Cervera. The existence of full gaps and deaf bands in two-dimensional sonic crystals. *Lightwave Technology, Journal of*, 17(11):2202–2207, Nov 1999.

[RI98] W. M. Robertson and J. F. Rudy III. Measurement of acoustic stop bands in two-dimensional periodic scattering arrays. *The Journal of the Acoustical Society of America*, 104(2):694–699, 1998.

[Sch06] D Schurig. Metamaterial electromagnetic cloak at microwave frequencies. *Science*, 314(5801):977–980, 2006.

[SHCSD03] Lorenzo Sanchis, Andreas Hkansson, Francisco Cervera, and Jose Sanchez-Dehesa. Acoustic interferometers based on two-dimensional arrays of rigid cylinders in air. *Physical Review B (Condensed Matter and Materials Physics)*, 67(3):035422, 2003.

[SSM05] R. Sainidou, N. Stefanou, and A. Modinos. Widening of phononic transmission gaps via anderson localization. *Physical Review Letters*, 94(20):205503, 2005.

[THCSD06] Daniel Torrent, Andreas Hakansson, Francisco Cervera, and Jose Sanchez-Dehesa. Homogenization of two-dimensional clusters of rigid rods in air. *Physical Review Letters*, 96(20):204302, 2006.

[Tho85] MF Thorpe. Elastic moduli of two-dimensional composite continua with elliptical inclusions. *The Journal of the Acoustical Society of America*, 77(5):1674–, 1985.

[Tre] Tretyakov. *Analytical modeling in Applied Electromagnetism.* Artech House, Norwood MA.

[TSD06] Daniel Torrent and José Sánchez-Dehesa. Effective parameters of clusters of cylinders embedded in a nonviscous fluid or gas. *Physical Review B (Condensed Matter and Materials Physics)*, 74(22):224305, 2006.

[TSD07] Daniel Torrent and José Sánchez-Dehesa. Acoustic metamaterials for new two-dimensional sonic devices. *New journal of physics*, 9(9):323, 2007.

[TSD08] Daniel Torrent and José Sánchez-Dehesa. Anisotropic mass density by two-dimensional acoustic metamaterials. *New journal of physics*, 10, 2008.

[W78] March E W. *Gradient Index Optics.* New York: Academic, 1978.

[XSK+07] J.-Q. Xi, M. F. Schubert, J. K. Kim, E. F. Schubert, M. Chen, S.-Y. Lin, W. Liu, and J. A. Smart. Optical thin-film materials with low refractive index for broadband elimination of Fresnel reflection. *Nature Photonics, Volume 1, Issue 3, pp. 176-179 (2007).*, 1:176–179, March 2007.

[YA98] Zhen Ye and Alberto Alvarez. Acoustic localization in bubbly liquid media. *Phys. Rev. Lett.*, 80(16):3503–3506, Apr 1998.

[ZL04] X. Zhang and Z. Liu. Negative refraction of acoustic waves in two-dimensional phononic crystals. *Applied Physics Letters*, 85:341–+, July 2004.

Printed with LaTeX